DETERMINATION OF THE CHANGE IN BUILDING CAPACITY DURING EARTHQUAKES

A THESIS SUBMITTED TO
THE GRADUATE SCHOOL OF NATURAL AND APPLIED SCIENCES
OF
MIDDLE EAST TECHNICAL UNIVERSITY

BY

DENİZ ÇEVİK

IN PARTIAL FULFILLMENT OF THE REQUIREMENTS
FOR
THE DEGREE OF MASTER OF SCIENCE
IN
CIVIL ENGINEERING

JANUARY 2006

Approval of the Graduate School of Natural and Applied Sciences

____

Prof. Dr. Canan ÖZGEN
Director

I certify that this thesis satisfies all the requirements as a thesis for the degree of Master of Science.

____

Prof. Dr. Erdal ÇOKÇA
Head of Department

This is to certify that we have read this thesis and that in our opinion it is fully adequate, in scope and quality, as a thesis for the degree of Master of Science.

____

Assoc. Prof. Dr. Ahmet YAKUT
Supervisor

Examining Committee Members

Prof. Dr. Polat GÜLKAN	(METU, CE)	________________
Assoc. Prof. Dr. Ahmet YAKUT	(METU, CE)	________________
Asst. Prof. Dr Barış BİNİCİ	(METU, CE)	________________
Asst. Prof. Dr. Altuğ ERBERİK	(METU, CE)	________________
MS. Yüksel TONGUÇ	(PROMER)	________________

I hereby declare that all information in this document has been obtained and presented in accordance with academic rules and ethical conduct. I also declare that, as required by these rules and conduct, I have fully cited and referenced all material and results that are not original to this work.

Name, Last name : Deniz ÇEVİK

Signature :

ABSTRACT

DETERMINATION OF THE CHANGE IN BUILDING CAPACITY DURING EARTHQUAKES

ÇEVİK, Deniz
M.Sc., Department of Civil Engineering
Supervisor: Assoc. Prof. Dr. Ahmet YAKUT

January 2006, 136 pages

There is a great amount of building stock built in earthquake regions where earthquakes frequently occur. It is very probable that such buildings experience earthquakes more than once throughout their economic life. The motivation of this thesis arose from the lack of procedures to determine the change in building capacity as a result of prior earthquake damage. This study focuses on establishing a method that can be employed to determine the loss in the building capacity after experiencing an earthquake.

In order to achieve this goal a number of frames were analyzed under several randomly selected earthquakes. Nonlinear time-history analyses and nonlinear static analyses were conducted to assess the prior and subsequent capacities of the frames under consideration. The structural analysis programs DRAIN-2DX and SAP2000 were employed for this purpose. The capacity curves obtained by these methods were investigated to propose a procedure by which the capacity of previously damaged structures can be determined.

For time-history analyses the prior earthquake damage can be taken into account by applying the ground motion histories successively to the structure under consideration. In the case of nonlinear static analyses this was achieved by modifying the elements of the damaged structure in relation to the plastic deformation they experience.

Finally a simple approximate procedure was developed using the regression analysis of the results. This procedure relies on the modification of the structure stiffness in proportion to the ductility demand the former earthquake imposes.

The proposed procedures were applied to an existing 3D building to validate their applicability.

Keywords: Change in building capacity, prior earthquake damage, nonlinear time-history analyses, nonlinear static analyses, approximate procedures.

ÖZ

BİNA DAYANIMININ DEPREM ANINDA DEĞİŞİMİNİN BELİRLENMESİ

ÇEVİK, Deniz
Yüksek Lisans, İnşaat Mühendisliği Bölümü
Tez Yöneticisi: Doç. Dr. Ahmet YAKUT

Ocak 2006, 136 sayfa

Depremlerin sürekli olarak oluştuğu deprem bölgelerinde birçok yapı mevcuttur. Bu yapıların birçoğu büyük bir olasılıkla ekonomik ömürleri boyunca birden fazla defa deprem kuvvetlerine maruz kalacaktır. Bu tezin hareket noktasını, mevcut analiz yöntemleri arasında daha önceden deprem geçirmiş yapıların dayanımında meydana gelen değişimin belirlenmesi için bir yöntem bulunmayışı oluşturmaktadır. Bu çalışma, deprem geçirmiş bir yapının dayanımında meydana gelen azalmayı tayin eden bir yöntem geliştirmeyi hedeflemiştir.

Bu amaç için değişik özelliklere sahip çerçeveler rastgele seçilmiş depremler altında analiz edilmiştir. Bu çerçevelerin dayanımlarının belirlenmesi için elastik ötesi dinamik analiz ve elastik ötesi statik analiz yöntemleri kullanılmıştır. Bu amaçla kullanılan analiz programları DRAIN-2DX ve SAP2000 olmuştur. Bu yöntemler ve programlarla elde edilen sonuçlar incelenerek deprem sırasında hasar görmüş bir yapının dayanımda meydana gelen değişimi belirleyen bir yöntem geliştirilmiştir.

Elastik ötesi dinamik analiz yöntemi için daha önceki depremin etkisi, deprem yer hareketlerini yapıya üst üste uygulayarak belirlenebilir. Elastik ötesi statik analiz yönteminde ise buna, zarar görmüş yapı elemanlarının rijitliğini maruz kaldıkları plastik deformasyonlarıyla orantılı olarak azaltarak ulaşılabilir.

Bu yöntemlerin sonuçlarını kullanarak elde edilen regresyon modeliyle, kullanması çok kolay bir yöntem geliştirilmiştir. Bu yöntemle, yapıya hasar veren ilk depremin oluşturduğu süneklik oranı kullanılarak yapının rijitliği azaltılmakta ve hasarlı binanın dayanımı bu şekilde tayin edilmektedir.

Önerilen yöntemler gerçek bir üç boyutlu binaya tatbik edilmiş; böylece bu yöntemlerin uygulanabilirliği tasdik edilmiştir.

Anahtar Kelimeler: Bina dayanımında değişim, önceki deprem hasarı, elastik ötesi dinamik analiz, elastik ötesi statik analiz, yaklaşık yöntemler.

To Dilek

ACKNOWLEDGMENTS

This study was conducted under the supervision of Assoc. Prof. Dr. Ahmet Yakut. I would like to express my deepest appreciation and sincere gratitude for the help, expert guidance, support, suggestions and continual supervision that he has provided me throughout the study. It was a great pleasure to work with him.

I also owe thanks to my friends Beyhan Bayhan, Serkan Çetinceli and İ. Cem Baskın for their friendship and support throughout my undergraduate and graduate life.

Sermin Oğuz deserves special thanks for her valuable suggestions and support during this study.

I would like to express my deepest appreciation to my wife Dilek, my parents Gisela and Abdullah, my sister Selma, and brother Selim – the most precious people in my life – for their confidence in me and for the support, love and understanding that they have provided me throughout my life.

TABLE OF CONTENTS

LIST OF TABLES

LIST OF FIGURES

CHAPTER 1

INTRODUCTION

1.1 BACKGROUND

Structures built in earthquake regions may be subjected to earthquake forces more than once throughout their life. Prior earthquake damage would lead to changes in the structural characteristics which in turn imply changes in the response of the structure against future earthquakes. This effect can be taken into account by performing successive time-history analyses or nonlinear static analyses of the structure under consideration. Although the time-history analysis produces the most reliable results, it is an impractical procedure due to its time consuming nature and the absence of ground motion data required to perform this analysis. These drawbacks lead to high computational costs which are undesirable for common use. The nonlinear static analysis on the other hand is a simplified procedure taking into consideration structural properties such as stiffness and strength and produces the pushover curve which is an illustration of the response characteristics of the structure. This procedure is preferred due to its simplicity yet the results obtained are approximate.

In this study a number of frames were analyzed under several earthquakes employing both methods mentioned above and a simple method for determining the changes in structural characteristics due to prior earthquake damage is proposed for use in seismic assessment.

1.2 PREVIOUS WORK

There has been very limited research focusing on the inclusion of the prior earthquake damage on the subsequent analyses of structures. In these studies, most of which were shake table test, the main objective was to determine the change in the displacement capability of the structures subjected to prior earthquake damage. This was achieved by subjecting the structures to successive ground motions and comparing the pre and post damage states. The important studies performed to determine the effects of prior earthquake damage will next be presented in chronological order.

Çeçen [12] performed shake table tests on ten-story three-bay reinforced concrete frames and concluded that the maximum roof displacement exercised only very slight changes for the damaged structure in comparison to the undamaged structure.

The shake table tests performed by Araki et al [5] in which reinforced concrete wall and frame wall structures were subjected to single and successive ground motions, indicated that damaged low rise structures were able to displace twice as much as their undamaged counterparts, whereas the increase in displacement capability for mid rise and high rise structures was limited to 10 percent.

Wolschlag [25] applied repeated ground motions to three story reinforced concrete walls but could not detect any considerable change in the peak displacement of each story.

Hanson [15] investigated the prior earthquake damage in terms of loss in lateral load carrying capacity of the structure. He proposed a procedure to express this loss in terms of observed crack widths in the damaged structure.

In the ATC-43 Project [3], a procedure based on global displacement and component deformation capacities was presented due to the disagreement on the suitability of using the force capacity. The study concluded that the maximum displacement occurring during larger future earthquakes is not affected in many cases by the prior earthquake. This was related to the fact that no significant strength degradation might have occurred during the smaller prior earthquake.

Aschheim and Black [6] modeled prior earthquake damage as a reduction in the initial stiffness under the assumption that residual displacements were negligible. They used three versions of the Takeda hysteresis model and observed minor influence on peak displacement response.

Sözen [22] investigated buildings in Düzce, which experienced two successive strong earthquakes in August and November 1999. He wondered that if the ground motion records of both earthquakes and the damage state for the earthquake in August had been given, could the damage occurring in November be predicted. He concluded that this was not possible on the basis of direct and indirect but simple methods and addressed the connection between ground motion measurement and potential damage.

Bazzuro et al [7] proposed guidelines for the assessment of the seismic performance of existing steel structures for a major electric utility. The procedure used in this study to determine the capacity curve of the damaged structure is as explained below;

- The building is assumed to unload linearly, see (Figure 1.1). The unloading stiffness, K_i, is determined using a linear model of the structure in Damage State i (DS_i). This model is constructed by reducing the stiffness of damaged beams. For beams whose end connections remain within the elastic or hardening region of the moment-rotation curve (Figure 1.2), the beam stiffness remains unchanged. For beams whose end connections have "fractured" or gone past point D on the moment-rotation curve (Figure 1.3), the stiffness is reduced to approximate that for a beam with fractured flanges. For a beam that fails on one end, the moment of inertia is reduced to 2/3 I, for a beam that fails on both ends it is reduced to 1/3 I.
- The residual deformation resulting from this unloading is Δ_{rs} as shown in Figure 1.1. The dynamic residual displacement, Δ_{rd}, is estimated to be $0.2\times\Delta_{rs}$ for low strength degradation and $0.6\times\Delta_{rs}$ for high strength degradation.
- The hardening stiffness, K_{hi}, for the damaged structure is determined by the ratio of fractured connections (N_f) to the total number of connections (N_c)

$$K_{hi} = \left(1 - \frac{N_f}{N_c}\right) \times K_i$$

- The Static Pushover (SPO) of the damaged structure meets the SPO of the intact structure at the defined DS_i point and then follows the SPO of the intact structure. Given the two points, DS_i and Δ_{rd}, and the two slopes K_i and K_{hi}, the SPO curves for the damaged structure can be created, see (Figure 1.4).

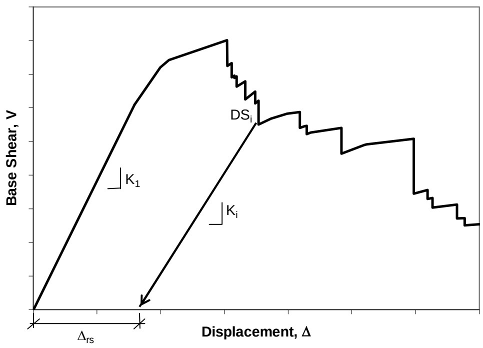

Figure 1.1: Assumed Global Unloading Stiffness from DS_i.

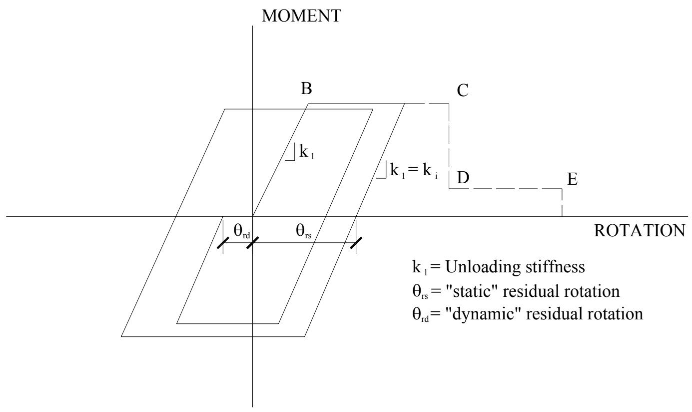

Figure 1.2: Assumed Unloading Cyclic Behavior for Connections Whose Flanges Have Not Fractured.

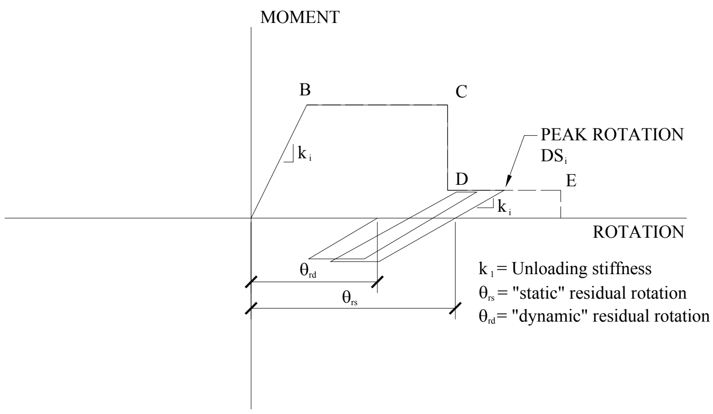

Figure 1.3: Assumed Unloading and Cyclic Behavior of Connections Whose Flanges Have Fractured.

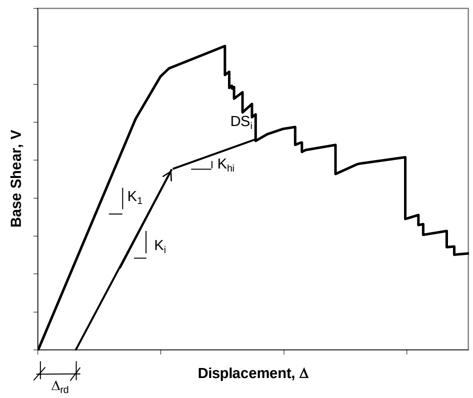

Figure 1.4: Assumed Global Reloading of a Structure That Has Been Subjected to DS_i

1.3 OBJECTIVE AND SCOPE

There is a great amount of buildings that have already suffered earthquakes but are still in use. It is also very probable that some of these buildings will be subjected once again to earthquake forces. Therefore it is necessary to approximately define the amount of damage that the building will suffer during an earthquake. In this manner, the response of the buildings due to the subsequent earthquakes can be estimated. This study aims at exploring a procedure to determine the change in building capacity during an earthquake.

In order to achieve this goal, six frames were analyzed under ten ground motion records. The frames were analyzed using two different methods; time-history analysis of the multi degree of freedom (MDOF) system and nonlinear static analysis (pushover analysis) of the frames in conjunction with time-history analysis of the single degree of freedom (SDOF) representation of the frames.

For all the analyses stated above the capacity curve of the undamaged state of the frames was established. As a next step the capacity curves of the damaged structures were explored.

In the case of time-history analyses of MDOF systems, the ground motion record was applied successively to the frames and the results obtained for the second record were used as the values for the damaged structure.

For the nonlinear static analysis procedure, elements were modified to represent their current damage state by taking into account the amount of plastic rotation they experience. The analyses were repeated to determine the capacity curve corresponding to the prior damage caused by the ground motion.

Time-history analysis of SDOF representation of the frames is achieved by approximating the capacity curve of the MDOF system as a bilinear curve thus for the damaged case the capacity curve of the damaged structure is used for the determination of this approximation.

This study makes use of various methods therefore there arose good occasions to compare the results and test the dependability of simplified procedures. Results obtained by the time-history analyses are considered to be the correct or exact values that the other procedures are going to be compared with.

The first assessment is the dependability of the simplified, nonlinear static analysis (pushover) and SDOF approximation methods. Results obtained via these two analysis methods are compared with the time-history analysis results to observe how well they can approximate the much more cumbersome time-history method.

The nonlinear static analyses of the frames were performed through two different structural analysis programs; DRAIN-2DX [20] and SAP2000 [11]. A comparison of the modeling assumptions and results obtained are also presented in this study.

The thesis also briefly explores the differences between three methods commonly used to obtain the bilinear approximation of capacity curves. These methods include the FEMA Method [13], the Initial Stiffness Procedure, and the Major Yield Method.

As a result of these analyses and the comparison of all the different methods used, a procedure to estimate the capacity of a building subjected to prior earthquake damage is proposed. This procedure facilitates the modification of the stiffness of a structure that experiences an earthquake given that the ductility demand imposed on the structure from a previous earthquake is known.

This thesis is comprised of four chapters. Chapter 1 presents a brief introduction and discusses the main points of the analysis tools used in addition to the aim of this study. Chapter 2 includes the analyses performed in this study. Initially the frames analyzed and earthquakes used are defined. Then the modeling assumptions and parameters are presented and the results obtained by the time-history analysis of the MDOF system, nonlinear static analysis (pushover analysis) of the frames, and time-history analysis of SDOF representation of the frames are compared. In Chapter 3 the results obtained from the previous chapter are processed and a procedure that can be used to determine the change in building capacity due to prior earthquakes is proposed. Additionally an approximate but very easy to implement procedure is defined and applied to a case study building. Chapter 4 contains the summary, conclusion, and future recommendations on the study. The Appendix contains detailed properties of the frames analyzed, the base shear roof displacement pairs obtained by the time-history analyses of both the MDOF and SDOF systems and finally the section properties for column and beams of the case building used in Chapter 3.

CHAPTER 2

INVESTIGATION OF PRIOR EARTHQUAKE DAMAGE ON FRAMES

2.1 GENERAL

The analyses in this study were conducted on six different frames. These frames include a two story-two bay frame which will be called F2S2B, a four story frame comprised of three bays entitled as F4S3B, three five story frames having two, four and seven bays and termed as, F5S2B, F5S4B, and F5S7B respectively, and finally an eight story-three bay frame named as F8S3B. Considering the building stock of Turkey, which consists mainly of four or five story buildings, the majority of frames chosen to be analyzed in this study were five story frames. Time-history analyses of these frames were performed under ten earthquakes. The earthquakes used, whose properties will be given in the following sections, were, Düzce, El Centro, Pacoima Dam, Parkfield, El Centro 79a, El Centro 79b, Chi-Chi, Northridge-Pacoima, Cape Mendocino, and Northridge. All of these earthquakes were scaled so that they push the structure into the Immediate Occupancy or Life Safety regions, which cover light to moderate damage states of the structure. The performance objective of Immediate Occupancy is defined as a post-earthquake damage state in which only very limited structural damage occurs. The basic vertical and lateral force resisting systems of the building retain nearly all of their pre-earthquake strength and stiffness. The Life Safety performance objective on the other hand is described as a post-earthquake damage state in which significant damage to the structure occurs, but some margin against either partial or total structural collapse remains. In this damage state, some structural elements and components are severely damaged, but this does not result in large falling debris hazards, either within or outside the building. In fact, there is also a third performance level defined on structures, namely the Collapse Prevention

Performance Level, where the building is on the verge of experiencing partial or total collapse. Here substantial damage to the structure occurs, potentially including significant degradation in the stiffness and strength of the lateral force resisting system, large permanent lateral deformation of the structure and – to a more limited extent – degradation in vertical load carrying capacity [13]. But since in this final damage state the structure may not be technically practical to repair and is not safe for re-occupancy, it was not included in the analyses performed throughout this study. The displacement limits corresponding to these three performance levels are determined as shown in Figure 2.1. Immediate Occupancy corresponds to the linear range of the bilinear approximation of the capacity curve. The portion between the yield displacement and ultimate displacement of the capacity curve is then divided into two equally long segments where the first segment makes up the Life Safety Level and the second one the Collapse Prevention Level. Six different performance points for each frame in the mentioned range of displacements were selected and the earthquakes were scaled accordingly.

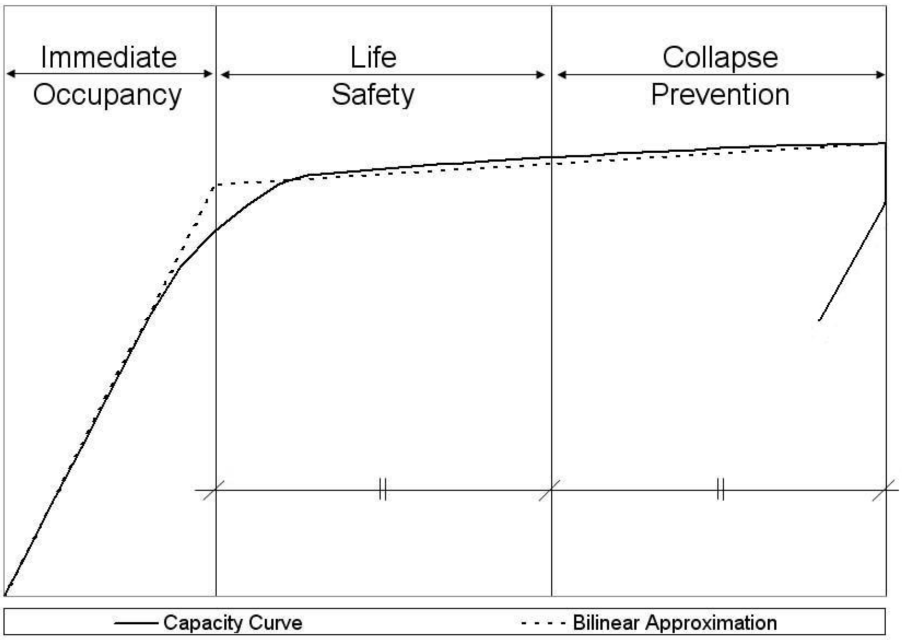

Figure 2.1: Performance Level Limits

In the next step, nonlinear static analyses of the frames were conducted. These analyses produce the capacity curve or the so called pushover curve, which is a plot of the base shear versus top displacement interaction of the frames. The overall capacity of a structure depends on the strength and deformation capacities of the individual components of the structure. In order to determine capacities beyond the elastic limits, the pushover procedure, which uses a series of sequential elastic analyses superimposed to approximate a force displacement capacity diagram of the overall structure, is implemented. The mathematical model of the structure is modified to account for reduced resistance of yielding components. A lateral force distribution is again applied until additional elements yield and this process is continued until the structure becomes unstable or a predetermined limit is reached [2]. In this analysis, hinges which reflect the moment-rotation properties of elements are assigned to both ends of columns and beams and the structure is pushed to failure under a lateral load arrangement generally reflecting the first mode shape of the frame.

The final type of analysis included in this work is the Single Degree of Freedom (SDOF) analysis of the frames. Multi Degree of Freedom (MDOF) frames are represented by SDOF systems which have equivalent dynamic properties. This was achieved by producing a bilinear representation of the capacity curve of the original MDOF structure. The time-history analyses of these simplified frames are carried out in order to approximately determine the response using the pushover curves.

This chapter presents the comparison of the results of the above stated procedures, namely; the time-history method and nonlinear static analysis along with the equivalent SDOF approximation.

2.2 DESCRIPTION OF SELECTED FRAMES

The six frames analyzed in this study are all reinforced concrete frames, possessing natural periods of vibration in the range 0.488-1.064 sec. Frames F2S2B, F5S4B, and F8S3B, were designed in California complying the Uniform

Building Code-1982 [16] whereas frames F4S3B, F5S2B, F5S7B are extracted from existing structures located in the city of Bursa in Turkey. Details like material properties, frame sections, dimensions, and reinforcements used are presented in Appendix A1. Free vibration analyses of these frames were conducted using the structural analysis programs SAP2000 [11] and DRAIN-2DX [20] and yielded identical results which are presented in Table 2.1.

Table 2.1 Dynamic Properties of Frames Selected

Frame	Mass (ton)	Period (T_1, sec)	Modal Participation Factor (Γ_1)	Modal Mass Factor (α_1)
F2S2B	275.255	0.488	1.336	0.834
F4S3B	195.125	0.838	1.249	0.828
F5S2B	260.171	0.615	1.285	0.808
F5S4B	1007.120	0.887	1.340	0.802
F5S7B	769.136	0.723	1.269	0.813
F8S3B	1816.070	1.064	1.409	0.727

2.3 SELECTED GROUND MOTIONS

Düzce (Bolu-Düzce, 12 November 1999, EW Component), El Centro (Imperial Valley, 18 May 1940, NS Component), Pacoima Dam (San Fernando, 9 February 1971, S16E Component), Parkfield (Parkfield, 27 June 1966, N65E Component [Chalome station]), El Centro 79a (Imperial Valley, 15 October 1979,140 Component), El Centro 79b (Imperial Valley, 15 October 1979, NS Component), Chi-Chi (Chi-Chi, Taiwan, 20 September 1999, 360 Component), Northridge-Pacoima (Northridge, 17 January 1994, 360 Component), Cape Mendocino (Cape Mendocino, 25 April 1992, 360 Component), and Northridge (Northridge, 17 January 1994, S00E) were the ground motion records used in this study. These ground motions, whose Peak Ground Accelerations vary within 0.319-1.17 g were selected to represent a broad range of differences in frequency, duration, and severity for the sake of coming up with a conclusion that can be generalized for common use. Table 2.2 summarizes the important features of these records. The earthquakes' acceleration-time histories are given in Figure 2.2 and their 5% damped elastic pseudo-acceleration response spectra are plotted in Figure 2.3.

These ground motions were scaled so that they strike the structure in the Immediate Occupancy-Life Safety performance states. After initially determining the capacity curve and limits of the performance states of the structure, the deformation levels are chosen so that one of them lies in the Immediate Occupancy range which also corresponds to the elastic range of the structure where no permanent damage occurs. The other five deformation levels are distributed along the Life Safety range as discussed in Section 2.1 and shown in Figure 2.4. Next the ground motion scale factors corresponding to these deformation levels were determined. This was achieved by SDOF analysis of the frames. The frames are converted to equivalent SDOF systems using the procedure that will be described in Section 2.6. Next the time-history analyses of these equivalent SDOF systems are performed and the peak ground acceleration of the earthquake is scaled until the peak roof displacement corresponding to the predetermined deformation level is reached. The results obtained are tabulated in Table 2.3.

Table 2.2 Features of Ground Motions Records

Rec. No	Record Name	Earthquake	Magnitude	Component	Site	PGA (g)	PGV (cm/s)	PGD (cm)
1	Düzce	Bolu-Düzce, 12/11/99	7.2	EW	Geomatrix or CWB (B) USGS ( )	0.513	86.1	170.12
2	Elcentro	Imperial Valley, 18/05/40	7.0	NS	Geomatrix or CWB (D) USGS (C)	0.319	29.8	13.32
3	Pacoima Dam	San Fernando, 09/02/1971	6.6	NS	Geomatrix or CWB (B) USGS ( )	1.170	54.3	11.73
4	Parkfield	Parkfield, 27/06/1966	6.1	N65E	Geomatrix or CWB (D) USGS (C)	0.476	75.1	22.49
5	El Centro 79a	Imperial Valley, 15/10/79	6.5	140	Geomatrix or CWB (D) USGS (C)	0.589	44.3	15.00
6	El Centro 79b	Imperial Valley, 15/10/79	6.5	NS	Geomatrix or CWB (D) USGS (C)	0.483	41.1	16.30
7	Chi-Chi	Chi-Chi, Taiwan, 20/09/99	7.6	360	Geomatrix or CWB (1) USGS (C)	0.359	42.1	16.40
8	Northridge-Pacoima	Northridge, 17/01/94	6.7	360	Geomatrix or CWB (A) USGS ( )	0.432	50.9	6.60
9	Cape Mendocino	Cape Mendocino, 25/04/92	7.0	360	Geomatrix or CWB (C) USGS (B)	0.549	42.6	13.40
10	Northridge	Northridge, 17/01/94	6.7	S00E	Geomatrix or CWB (D) USGS (C)	0.437	59.8	17.60

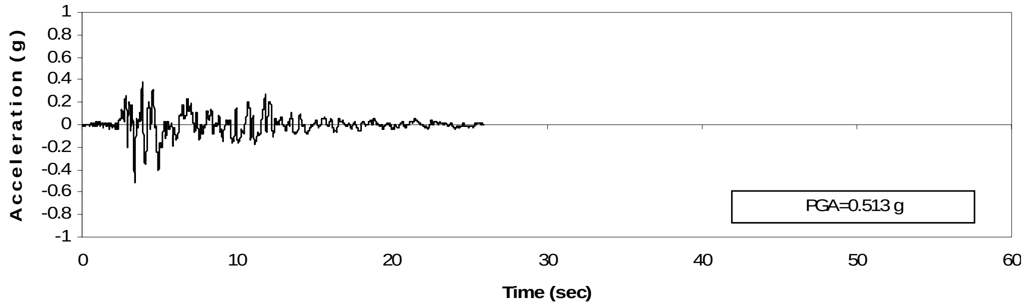

a) Düzce (Bolu-Düzce, 12 November 1999, EW Component)

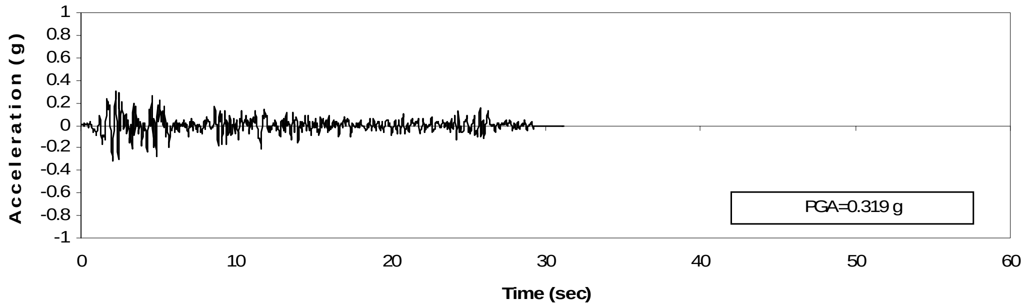

b) El Centro (Imperial Valley, 18 May 1940, NS Component)

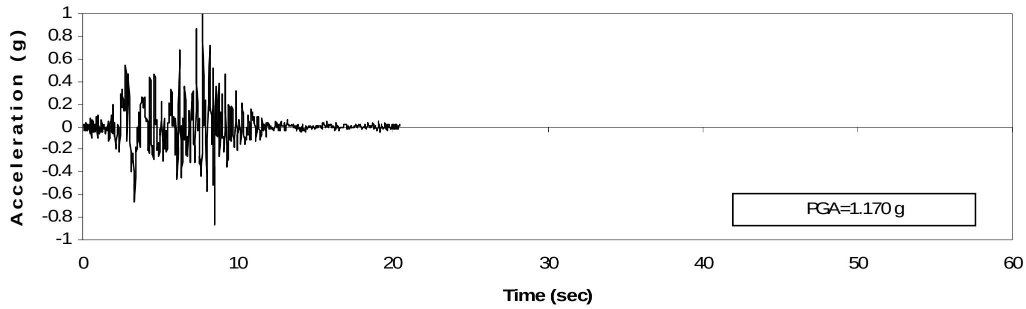

c) Pacoima Dam (San Fernando, 9 February 1971, S16E Component)

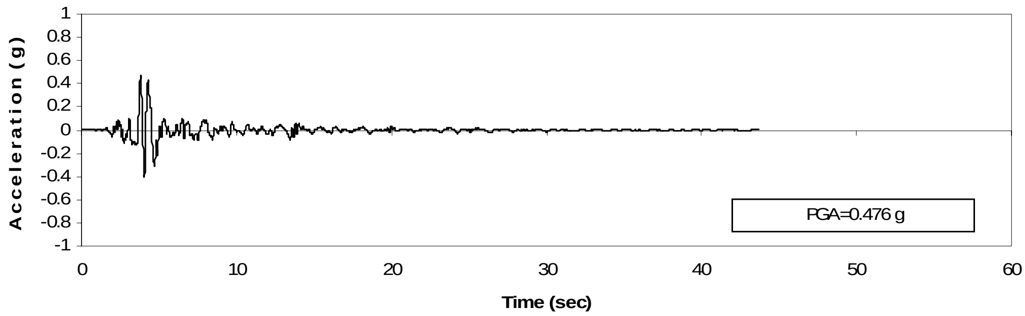

d) Parkfield (Parkfield, 27 June 1966, N65E Component)

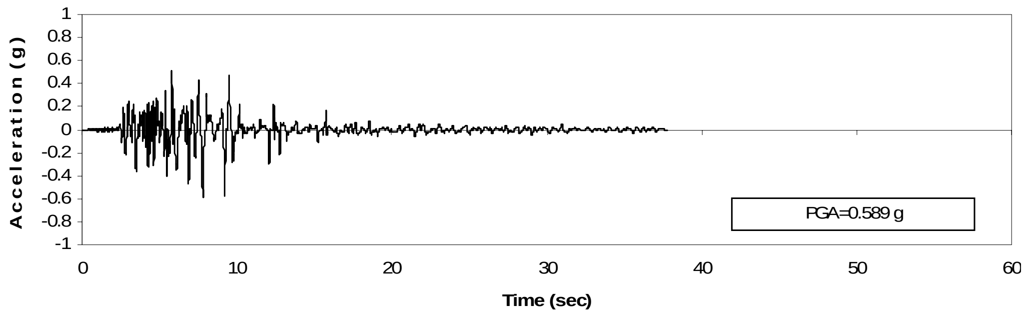

e) El Centro 79a (Imperial Valley, 15 October 1979, 140 Component)

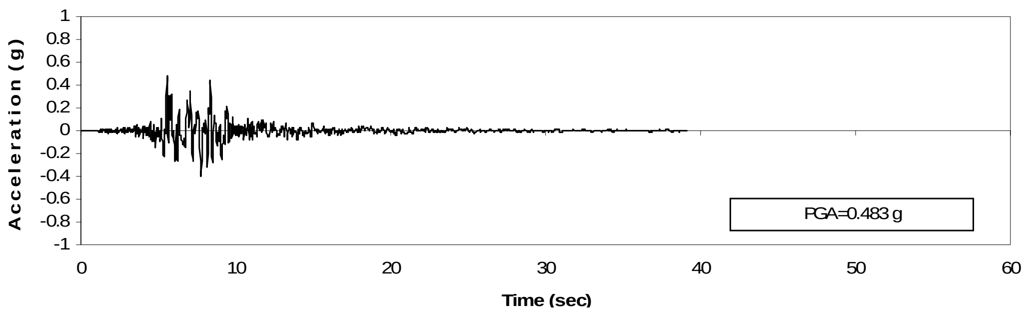

f) El Centro 79b (Imperial Valley, 15 October 1979, NS Component)

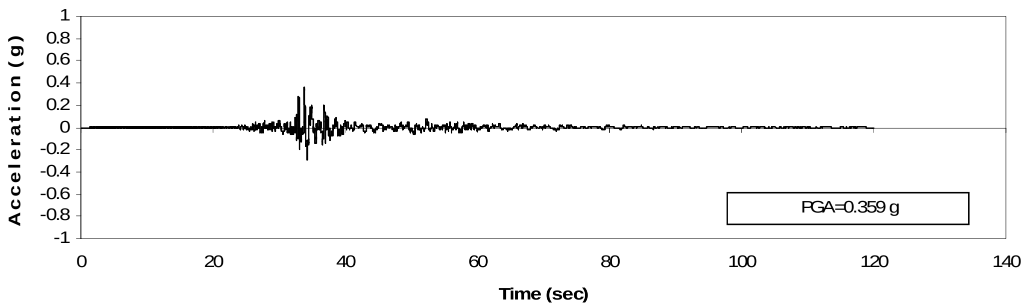

g) Chi-Chi (Chi-Chi, Taiwan, 20 September 1999, 360 Component)

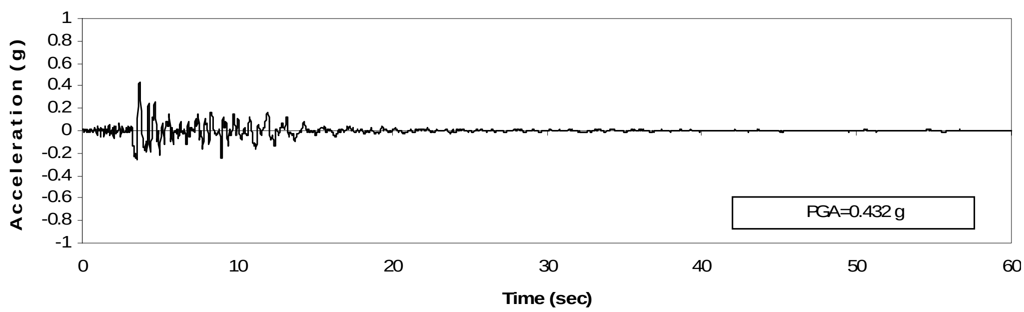

h) Northridge-Pacoima (Northridge, 17 January 1994, 360 Component)

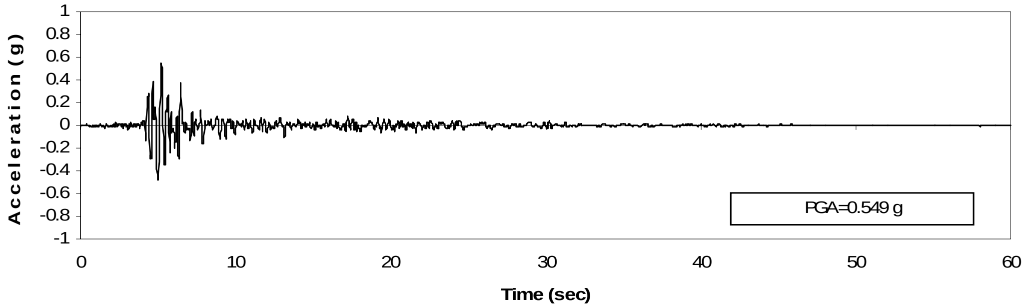

i) Cape Mendocino (Cape Mendocino, 25 April 1992, 360 Component)

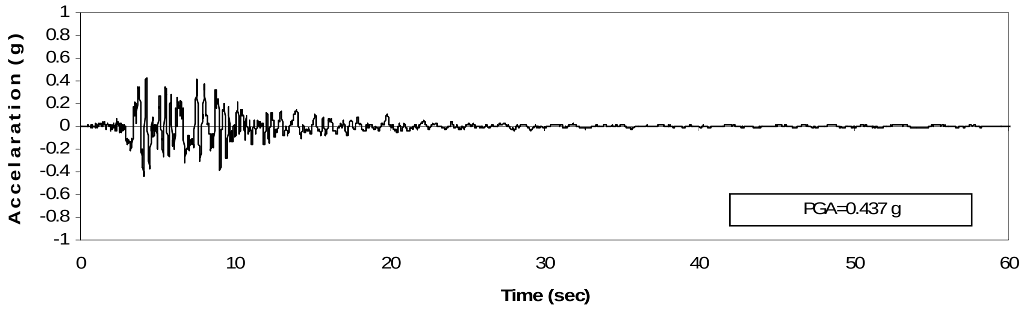

j) Northridge (Northridge, 17 January 1994, S00E)

Figure 2.2 Acceleration-Time Histories of Ground Motion Records

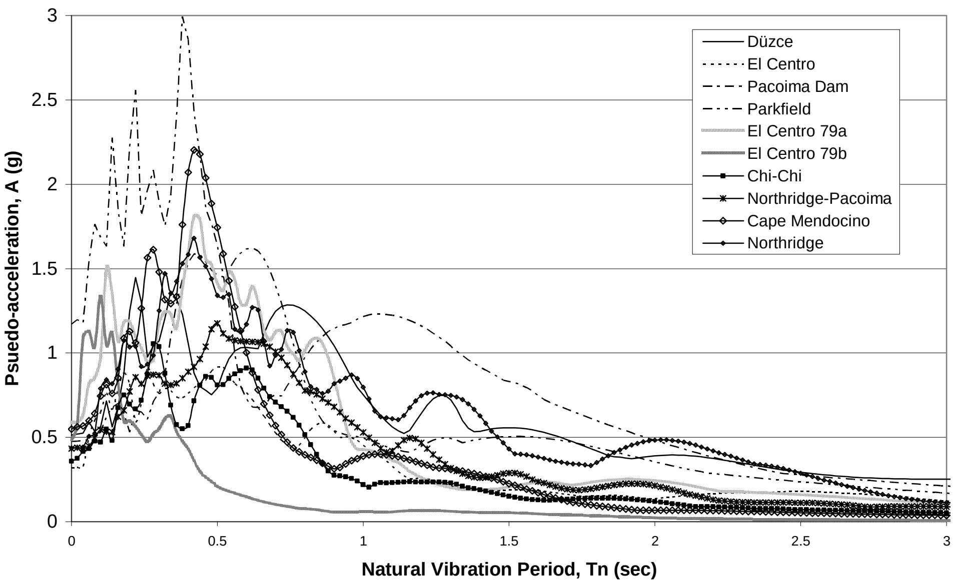

Figure 2.3 Pseudo-Acceleration Response Spectra of Ground Motions (5% Damped)

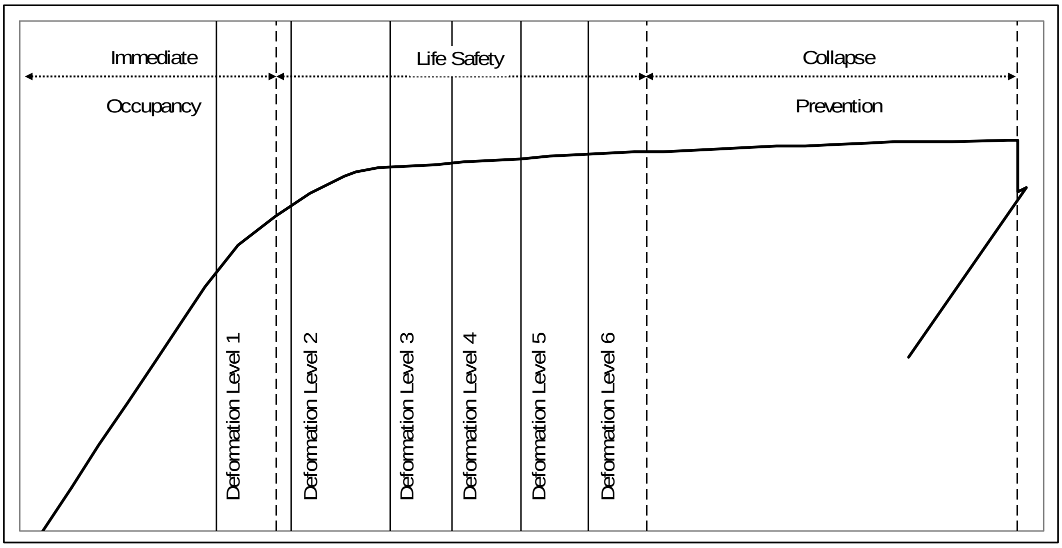

Figure 2.4 Deformation Levels

Table 2.3 Ground Motion Scale Factors Corresponding to the Deformation Levels Considered

Deformation Level	Düzce					
	F2S2B	F4S3B	F5S2B	F5S4B	F5S7B	F8S3B
I	0.34	0.04	0.26	0.27	0.19	0.31
II	0.51	0.07	0.39	0.38	0.33	0.44
III	0.69	0.26	0.56	0.65	0.43	0.80
IV	0.74	0.29	0.62	0.85	0.53	0.83
V	0.84	0.41	0.78	1.10	0.80	0.97
VI	0.87	0.45	0.82	1.35	0.86	1.02
Deformation Level	El Centro					
	F2S2B	F4S3B	F5S2B	F5S4B	F5S7B	F8S3B
I	0.35	0.08	0.37	0.50	0.52	0.50
II	0.52	0.16	0.55	0.70	0.91	0.71
III	0.70	0.31	1.08	1.20	1.13	1.50
IV	0.75	0.39	1.15	1.35	1.53	1.60
V	1.28	0.81	1.86	2.00	1.84	2.13
VI	1.35	1.01	2.15	2.30	1.92	2.39
Deformation Level	Pacoima Dam					
	F2S2B	F4S3B	F5S2B	F5S4B	F5S7B	F8S3B
I	0.23	0.05	0.41	0.25	0.31	0.16
II	0.35	0.08	0.56	0.35	0.55	0.22
III	0.58	0.18	0.71	0.50	0.71	0.37
IV	0.63	0.20	0.74	0.52	0.81	0.40
V	0.74	0.27	0.88	0.68	0.96	0.75
VI	0.79	0.30	0.90	0.72	0.99	0.98

Table 2.3 Continued

Deformation Level	Parkfield					
	F2S2B	F4S3B	F5S2B	F5S4B	F5S7B	F8S3B
I	0.21	0.07	0.17	0.50	0.20	0.42
II	0.32	0.13	0.24	0.75	0.34	0.60
III	0.40	0.24	0.57	1.03	0.44	1.00
IV	0.43	0.28	0.61	1.10	0.62	1.04
V	0.76	0.43	0.76	1.39	0.79	1.44
VI	0.81	0.48	0.80	1.45	0.84	1.55
Deformation Level	El Centro 79a					
	F2S2B	F4S3B	F5S2B	F5S4B	F5S7B	F8S3B
I	0.22	0.04	0.20	0.31	0.22	0.50
II	0.33	0.08	0.30	0.44	0.38	0.69
III	0.41	0.42	0.59	0.98	0.53	1.02
IV	0.44	0.46	0.63	1.02	0.75	1.54
V	0.52	0.73	0.78	1.21	1.05	2.22
VI	0.55	0.84	0.81	1.29	1.10	2.43
Deformation Level	El Centro 79b					
	F2S2B	F4S3B	F5S2B	F5S4B	F5S7B	F8S3B
I	0.29	0.08	0.28	0.52	0.40	0.42
II	0.44	0.14	0.44	0.73	0.71	0.59
III	0.54	0.31	0.99	1.40	0.92	1.01
IV	0.58	0.32	1.05	1.47	1.05	1.07
V	1.01	0.43	1.24	1.80	1.64	1.26
VI	1.05	0.46	1.29	1.85	1.71	1.38
Deformation Level	Chi-Chi					
	F2S2B	F4S3B	F5S2B	F5S4B	F5S7B	F8S3B
I	0.41	0.06	0.50	0.34	0.28	0.25
II	0.60	0.11	0.71	0.47	0.50	0.35
III	0.73	0.38	0.90	0.67	0.64	0.95
IV	0.77	0.44	0.95	1.05	0.74	1.01
V	0.93	0.78	1.54	1.43	1.35	2.18
VI	1.03	0.89	1.59	1.68	1.46	2.40
Deformation Level	Northridge-Pacoima					
	F2S2B	F4S3B	F5S2B	F5S4B	F5S7B	F8S3B
I	0.29	0.06	0.26	0.42	0.26	0.44
II	0.43	0.12	0.42	0.61	0.44	0.63
III	0.58	0.27	0.63	0.82	0.58	0.94
IV	0.62	0.47	0.68	0.86	0.75	0.98
V	0.76	0.81	0.84	1.08	0.96	1.83
VI	0.80	0.93	0.89	1.14	1.01	1.97
Deformation Level	Cape Mendocino					
	F2S2B	F4S3B	F5S2B	F5S4B	F5S7B	F8S3B
I	0.21	0.13	0.30	0.90	0.49	0.48
II	0.31	0.27	0.44	1.26	0.86	0.69
III	0.38	0.53	0.86	1.78	1.12	1.37
IV	0.41	0.57	1.10	1.89	1.53	1.44
V	0.69	0.89	1.40	2.92	2.02	1.84
VI	0.73	1.00	1.51	3.01	2.15	2.02

Table 2.3 Continued

Deformation Level	Northridge					
	F2S2B	F4S3B	F5S2B	F5S4B	F5S7B	F8S3B
I	0.23	0.06	0.22	0.37	0.22	0.32
II	0.35	0.10	0.39	0.52	0.39	0.44
III	0.56	0.23	0.82	0.65	0.51	0.58
IV	0.60	0.25	0.87	0.70	0.64	0.67
V	0.83	0.35	1.05	1.17	0.73	0.97
VI	0.98	0.39	1.33	1.23	0.78	1.08

2.1 NONLINEAR TIME HISTORY ANALYSIS

The nonlinear time-history analyses of the frames were conducted by utilizing the software DRAIN-2DX [20]. The following sections describe the modeling rules, assumptions, and the procedure followed.

2.1.1 Assumptions and Modeling

The frames are composed of elements that can simulate nonlinear behavior at the nodes. The columns at the ground floor were assumed to be rigidly connected to the foundations. In order to take into consideration the behavior of the slabs, all joints at the same story level were constrained to move together as a planar diaphragm that is rigid against in plane membrane deformations. Beams and columns were modeled as massless elements and the mass of each story, considering dead loads and 25% of live loads, was lumped at the mass center of that story. Element Type 02 of the DRAIN-2DX [19] element library was used in order to represent the beam and columns of the frames. This element consists of an elastic beam and rigid-plastic hinges at both sides of this beam where the yielding occurs. The modulus of elasticity, area, moment of inertia, flexural stiffness coefficients, shear areas and poisson ratios are used to define the attributes of each element. The hinge properties of elements are also characterized by various parameters.

Column elements' hinge properties are identified by a shape code 3 [19] shown in Figure 2.5, which requires positive (M_y^+) and negative (M_y^-) yield moments, compression (P_{yc}) and tension (P_{yt}) yield forces, the ratio of maximum moment to the yield moment in both positive (M_A/M_y^+) and negative (M_B/M_y^-) moment regions of the M-N interaction curve of the column as well as the ratio of axial forces at the same points to the compressive yield force [(P_A/P_{yc}), (P_B/P_{yc})] to be identified. In the case of beam elements it is sufficient to identify the positive (M_y^+) and negative (M_y^-) yield moments of the elements.

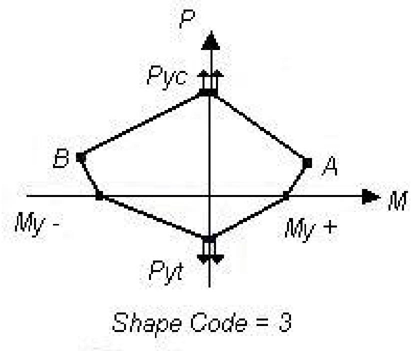

Figure 2.5 Shape Code 3

The interaction diagrams required to establish these hinge properties were calculated by making use of the software RESPONSE-2000 [8]. The concrete model defined in this program does not take into consideration confinement effects which are neglected as well in this study

DRAIN-2DX [20] permits the specification of a viscous damping matrix which is proportional to element stiffness and masses. This introduces a damping matrix of the form;

$$C=\alpha M+\beta K \qquad 2\text{-}1$$

Where,C: damping matrix

M: mass matrix

K: stiffness matrix

For the calculation of the coefficients α and β, which are the mass and stiffness proportional damping coefficients respectively, the following assumptions were made; in the analysis of the frame F2S2B the damping ratios of the first two modes were assumed to be 5%. For the four and five story frames the damping ratios of the first and third modes, and for the eight story frame that for the first and fifth modes were equated to 5%. By equating the damping ratios as described above, the mentioned coefficients can be calculated as follows;

$$\alpha=\zeta\frac{2\omega_i\omega_j}{\omega_i+\omega_j} \qquad 2\text{-}2$$

$$\beta=\zeta\frac{2}{\omega_i+\omega_j} \qquad 2\text{-}3$$

Where,

i, j: indices indicating the modes whose damping ratios are equated

ζ=0.05: damping ratio

ω: natural frequency of vibration

2.4.2 Analyses of Undamaged Structure

Some parameters included in the time-history analysis require the natural frequency of the structure to be analyzed therefore a modal analysis has to be performed initially. After the definition of the geometry, the hinge properties of each element are identified. The axial load on columns is assumed to be constant and assigned a value computed from the vertical loading for all columns. This assumption leads to a unique hinge property for all columns with the same section properties in the structure. The interaction diagram obtained for columns has to be approximated by a tri-linear curve in line with the shape code 3 definition of DRAIN-2DX [20]. The conversion of the M-N Interaction obtained by the software RESPONSE-2000 is displayed in Figure 2.6.

Time-history analyses were performed for each of the six scales of the above given ten earthquakes. Then the output data was processed to filter out the maximum top displacement and base shear force occurring under each loading. The results are presented in Appendix A2.

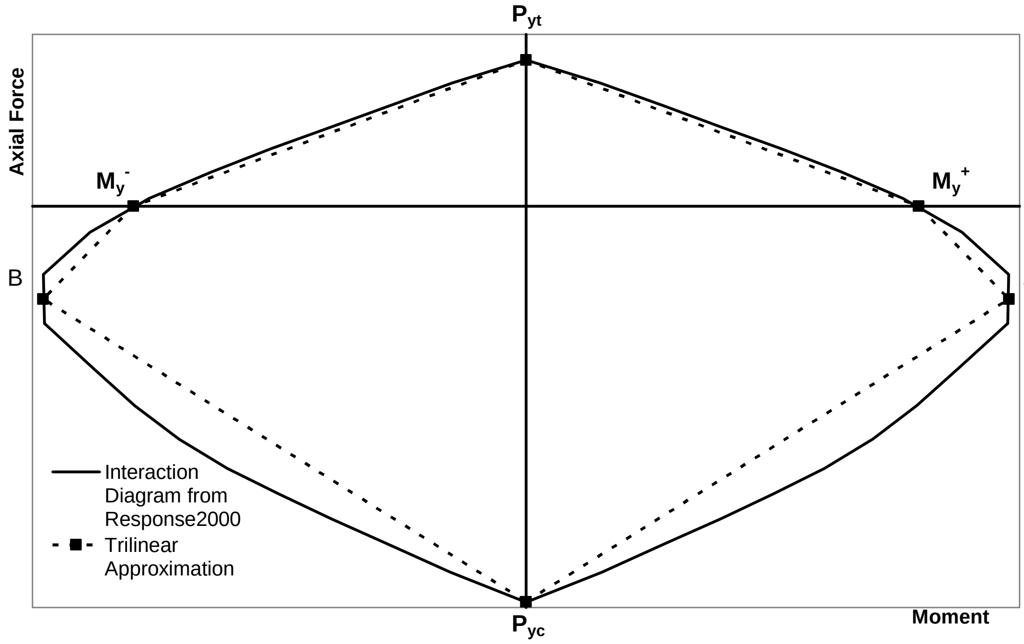

Figure 2.6 M-N Interaction and Tri-linear Approximation

2.5 NONLINEAR STATIC ANALYSES

The nonlinear time-history analysis described in the previous section is considered overly complex and impractical for general use. This is due to its high computation costs which result from the long computation time and large output data which have to be processed. To overcome these disadvantages, available simplified nonlinear analysis methods referred to as nonlinear static analysis procedures are usually preferred for the nonlinear analysis of structures. The following paragraphs present the nonlinear static analyses of the above evaluated frames and comparisons of the results with the time-history analyses to test the reliability of such simplified analysis procedures.

2.5.1 Assumptions and Modeling

The nonlinear static analyses of the frames were performed using the software DRAIN-2DX [20] and SAP2000 [11] to make sure that both software provide consistent results. A main disadvantage of DRAIN-2DX is that the deformability limits of individual elements cannot be defined. Therefore the pushover curve obtained from this software does not produce an ultimate deformation at which the structure fails. That is, the pushover curve extends up to very large displacement values, which cannot be correct. SAP2000 on the other hand allows the definition of a load-deformation relation as shown in Figure 2.7 for all individual elements.

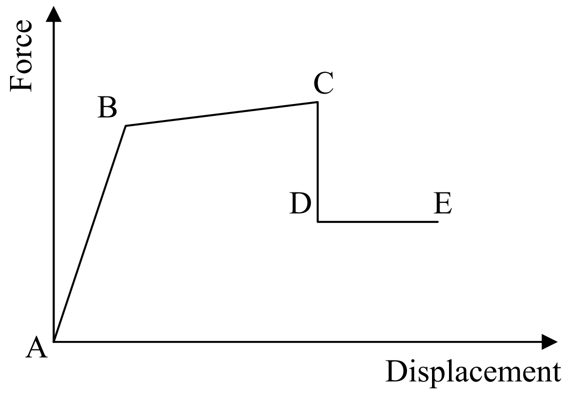

Figure 2.7: Generalized Load-Deformation Relation for beams and columns

This relation is described by linear response from A (unloaded element) to an effective yield B. Subsequently, there is linear response, at reduced stiffness from B to C, with sudden reduction in lateral load resistance to D, response at reduced resistance to E, and final loss of resistance thereafter [13]. The force-displacement relation for all beams and columns are determined from their corresponding moment-curvature relations, which were evaluated through the utilization of the software RESPONSE2000 [8]. The section and material properties given in Section 2.2 and Appendix A1 were used for this purpose. Although the axial force in columns is not constant throughout the analysis, a constant axial load level equal to the axial load occurring due to dead load and 25% of live load was assumed for the determination of the moment-curvature relation. Axial forces on beams on the other hand were taken to be zero. These assumptions are valid for both DRAIN-2DX [20] and SAP2000 [11] solutions.

In order to convert the moment-curvature relation to moment-rotation, it was assumed that the member is in symmetrical double curvature. This procedure was used by Saidii and Sozen [21] and Park and Paulay [17]. Although this is not exactly correct for all members in the structure it is a reasonable approximation. For this condition, elastic theory shows that the end rotation is;

$$\theta=\frac{M\,L}{6\,EI} \qquad 2\text{-}4$$

where L : Member length

EI : Flexural rigidity of section

When yield is just reached at the ends, $\theta = \theta_y$ and $M = M_y$,

where M_y : Moment at first yield

The yield curvature is; $\varphi_y=\frac{M_y}{EI}$ 2-5

$$\therefore\ \theta_y=\frac{\varphi_y\,L}{6} \qquad 2\text{-}6$$

where θ_y : Rotation at yield

φ_y : Curvature at yield

Further rotation at the ends of the member will impose plastic rotation θ_P, which can be calculated by the following equation;

$$\theta_P=\left(\varphi_u-\varphi_y\right)l_P \qquad 2\text{-}7$$

where θ_P : Plastic rotation

φ_u : Curvature at ultimate moment

l_P : Equivalent plastic hinge length

Finally the rotation occurring at the ultimate moment is calculated by adding the rotation at yield and the plastic rotation. That is;

$$\theta_u= \theta_y+\theta_P \qquad 2\text{-}8$$

There are several empirical expressions proposed for the equivalent plastic hinge length (l_P) but in this study l_P was assumed to be equal to the depth (d) of the member under consideration. [17]

With the definitions made above, the moment rotation relationships for beam and column elements are defined as shown in Figure 2.8.

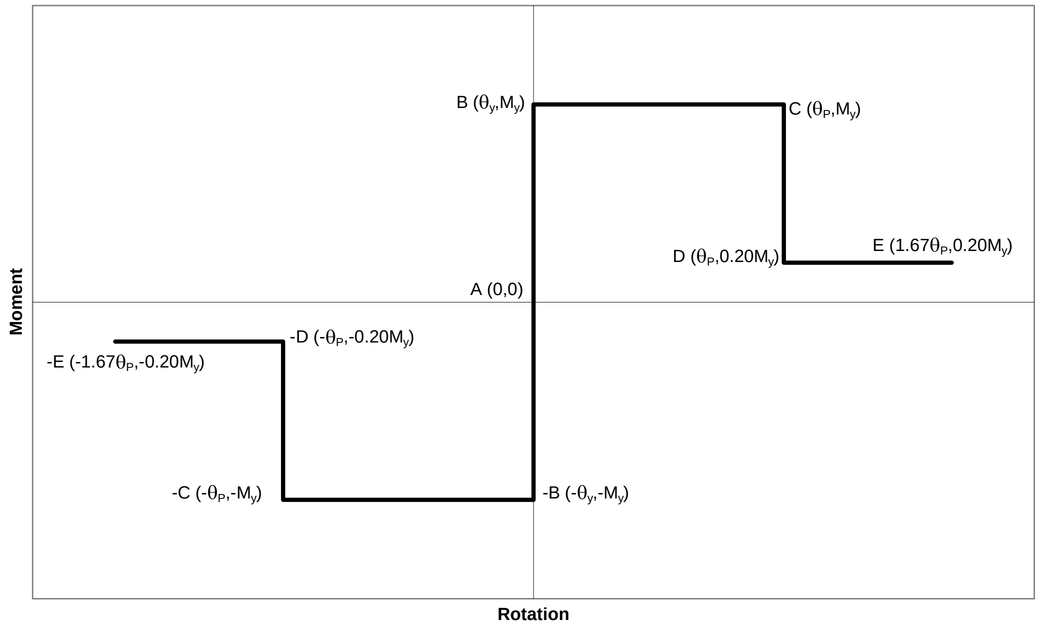

Figure 2.8: Load-Deformation Relation for beams and columns

The software SAP2000 [11] does not take into consideration the rotation at yield (θ_y) of the element; therefore it is input as zero in the definition of the hinge properties. The rotation occurring at point C, which is the point of ultimate moment, thus becomes equal to the plastic rotation. The residual strength ratio at point D and the final rotation value at point E are average values taken from ATC-40 [2]. Strain hardening between the segment from B to C is ignored hence this line segment is parallel to the rotation axis.

For elements with symmetrical cross-sections the moment-rotation relation will also be symmetrical. Sections with unsymmetrical cross-sections, which are usually the case for beams, on the other hand, exhibit unsymmetrical moment rotation relations therefore an analysis considering both positive and negative moments has to be performed for them.

The capacity curve is generally constructed to represent the first mode response of the structure based on the assumption that the fundamental mode of vibration is the predominant response of the structure. This is generally valid for regular buildings with fundamental periods of vibration up to one second, and since the frames analyzed satisfy this constraint the lateral forces (F_x) are applied in proportion to the product of story masses and first mode shape of the elastic model of the structure. That is for the base shear, V;

$$F_x = \left[\frac{m_x \phi_x}{\sum m_x \phi_x} \right] V \qquad \text{2-9}$$

2.5.2 Results

Pushover curves obtained for each frame using DRAIN-2DX and SAP2000 (Figure 2.9), revealed similar results indicating that these software are comparable. It has been observed that any of these two software can be used for pushover analyses provided that hinge properties defined are the same. Since SAP2000 is able to take into account the limit deformation values for each component of the structure it has been used for further pushover analyses.

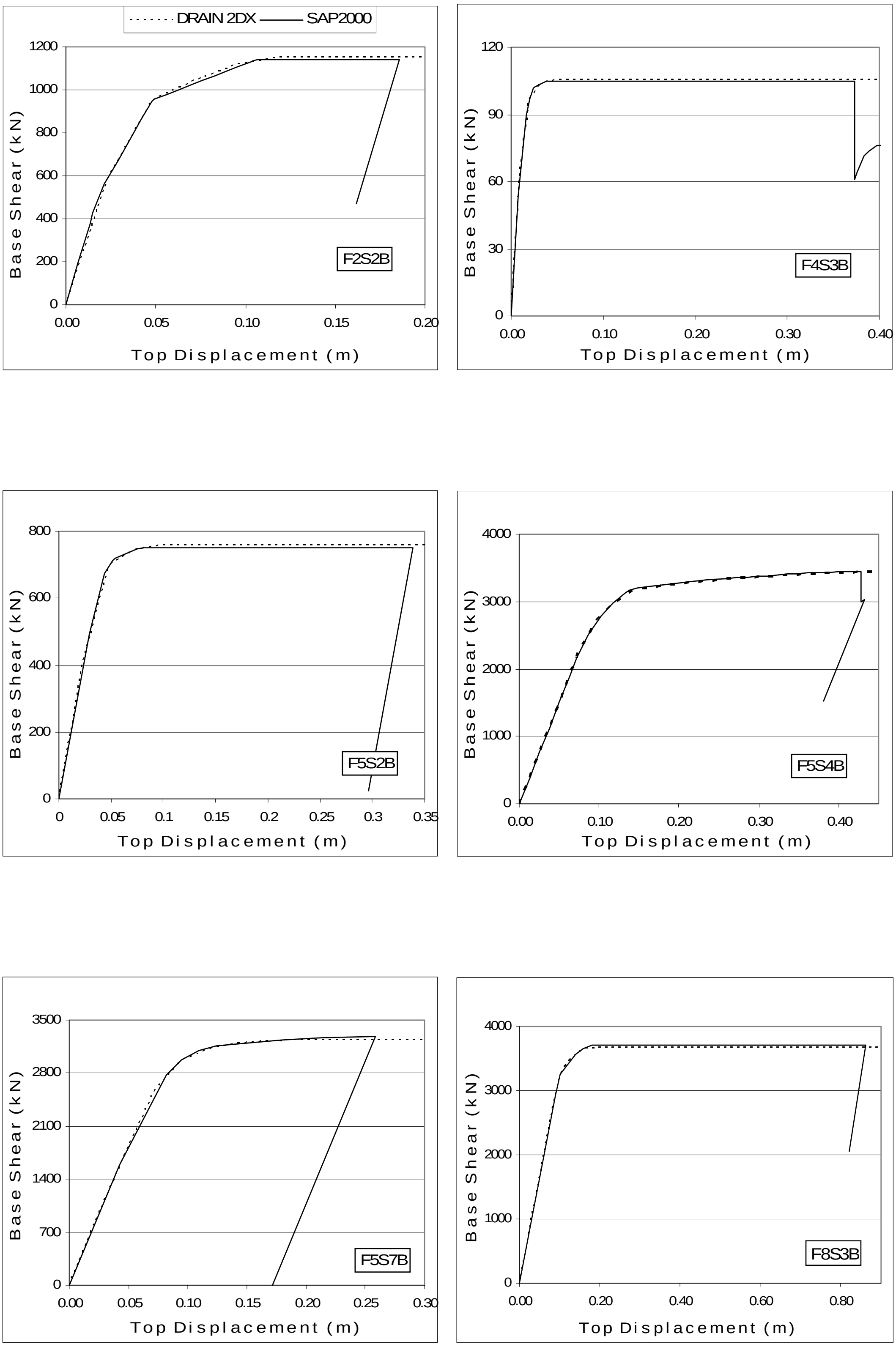

Figure 2.9: Capacity Curves of Frames

The pushover analysis procedure is capable of predicting the location of weak points and potential failure modes that the structure would experience in case of a seismic event. This is achieved by the determination of the hinge locations, by which the failure mechanism of the structure can be identified. The locations of plastic hinges for frames F4S3B and F5S4B corresponding to deformation levels 1, 2, 4, and 6 are presented in Figure 2.10 and 2.11 respectively. From these figures it can be visualized that hinging starts at the lower and middle story beams and then shifts to the ground story columns. This type of hinging mechanism corresponds to a mixed failure mechanism. The behavior of the other frames under consideration was observed to be similar therefore they were not illustrated in this study.

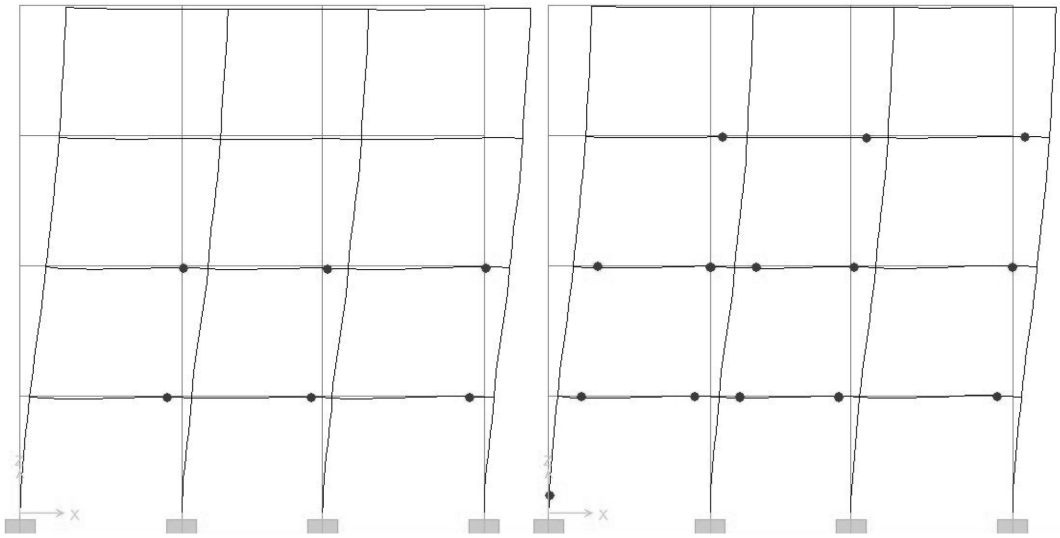

a) Deformation Level 1 b) Deformation Level 2

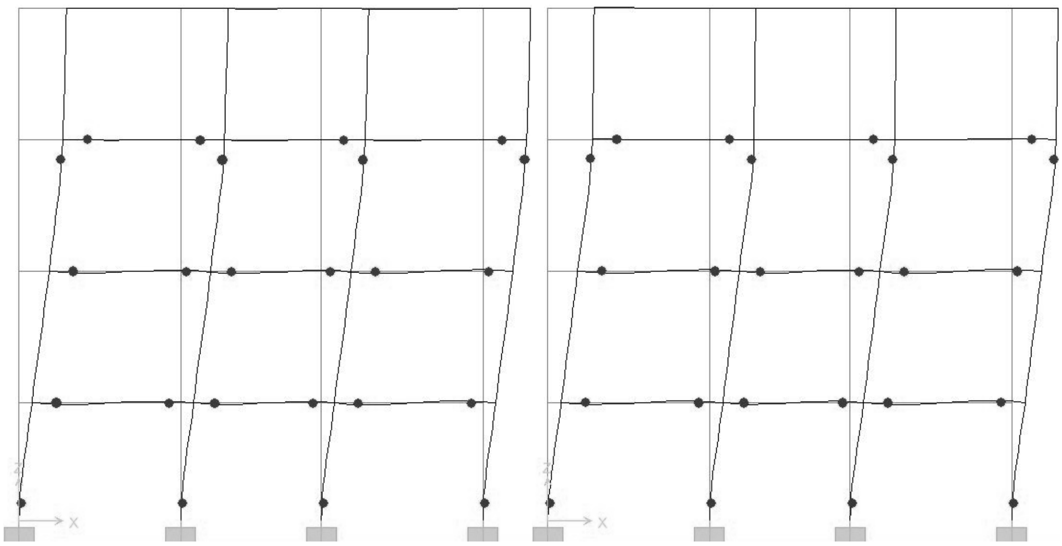

a) Deformation Level 4 b) Deformation Level 6

Figure 2.10: Hinge Patterns for F4S3B

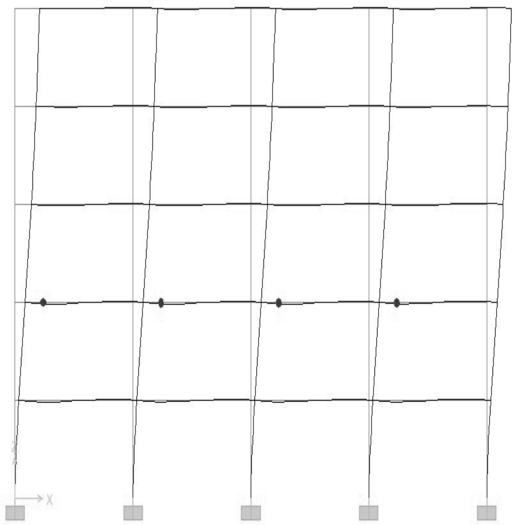

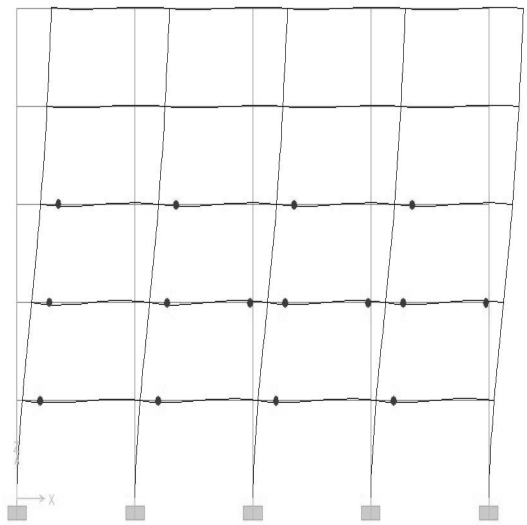

a) Deformation Level 1 b) Deformation Level 2

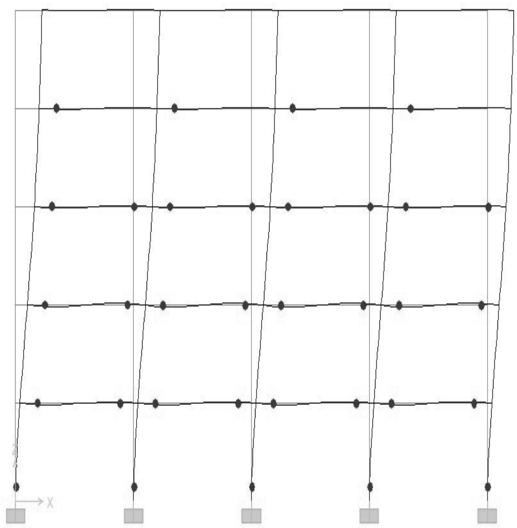

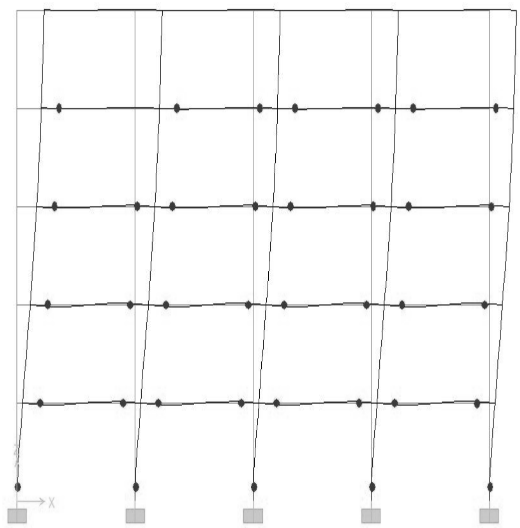

a) Deformation Level 4 b) Deformation Level 6

Figure 2.11: Hinge Patterns for F5S4B

2.6 SINGLE DEGREE OF FREEDOM ANALYSES

It is possible to characterize each mode of a Multi Degree of Freedom (MDOF) system by an equivalent Single Degree of Freedom (SDOF) system [2], [10]. This procedure is a commonly used practice in order to determine the performance point of structures. In this method the original structure, which is a MDOF system is converted into a SDOF system and the time-history analysis of this simplified system is performed in order to calculate the maximum displacement that this structure will suffer. The equivalent SDOF system possesses a mass M^* and stiffness K^*, which are functions of the mode shape, mass, and stiffness of the original structure. All the frames analyzed in this study have natural periods of vibration up to one second, therefore as previously discussed; the fundamental mode of vibration is the predominant response of these structures. Consequently the equivalent SDOF system is constructed for the fundamental mode shape corresponding to each frame. With these considerations the equivalent SDOF system will have a period of

$$T_n = 2\pi\sqrt{\frac{M^*}{K^*}} \qquad 2\text{-}10$$

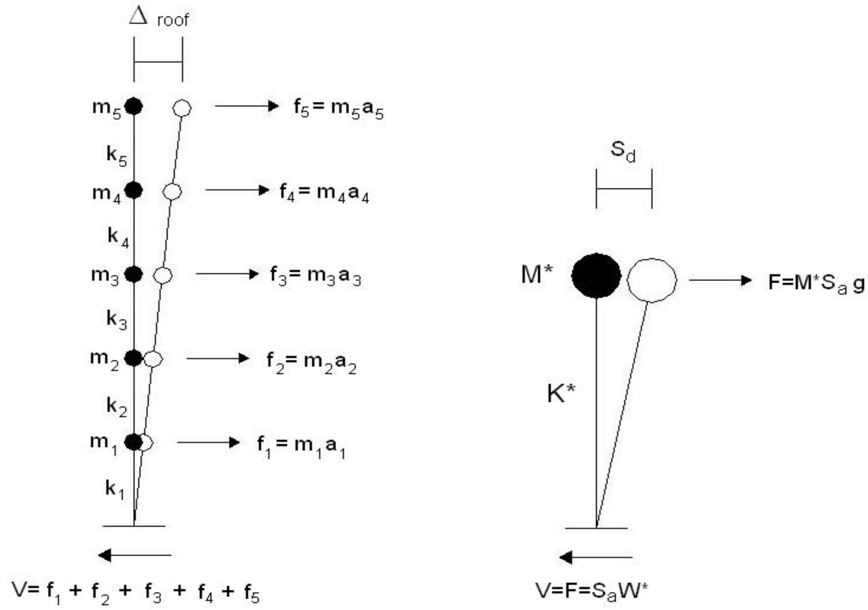

Figure 2.12: MDOF System Represented by a SDOF System

Figure 2.12 shows the computational basis for converting a MDOF System into a SDOF System. Both systems in the figure are equivalent; that is if during an earthquake the mass M^* moves a distance S_d, the top story of the original building will undergo a displacement of Δ_{roof}. The ratio of Δ_{roof} to S_d is used here as the modal participation factor (Γ_1) for the fundamental mode. This factor implies a measure of the degree to which the fundamental mode participates in the response. The modal participation factor for the fundamental mode is analytically defined as;

$$\Gamma_1 = \frac{\sum_{i=1}^{N} m_i \phi_i}{\sum_{i=1}^{N} m_i \phi_i^2} \phi_{1\,roof} \qquad 2\text{-}11$$

and

$$\Delta_{roof} = \Gamma_1\ S_d \qquad 2\text{-}12$$

where, N: number of stories

m_i: mass of story i

ϕ_i: mode shape for fundamental mode at story i

$\phi_{1\,roof}$: mode shape for fundamental mode at roof story

M^*, as stated above is the effective mass of the equivalent SDOF system. The values M and M^* are related to each other by a coefficient α_1, which is termed as the Effective Mass Coefficient for the fundamental mode of vibration and defined as;

$$\alpha_1 = \frac{\left[\sum_{i=1}^{N} m_i \phi_i\right]^2}{\left[\sum_{i=1}^{N} m_i\right]\left[\sum_{i=1}^{N} m_i \phi_i^2\right]} \qquad 2\text{-}13$$

and

$$M^* = \alpha_1\ M \qquad 2\text{-}14$$

where, $M = \sum_{i=1}^{N} m_i$: total mass of structure

2.6.1 Equivalent SDOF System Representation of Selected Frames

In this section, the procedure used to determine the equivalent SDOF of the corresponding frames will be described. For this purpose the previously determined capacity curves are used. At first, the capacity curve has to be converted into a capacity spectrum whose abscissa is the spectral displacement (S_d) and ordinate is the spectral acceleration (S_a). In order to develop the capacity spectrum from the capacity curve, it is necessary to do a point to point conversion to first mode spectral coordinates. Every top displacement - base shear (Δ_i, V_i) pair on the capacity curve is converted to their corresponding points (S_d, S_a) on the capacity spectrum with the aid of the following equations;

$$S_{d\,i} = \frac{\Delta_{roof\,i}}{\Gamma_1} \qquad \text{2-15}$$

$$S_{a\,i} = \frac{V_i / W}{\alpha_1} \qquad \text{2-16}$$

After this conversion, the next step is to approximate the capacity curve by a bilinear representation. There are various methods used for this purpose among which, the FEMA 273 Approach [13], Initial Stiffness Approach [2], and Major Yield Approach are the most widely used ones. These approaches are going to be discussed in detail in the following section. The bilinear representation method used in this study is the FEMA 273 Approach therefore the main features of this method will be discussed next.

The bilinear capacity curve, as its name suggests is comprised of two line segments and four points with the help of which these lines are constructed. Two of these points; the origin (0, 0) and the ultimate point (Δ_{ult}, V_{ult}) are fixed. The ultimate point defines the point at which the structure fails. The next step is to identify the yield point such that the summation of the areas lying below and above the original curve are equal meanwhile the point corresponding to a base shear of 0.6 V_y should intersect the original pushover curve. Figure 2.13 shows the construction of the bilinear representation of the capacity curve graphically. As can be observed from this figure, the first line segment of the bilinear curve extends from the origin to the yield point and the second one from the yield point to the ultimate point. The point corresponding to 0.6 V_y intersects the original curve and the summation of A_1 and A_3 is approximately equal to A_2.

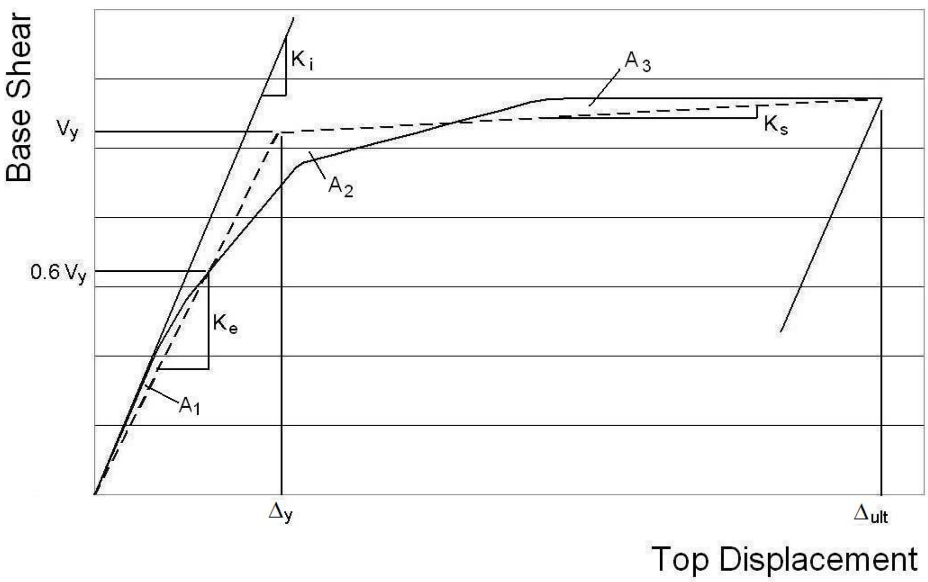

Figure 2.13: Bilinear Representation of Capacity Curve

Equations 2-15 and 2-16 are used to calculate the spectral coordinates of these four points in order to determine the bilinear capacity spectrum. The effective natural frequency and period, which are the dynamic properties of the equivalent SDOF system, are computed by the following formulae;

$$\omega_{eff} = \sqrt{\frac{S_a g}{S_d}} \qquad 2\text{-}17$$

$$T_{eff} = \frac{2\pi}{\omega_{eff}} \qquad 2\text{-}18$$

M^*, the effective mass of the equivalent SDOF System, is calculated through Equation 2-14 presented in the previous section. The effective stiffness (K^*), which will be equal to the initial stiffness of the equivalent SDOF system (K_1), can be calculated through the basic structural dynamics equation presented below;

$$\omega = \sqrt{\frac{K}{M}} \text{ and } K_1 = K^* = \omega^2 M^* \qquad 2\text{-}19$$

The ratio of the post elastic stiffness (K_s) to the elastic stiffness (K_e) of the bilinear capacity curve ($\frac{K_s}{K_e}$) will also be preserved in the equivalent SDOF system, therefore K_2, the secondary or yielding stiffness is calculated as below;

$$K_2 = K_1 \frac{K_s}{K_e} \quad \text{2-20}$$

After all these calculations, the force-displacement characteristics of the equivalent SDOF system turn out to be as presented in Figure 2.14.

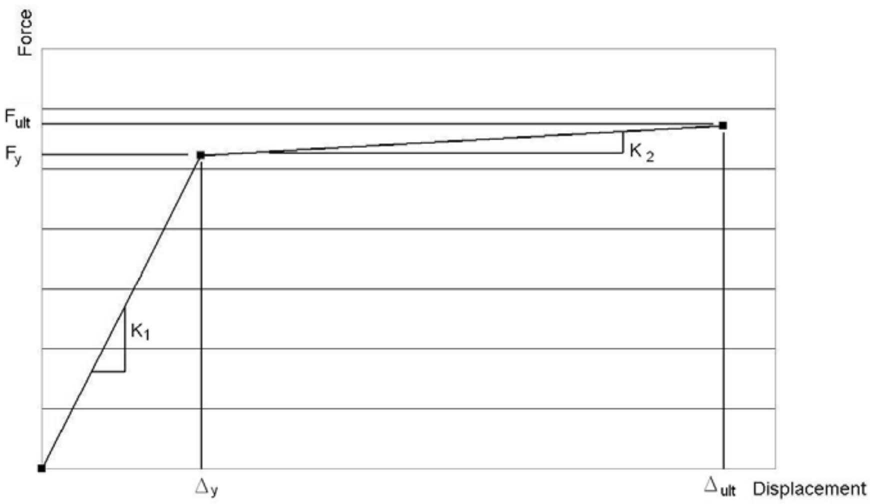

Figure 2.14: Force Deformation Characteristics of SDOF System

The software NONLIN [9] was used to perform the time-history analyses of the SDOF systems. The attributes of the systems that have to be input to the software are; mass, damping, initial stiffness of the system, secondary stiffness, yield strength, and finally the ground acceleration record.

NONLIN [9] calculates the maximum displacement of the SDOF system; therefore it has to be modified in order to determine the displacement of the original MDOF system. This is achieved by multiplying the displacement of the SDOF system by the modal participation factor for the fundamental mode (Γ_1);

$$\Delta_{MDOF} = \Delta_{SDOF} \times \Gamma_1 \quad \text{2-21}$$

Finally the base shear corresponding to this displacement value is determined through interpolation on the bilinear pushover curve.

Force Displacement Relationships employed for the SDOF representation of the frames analyzed are given in Table 2.4

Table 2.4 Force Displacement Relationships of SDOF System Representations of Frames Analyzed

Frame	T_{eff} (sec)	M* (ton)	K_1 (kN/m)	K_2 (kN/m)	F_y (kN)	Γ_1	α_1
F2S2B	0.531	229.57	32172.90	912.62	1045.00	1.3362	0.8340
F4S3B	0.841	161.59	9014.58	5.43	103.20	1.2491	0.8281
F5S2B	0.618	210.24	21756.65	74.65	735.00	1.2847	0.8081
F5S4B	0.884	807.65	40771.82	1303.95	3131.00	1.3400	0.8019
F5S7B	0.729	625.21	46447.13	1771.28	3038.00	1.2690	0.8129
F8S3B	1.059	1319.62	46411.72	108.73	3656.00	1.4091	0.7266

2.6.2 Idealization of Pushover Curves

There are various methods used for the aid of converting the pushover curve into a bilinear model. The most widely used three methods for this idealization include the FEMA Method [13], the Initial Stiffness Procedure [2], and the Major Yield Method. It has been observed from the bilinear approximations of the frames that for all frames except Frame “F2S2B”, the FEMA Method and the Initial Stiffness Procedure produce the same bilinear capacity curve. Therefore, this is a good opportunity to test the consistency of the FEMA Method used throughout the analysis of this study. The main features of the FEMA Method were outlined in the previous section; hence it is not going to be repeated at this point.

In the Initial Stiffness Procedure, the bilinear capacity curve is formed such that the elastic portion of the idealized curve is congruent with the initial stiffness of the original curve. The Major Yield idealization on the other hand is made such that the elastic portion of the bilinear curve passes through the major yield point of the original capacity curve. The consideration of the FEMA approach that, the summation of the areas below and above the original curve are equal is also valid for these two methods. Calculations of parameters like the natural frequency and period of vibration, effective mass, and initial and secondary stiffness are carried out as well in a similar fashion as done in the FEMA method. Figure 2.15 compares the idealization methods for frame F2S2B graphically and the calculated parameters are given in Table 2.5.

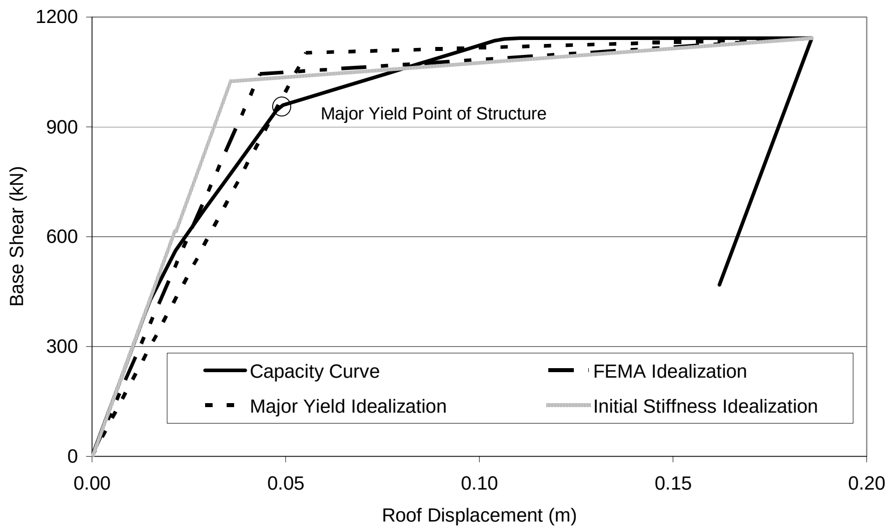

Figure 2.15: Comparison of Idealization Methods for Frame F2S2B

Table 2.5 Comparison of Force Displacement Relationships of Idealization Methods for Frame 2S2B

Idealization Method	T_{eff} (sec)	M* (ton)	K_1 (kN/m)	K_2 (kN/m)	F_y (kN)
FEMA	0.531	229.57	32172.90	912.62	1045.00
Major Yield	0.583	229.57	26626.87	412.22	1102.00
Initial Stiffness	0.488	229.57	38006.79	1054.85	1024.00

The SDOF analyses results of frame F2S2B using these idealization methods are presented in Appendix A3.

In Table 2.6 these three methods are compared in terms of percentage errors with relation to the time-history analyses results. That is, the absolute difference of the displacements obtained by the time-history analyses of the MDOF and equivalent SDOF systems is divided by the MDOF system solution and these error terms are averaged for each deformation level separately.

Table 2.6 Mean of Percentage Errors for Different Idealization Methods of Frame F2S2B

Deformation Level	FEMA	Initial Stiffness	Major Yield
I	21.40	8.42	38.60
II	26.59	12.07	40.71
III	21.46	13.59	36.52
IV	24.70	12.36	34.00
V	19.16	9.84	25.47
VI	20.94	7.92	26.98

The results in Table 2.6 clearly demonstrate that the Initial Stiffness Method yields much more satisfying results than the other two methods. The initial stiffness procedure is more successful in estimating especially the behavior of the structure in the elastic range and thus at points close to the global yield of the structure. The performance points used through the analyses in this study are all within the life safety performance limit, thus the above mentioned results are expected in this context.

2.6.3 SDOF Analyses Results

It was stated that the ground motions were scaled so that the SDOF system solutions of the frames correspond to the predetermined deformation levels. Therefore it is obvious that the SDOF System solutions of all frames yield the same roof displacement and base shear values under each earthquake which are presented in Table 2.7.

Table 2.7 Peak Roof Displacements and Base Shears of Undamaged Structure Obtained by TH Analysis of Equivalent SDOF System

Deformation Level	F2S2B		F4S3B		F5S2B	
	Δ_{max} (m)	V_{max} (kN)	Δ_{max} (m)	V_{max} (kN)	Δ_{max} (m)	V_{max} (kN)
I	0.029	707.804	0.010	72.117	0.033	565.673
II	0.044	1045.474	0.019	103.219	0.049	735.315
III	0.055	1052.775	0.042	103.322	0.082	737.256
IV	0.060	1056.425	0.051	103.360	0.091	737.778
V	0.079	1069.202	0.094	103.545	0.126	739.794
VI	0.086	1073.765	0.111	103.621	0.137	740.466
Deformation Level	F5S4B		F5S7B		F8S3B	
	Δ_{max} (m)	V_{max} (kN)	Δ_{max} (m)	V_{max} (kN)	Δ_{max} (m)	V_{max} (kN)
I	0.076	2323.993	0.041	1486.308	0.076	2506.233
II	0.107	3135.181	0.071	2601.039	0.109	3573.702
III	0.153	3179.516	0.093	3051.448	0.182	3661.461
IV	0.165	3191.251	0.109	3074.475	0.197	3662.657
V	0.222	3247.321	0.148	3129.384	0.289	3669.725
VI	0.240	3264.273	0.160	3145.326	0.334	3673.205

2.7 COMPARISON OF RESULTS

In Figures 2.16-2.21 results of the time-history analyses, nonlinear static analyses, and SDOF analyses of the undamaged structure are presented graphically. All data are plotted on the same graph so that the comparison can be easily visualized. The points refer to the results obtained from the time-history analyses and the vertical lines correspond to the SDOF solutions.

These figures clearly demonstrate that the nonlinear static analysis underestimates the base shear capacity of structures. The capacity curves lie below the base shear-top displacement pairs obtained from the nonlinear time-history analyses in almost all of the cases. This fact indicates that the pushover analysis, which is much easier to perform when compared to a full time-history analysis, can be used with confidence in most cases because the results obtained are conservative and usually form a lower bound to the actual behavior.

Another fact that can be visualized is that the SDOF and time-history solutions produce comparable results at performance points in the range of the global yield and the accuracy diminishes as the ductility ratio increases. The validity of this behavior is further explored in Table 2.8. The TH and SDOF columns of Table 2.8 correspond to the displacements in meters obtained from SDOF and time-history analyses respectively. The Error (%) column refers to the percentage error of the two analyses and is calculated as given below;

$$\text{Error (\%)} = \frac{\left|\Delta_{SDOF} - \Delta_{TH}\right|}{\Delta_{TH}} \times 100 \qquad \text{2-22}$$

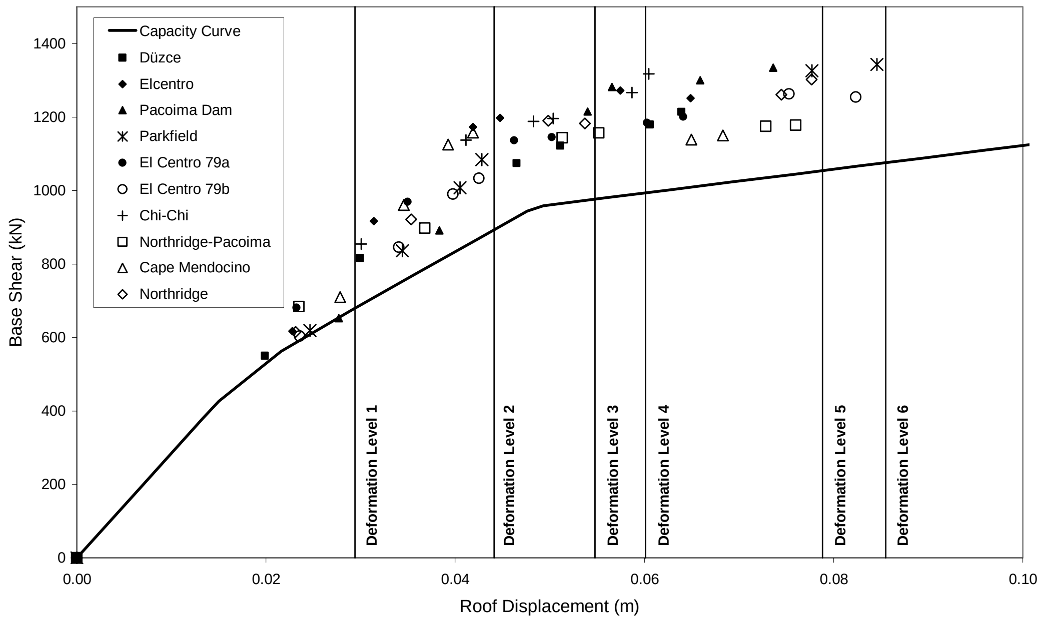

Figure 2.16: Time-History, Capacity Curve, SDOF System Comparison for Frame "F2S2B"

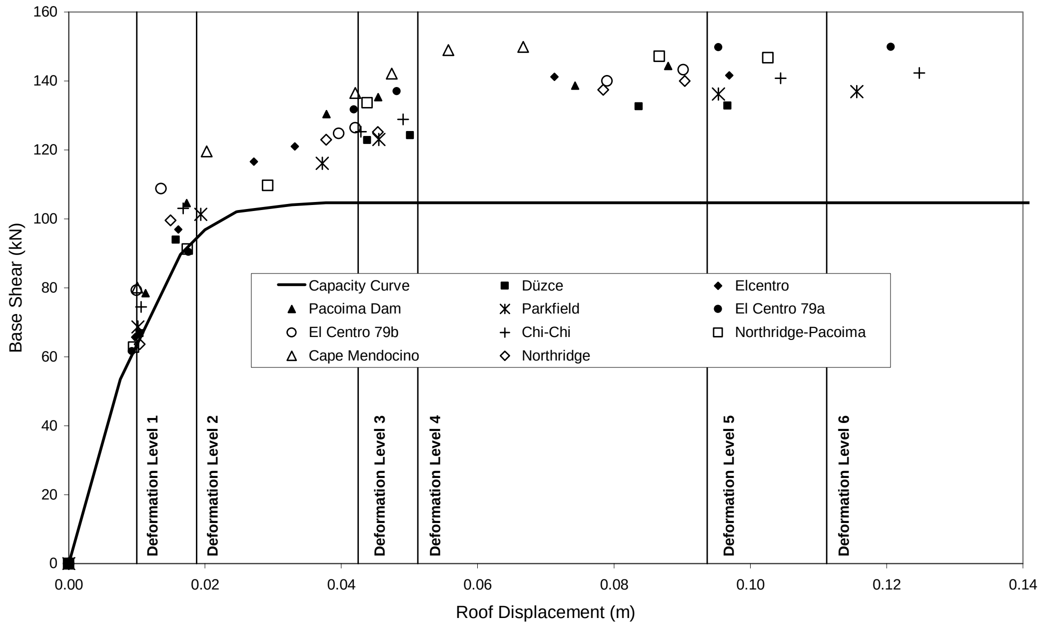

Figure 2.17: Time-History, Capacity Curve, SDOF System Comparison for Frame "F4S3B"

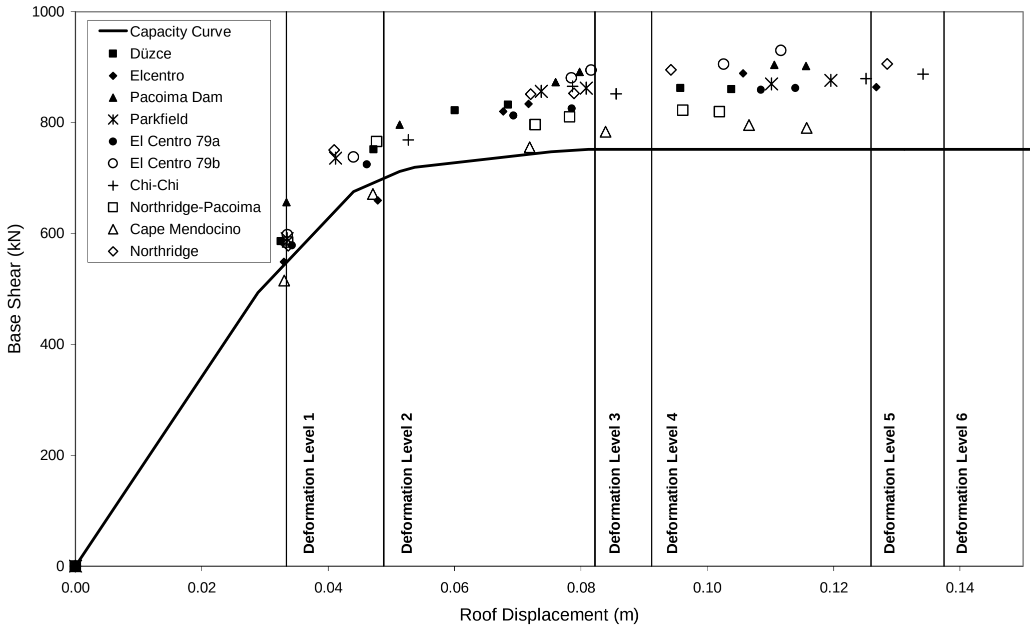

Figure 2.18: Time-History, Capacity Curve, SDOF System Comparison for Frame "F5S2B"

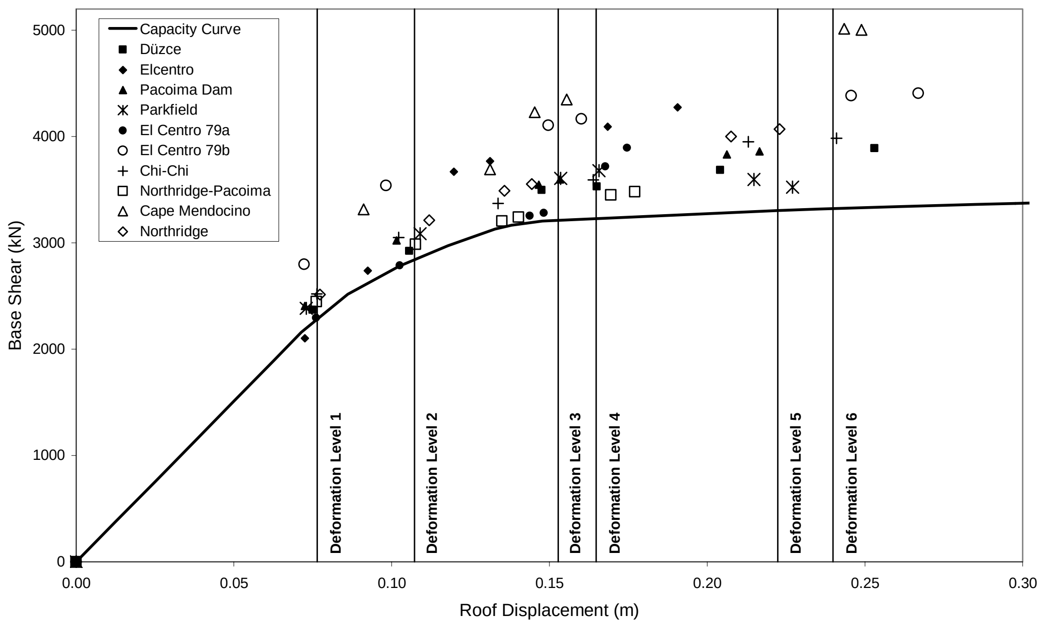

Figure 2.19: Time-History, Capacity Curve, SDOF System Comparison for Frame "F5S4B"

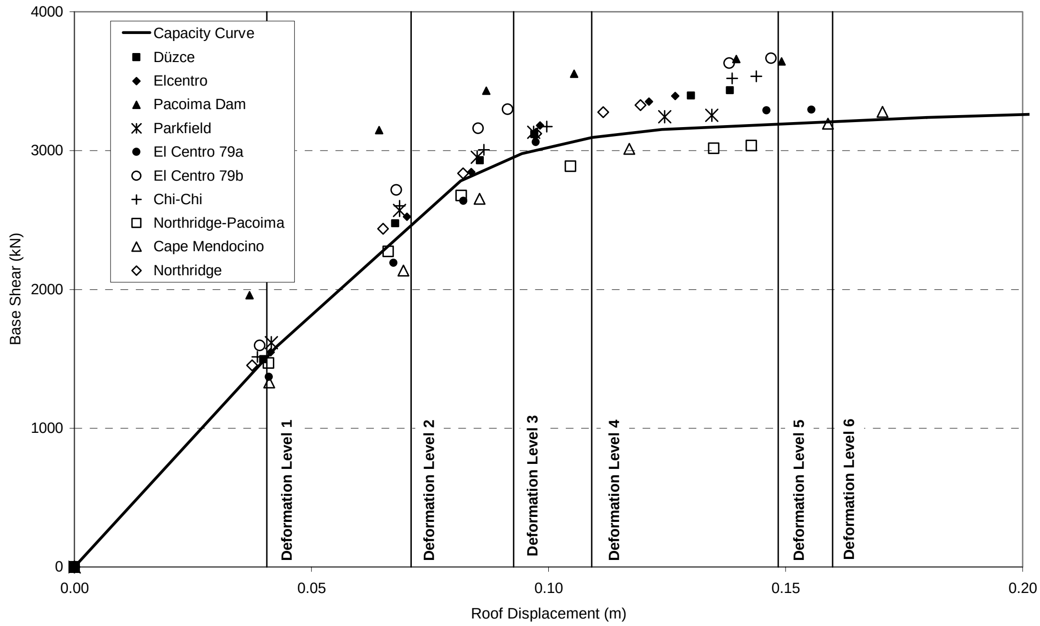

Figure 2.20: Time-History, Capacity Curve, SDOF System Comparison for Frame "F5S7B"

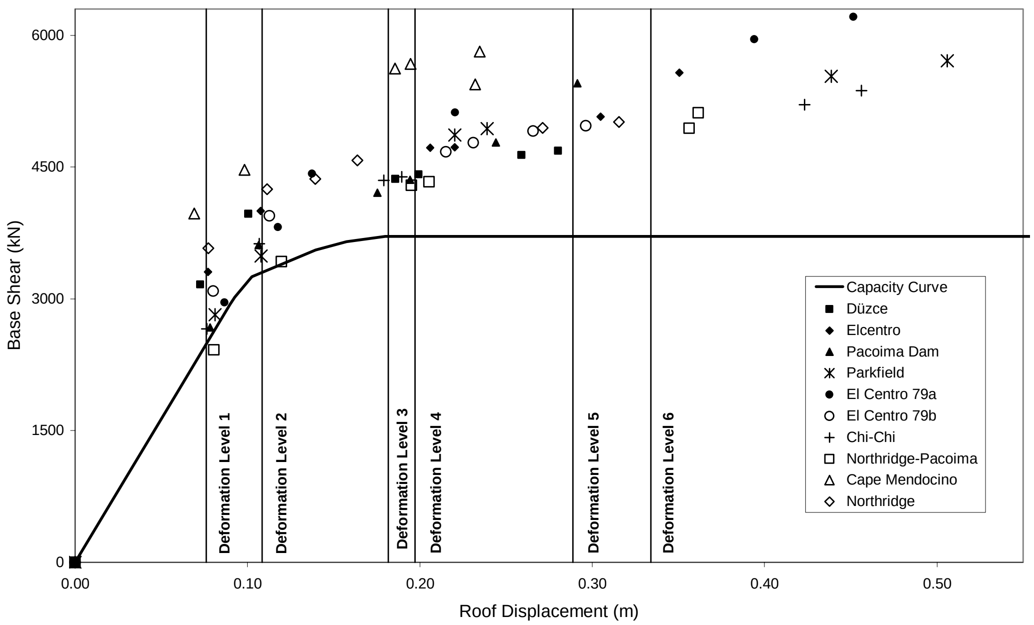

Figure 2.21: Time-History, Capacity Curve, SDOF System Comparison for Frame "F8S3B"

Table 2.8 SDOF System – Time-History Analysis Comparison

Deformation Level	F2S2B			F4S3B			F5S2B			F5S4B			F5S7B			F8S3B		
Düzce																		
	Δ_{max} (m) TH	Δ_{max} (m) SDOF	Error (%)	Δ_{max} (m) TH	Δ_{max} (m) SDOF	Error (%)	Δ_{max} (m) TH	Δ_{max} (m) SDOF	Error (%)	Δ_{max} (m) TH	Δ_{max} (m) SDOF	Error (%)	Δ_{max} (m) TH	Δ_{max} (m) SDOF	Error (%)	Δ_{max} (m) TH	Δ_{max} (m) SDOF	Error (%)
I	0.020	0.029	47.86	0.010	0.010	4.06	0.032	0.033	2.86	0.075	0.076	1.88	0.040	0.041	1.83	0.073	0.076	4.74
II	0.030	0.044	47.21	0.016	0.019	19.31	0.047	0.049	3.51	0.106	0.107	1.59	0.068	0.071	4.97	0.101	0.109	7.81
III	0.047	0.055	17.80	0.044	0.042	3.03	0.060	0.082	36.93	0.148	0.153	3.50	0.086	0.093	8.26	0.186	0.182	2.21
IV	0.051	0.060	17.71	0.050	0.051	2.24	0.068	0.091	33.32	0.165	0.165	0.11	0.097	0.109	12.49	0.199	0.197	1.03
V	0.061	0.079	30.17	0.084	0.094	12.05	0.096	0.126	31.51	0.204	0.222	8.99	0.130	0.148	14.17	0.259	0.289	11.52
VI	0.064	0.086	33.77	0.097	0.111	15.01	0.104	0.137	32.40	0.253	0.240	5.18	0.138	0.160	15.61	0.280	0.334	19.21
El Centro																		
Deformation Level	F2S2B			F4S3B			F5S2B			F5S4B			F5S7B			F8S3B		
	Δ_{max} (m) TH	Δ_{max} (m) SDOF	Error (%)	Δ_{max} (m) TH	Δ_{max} (m) SDOF	Error (%)	Δ_{max} (m) TH	Δ_{max} (m) SDOF	Error (%)	Δ_{max} (m) TH	Δ_{max} (m) SDOF	Error (%)	Δ_{max} (m) TH	Δ_{max} (m) SDOF	Error (%)	Δ_{max} (m) TH	Δ_{max} (m) SDOF	Error (%)
I	0.023	0.029	29.11	0.010	0.010	2.70	0.033	0.033	1.27	0.073	0.074	1.63	0.041	0.041	1.98	0.077	0.076	1.41
II	0.031	0.044	40.36	0.016	0.019	16.44	0.048	0.049	1.97	0.092	0.103	11.69	0.070	0.071	1.33	0.108	0.109	0.82
III	0.042	0.055	30.80	0.027	0.042	56.26	0.068	0.082	21.42	0.120	0.150	25.36	0.084	0.091	9.14	0.206	0.182	11.71
IV	0.045	0.060	34.39	0.033	0.051	54.38	0.072	0.091	27.17	0.131	0.169	28.74	0.098	0.109	11.13	0.220	0.197	10.41
V	0.057	0.079	37.26	0.071	0.094	31.48	0.106	0.126	19.16	0.169	0.220	30.40	0.121	0.147	21.48	0.305	0.289	5.27
VI	0.065	0.086	31.81	0.097	0.111	14.72	0.127	0.137	8.45	0.191	0.241	26.52	0.127	0.160	26.17	0.351	0.334	4.73
Pacoima Dam																		
Deformation Level	F2S2B			F4S3B			F5S2B			F5S4B			F5S7B			F8S3B		
	Δ_{max} (m) TH	Δ_{max} (m) SDOF	Error (%)	Δ_{max} (m) TH	Δ_{max} (m) SDOF	Error (%)	Δ_{max} (m) TH	Δ_{max} (m) SDOF	Error (%)	Δ_{max} (m) TH	Δ_{max} (m) SDOF	Error (%)	Δ_{max} (m) TH	Δ_{max} (m) SDOF	Error (%)	Δ_{max} (m) TH	Δ_{max} (m) SDOF	Error (%)
I	0.028	0.029	6.14	0.011	0.011	0.32	0.033	0.033	0.03	0.073	0.072	0.25	0.037	0.041	9.97	0.078	0.078	1.11
II	0.038	0.044	15.11	0.017	0.020	15.43	0.051	0.049	4.88	0.102	0.102	0.25	0.064	0.071	10.55	0.106	0.107	0.69
III	0.054	0.055	1.48	0.038	0.040	5.71	0.076	0.081	6.50	0.147	0.155	5.98	0.087	0.093	6.59	0.175	0.180	2.82
IV	0.057	0.060	6.28	0.045	0.050	10.06	0.080	0.091	14.31	0.153	0.165	7.50	0.105	0.108	2.30	0.194	0.200	2.91
V	0.066	0.079	19.65	0.074	0.092	24.44	0.111	0.126	13.82	0.206	0.226	9.80	0.140	0.148	6.30	0.244	0.289	18.29
VI	0.074	0.086	16.16	0.088	0.112	27.78	0.116	0.137	18.91	0.217	0.240	10.74	0.149	0.159	6.33	0.292	0.334	14.56

Table 2.8 Continued

Deformation Level	Parkfield																	
	F2S2B			F4S3B			F5S2B			F5S4B			F5S7B			F8S3B		
	Δ_{max} (m)		Error (%)	Δ_{max} (m)		Error (%)	Δ_{max} (m)		Error (%)	Δ_{max} (m)		Error (%)	Δ_{max} (m)		Error (%)	Δ_{max} (m)		Error (%)
	TH	SDOF		TH	SDOF		TH	SDOF		TH	SDOF		TH	SDOF		TH	SDOF	
I	0.025	0.029	19.36	0.010	0.010	1.52	0.033	0.033	0.24	0.073	0.072	0.76	0.042	0.042	0.74	0.081	0.076	6.28
II	0.034	0.044	28.13	0.019	0.019	3.36	0.041	0.048	15.51	0.109	0.106	2.94	0.069	0.071	3.64	0.108	0.109	0.55
III	0.041	0.056	38.52	0.037	0.042	14.23	0.074	0.082	11.51	0.154	0.151	1.36	0.085	0.093	9.08	0.220	0.183	16.83
IV	0.043	0.061	43.54	0.045	0.050	9.87	0.081	0.090	11.23	0.166	0.163	1.34	0.097	0.108	11.36	0.239	0.196	18.04
V	0.078	0.079	1.44	0.095	0.092	3.04	0.110	0.127	15.45	0.215	0.222	3.57	0.125	0.148	19.21	0.439	0.287	34.46
VI	0.085	0.086	1.12	0.116	0.110	4.94	0.120	0.139	16.06	0.227	0.240	5.62	0.134	0.160	18.95	0.506	0.335	33.70
Deformation Level	El Centro 79a																	
	F2S2B			F4S3B			F5S2B			F5S4B			F5S7B			F8S3B		
	Δ_{max} (m)		Error (%)	Δ_{max} (m)		Error (%)	Δ_{max} (m)		Error (%)	Δ_{max} (m)		Error (%)	Δ_{max} (m)		Error (%)	Δ_{max} (m)		Error (%)
	TH	SDOF		TH	SDOF		TH	SDOF		TH	SDOF		TH	SDOF		TH	SDOF	
I	0.023	0.029	26.65	0.009	0.010	7.72	0.034	0.033	2.55	0.076	0.076	0.44	0.041	0.041	1.03	0.087	0.079	9.06
II	0.035	0.044	26.11	0.018	0.019	6.73	0.046	0.049	5.86	0.103	0.107	4.50	0.067	0.070	3.65	0.118	0.109	7.81
III	0.046	0.055	18.48	0.042	0.042	1.51	0.069	0.082	18.57	0.144	0.154	7.20	0.082	0.093	12.88	0.137	0.182	32.29
IV	0.050	0.060	19.73	0.048	0.051	6.46	0.079	0.091	16.11	0.148	0.165	11.21	0.097	0.108	10.80	0.220	0.196	11.11
V	0.060	0.077	28.55	0.095	0.094	1.72	0.108	0.127	17.25	0.168	0.222	32.63	0.146	0.147	0.84	0.394	0.289	26.68
VI	0.064	0.086	33.39	0.121	0.111	7.85	0.114	0.137	20.66	0.175	0.241	38.11	0.155	0.160	2.86	0.451	0.334	26.02
Deformation Level	El Centro 79b																	
	F2S2B			F4S3B			F5S2B			F5S4B			F5S7B			F8S3B		
	Δ_{max} (m)		Error (%)	Δ_{max} (m)		Error (%)	Δ_{max} (m)		Error (%)	Δ_{max} (m)		Error (%)	Δ_{max} (m)		Error (%)	Δ_{max} (m)		Error (%)
	TH	SDOF		TH	SDOF		TH	SDOF		TH	SDOF		TH	SDOF		TH	SDOF	
I	0.024	0.029	24.68	0.010	0.010	0.50	0.034	0.033	0.41	0.072	0.076	5.75	0.039	0.041	3.73	0.080	0.078	3.30
II	0.034	0.044	29.57	0.014	0.019	38.15	0.044	0.049	10.86	0.098	0.107	9.11	0.068	0.071	4.61	0.113	0.109	3.76
III	0.040	0.055	37.78	0.040	0.044	10.27	0.078	0.082	4.76	0.150	0.154	2.98	0.085	0.093	8.74	0.215	0.180	16.18
IV	0.043	0.060	41.39	0.042	0.049	15.88	0.082	0.091	11.72	0.160	0.165	2.93	0.091	0.109	19.40	0.231	0.196	15.22
V	0.075	0.079	4.71	0.079	0.095	20.17	0.103	0.127	23.93	0.246	0.224	8.91	0.138	0.148	7.46	0.266	0.290	9.22
VI	0.082	0.086	3.84	0.090	0.114	26.02	0.112	0.139	24.26	0.267	0.243	9.12	0.147	0.160	8.80	0.296	0.335	13.21

Table 2.8 Continued

Deformation Level	Chi-Chi																	
	F2S2B			F4S3B			F5S2B			F5S4B			F5S7B			F8S3B		
	Δ_{max} (m)		Error (%)	Δ_{max} (m)		Error (%)	Δ_{max} (m)		Error (%)	Δ_{max} (m)		Error (%)	Δ_{max} (m)		Error (%)	Δ_{max} (m)		Error (%)
	TH	SDOF		TH	SDOF		TH	SDOF		TH	SDOF		TH	SDOF		TH	SDOF	
I	0.030	0.029	2.24	0.011	0.011	6.15	0.033	0.033	0.07	0.076	0.076	0.14	0.039	0.041	5.21	0.076	0.078	1.37
II	0.041	0.044	7.20	0.017	0.020	18.93	0.053	0.049	7.37	0.102	0.106	3.57	0.069	0.071	3.65	0.107	0.109	1.52
III	0.048	0.055	13.50	0.043	0.042	0.98	0.079	0.081	2.85	0.134	0.153	14.23	0.086	0.091	5.77	0.179	0.182	1.56
IV	0.050	0.060	19.41	0.049	0.050	1.89	0.086	0.091	6.61	0.164	0.165	0.52	0.100	0.109	9.54	0.189	0.197	4.11
V	0.059	0.079	34.38	0.104	0.094	10.29	0.125	0.126	0.63	0.213	0.222	4.41	0.139	0.148	7.00	0.423	0.289	31.74
VI	0.060	0.086	41.47	0.125	0.111	10.91	0.134	0.137	2.49	0.241	0.240	0.47	0.144	0.160	11.15	0.456	0.334	26.78

Deformation Level	Northridge-Pacoima																	
	F2S2B			F4S3B			F5S2B			F5S4B			F5S7B			F8S3B		
	Δ_{max} (m)		Error (%)	Δ_{max} (m)		Error (%)	Δ_{max} (m)		Error (%)	Δ_{max} (m)		Error (%)	Δ_{max} (m)		Error (%)	Δ_{max} (m)		Error (%)
	TH	SDOF		TH	SDOF		TH	SDOF		TH	SDOF		TH	SDOF		TH	SDOF	
I	0.023	0.029	25.23	0.010	0.010	5.02	0.034	0.033	0.56	0.076	0.076	0.25	0.041	0.042	2.31	0.080	0.076	5.43
II	0.037	0.044	19.80	0.017	0.019	7.63	0.048	0.049	2.43	0.108	0.107	0.40	0.066	0.070	5.38	0.120	0.109	9.42
III	0.051	0.055	6.71	0.029	0.042	45.29	0.073	0.081	11.22	0.135	0.154	14.20	0.082	0.093	13.52	0.195	0.180	7.55
IV	0.055	0.060	8.98	0.044	0.051	16.90	0.078	0.091	16.61	0.140	0.165	17.54	0.105	0.109	4.27	0.205	0.196	4.64
V	0.073	0.079	8.25	0.087	0.094	8.07	0.096	0.126	30.93	0.169	0.222	31.27	0.135	0.148	10.06	0.356	0.287	19.33
VI	0.076	0.086	12.51	0.103	0.111	8.39	0.102	0.137	34.87	0.177	0.240	35.49	0.143	0.160	11.95	0.361	0.335	7.23

Deformation Level	Cape Mendocino																	
	F2S2B			F4S3B			F5S2B			F5S4B			F5S7B			F8S3B		
	Δ_{max} (m)		Error (%)	Δ_{max} (m)		Error (%)	Δ_{max} (m)		Error (%)	Δ_{max} (m)		Error (%)	Δ_{max} (m)		Error (%)	Δ_{max} (m)		Error (%)
	TH	SDOF		TH	SDOF		TH	SDOF		TH	SDOF		TH	SDOF		TH	SDOF	
I	0.028	0.029	5.62	0.010	0.010	0.35	0.033	0.033	1.00	0.091	0.076	16.18	0.041	0.041	1.14	0.069	0.076	10.00
II	0.035	0.044	27.66	0.020	0.019	7.48	0.047	0.049	3.68	0.131	0.107	18.27	0.069	0.071	2.41	0.098	0.109	10.32
III	0.039	0.055	39.64	0.042	0.044	3.95	0.072	0.082	14.38	0.145	0.153	5.10	0.085	0.093	8.37	0.186	0.180	2.85
IV	0.042	0.060	43.52	0.047	0.051	8.08	0.084	0.091	8.69	0.155	0.165	6.00	0.117	0.109	6.78	0.195	0.196	0.68
V	0.065	0.079	21.40	0.056	0.094	68.21	0.107	0.126	18.09	0.243	0.222	8.63	0.159	0.148	6.59	0.232	0.290	25.09
VI	0.068	0.086	25.21	0.067	0.111	66.69	0.116	0.137	18.80	0.249	0.240	3.61	0.170	0.160	6.18	0.235	0.335	42.83

Table 2.8 Continued

Deformation Level	Northridge																	
	F2S2B			F4S3B			F5S2B			F5S4B			F5S7B			F8S3B		
	Δ_{max} (m)		Error (%)	Δ_{max} (m)		Error (%)	Δ_{max} (m)		Error (%)	Δ_{max} (m)		Error (%)	Δ_{max} (m)		Error (%)	Δ_{max} (m)		Error (%)
	TH	SDOF		TH	SDOF		TH	SDOF		TH	SDOF		TH	SDOF		TH	SDOF	
I	0.023	0.029	27.09	0.010	0.010	3.76	0.034	0.033	0.79	0.077	0.075	2.91	0.037	0.041	8.33	0.077	0.078	0.36
II	0.035	0.044	24.74	0.015	0.019	25.42	0.041	0.048	16.13	0.112	0.106	5.39	0.065	0.071	9.11	0.111	0.107	3.74
III	0.050	0.055	9.92	0.038	0.042	12.49	0.072	0.082	14.09	0.136	0.154	13.52	0.082	0.093	12.94	0.139	0.180	29.45
IV	0.054	0.060	12.00	0.045	0.051	12.90	0.079	0.090	13.95	0.144	0.165	14.10	0.097	0.110	13.38	0.164	0.197	20.53
V	0.074	0.079	5.84	0.078	0.094	19.46	0.094	0.126	33.57	0.208	0.222	7.13	0.112	0.148	33.08	0.271	0.287	5.95
VI	0.078	0.086	10.13	0.090	0.112	24.36	0.128	0.139	8.00	0.223	0.240	7.58	0.119	0.160	33.94	0.315	0.335	6.32

As a general trend, the variation of the percentage error increases as the earthquake acceleration scale increases but when all data are examined this rule is not precisely correct. It can be stated that the variation in error depends both on the acceleration scale and the ground motion itself. In order to come up with a more reliable conclusion the average errors for each earthquake scale are calculated and compared in Table 2.9.

Table 2.9 Mean of Percentage Error

Deformation Level	F2S2B	F4S3B	F5S2B	F5S4B	F5S7B	F8S3B
I	21.40	3.21	0.98	3.02	3.63	4.31
II	26.59	15.89	7.22	5.77	4.93	4.65
III	21.46	15.37	14.22	9.34	9.53	12.35
IV	24.70	13.87	15.97	9.00	10.14	8.87
V	19.16	19.89	20.43	14.57	12.62	18.76
VI	20.94	20.67	18.49	14.24	14.19	19.46

In Table 2.9, the mean of the percentage errors of the ten ground motions the structure is analyzed for are presented. The error is generally within 20 percent. The higher mean percentage errors of frame F2S2B repeat the conclusion of the previous section and Table 2.6 that the Initial Stiffness Procedure produces the best results among the introduced three idealization methods.

The overall trend reveals the expectation that; the percentage error increases as the degree of inelasticity (ductility ratio) increases. The higher error values at larger acceleration scales put in the picture that the discrepancy in error of the SDOF analyses amplify at performance points that are further away from the global yield of the structure.

To visualize this trend and give a better understanding of the case, Figure 2.22 will be used. In this figure the time-history results are plotted against the SDOF results together with the 45° line dividing the first quadrant. On this line the time-history and SDOF solutions will yield identical results therefore increasing discrepancies from this line indicate that there is more error involved in the SDOF solution.

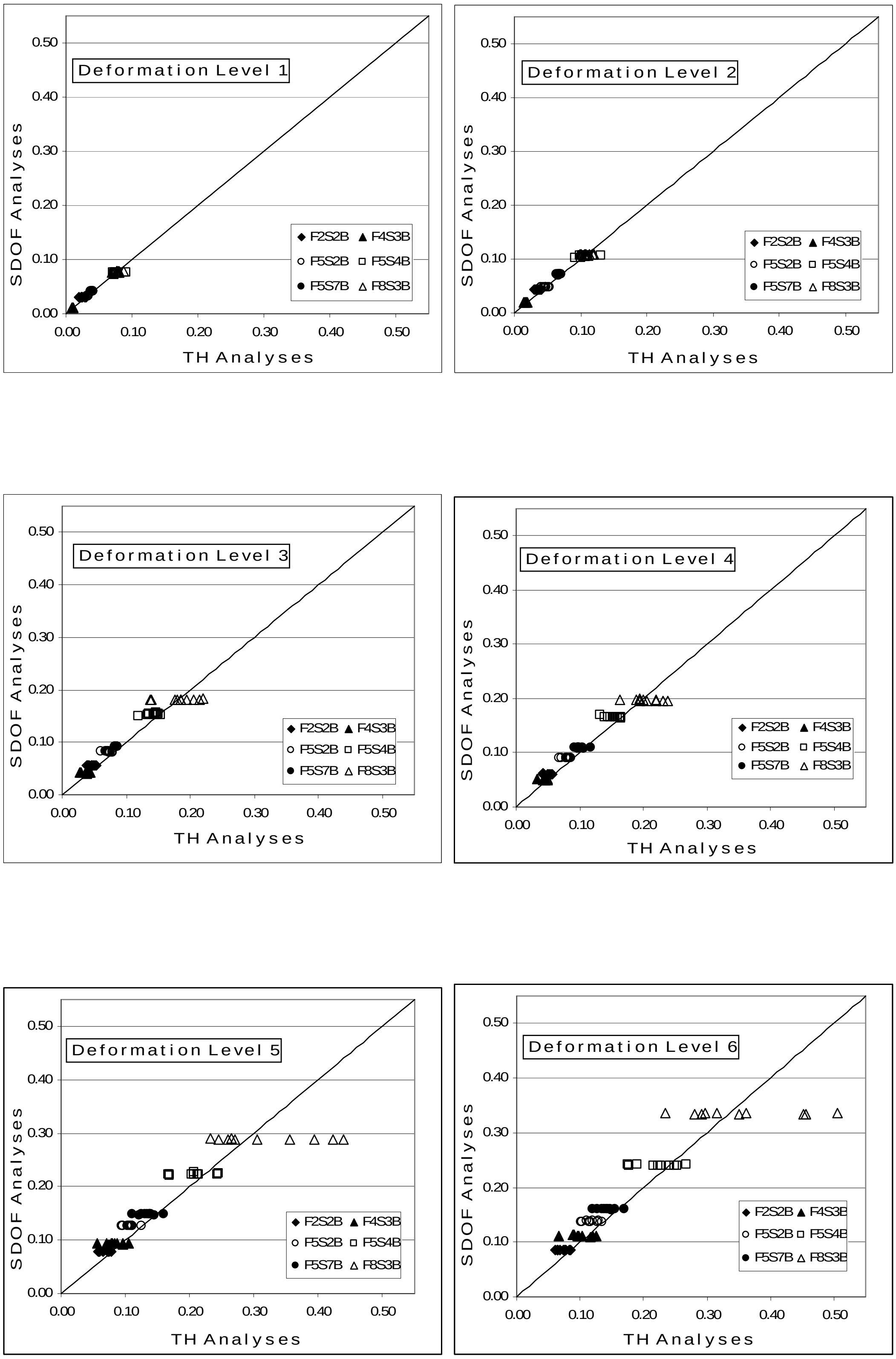

Figure 2.22: SDOF System – Time-History Analysis Comparison

CHAPTER 3

ASSESMENT OF BUILDING CAPACITY SUBJECTED TO PRIOR EARTHQUAKES

In this chapter, a procedure to determine the building capacity subjected to prior earthquakes will be developed. This procedure employs the methods discussed in the previous chapter and relies on modifying the earthquake ground motion records and/or the properties of the elements making up the structure. Initially the process developed to determine the nonlinear time-history results of the MDOF systems will be given. Afterwards, based on the results obtained through this method, a procedure, by which the nonlinear static analysis of a structure damaged from prior earthquakes can be determined, is developed.

3.1 TIME HISTORY ANALYSES OF DAMAGED STRUCTURE

The determination of the base shear and top story displacements of the damaged structure was made in a similar manner as that for the undamaged structure as described in Section 2.4.2. Here, as seen in Figure 3.1 the same earthquake was applied two times successively to determine the response for a subsequent earthquake of the same intensity and the response corresponding to the second application was taken into concern. For instance if the Düzce record is considered, the acceleration history for this earthquake lasts 25.905 s. In order to determine the forces and displacements for the damaged structure, the maximum forces and displacements in the time span 25.91 – 51.815 s. are used. The results obtained in this manner are summarized in Appendix A4.

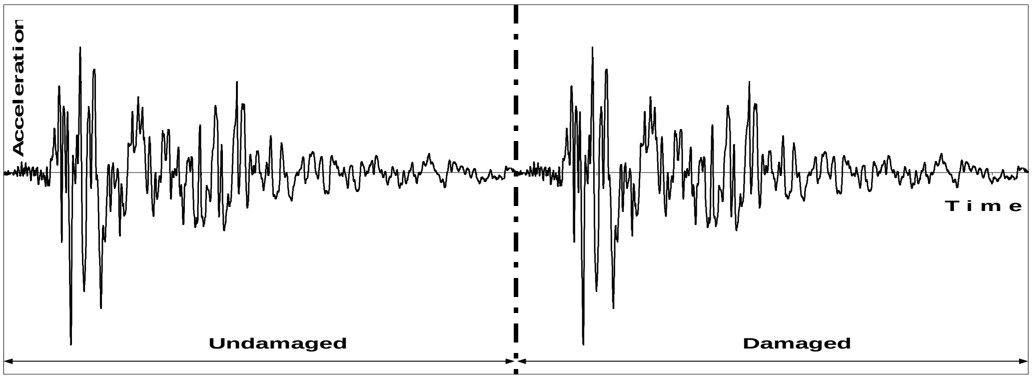

Figure 3.1: Successive Application of Ground Motions

3.2 NONLINEAR STATIC ANALYSIS OF DAMAGED STRUCTURE

This procedure relies on modifying the moment-rotation relationships of members in accordance with the plastic rotation that they attain during the prior earthquake. All members' rigidities are altered taking into consideration their plastic rotation (θ_P) in proportion to their yield rotation (θ_y). For this aim, the yield and plastic rotations of all yielding members have to be determined and the rigidity of each element has to be modified accordingly. This is a very cumbersome procedure and thus not very practical for common use. Concerning this drawback, using the results obtained from the detailed analysis of the six frames evaluated in this study, a simplified procedure, which is based on the global damage level and rigidity of the structure is also proposed. The former procedure, which is the detailed one requiring modification of all elements, will be referred to as "Procedure 1", and the simplified one will be called "Procedure 2" in the remaining of the study.

3.2.1 Procedure 1

The nonlinear static analysis, which makes use of the pushover procedure, is a very practical tool used to determine the global capacity of structures. The reliability of this procedure was tested in the previous chapter and yielded quite satisfying results both in applicability and dependability.

The pushover procedure produces the capacity curve of the structure. The demand, which is the maximum expected response of the structure during the earthquake, can be determined by the analysis of the equivalent SDOF system of the structure. Results of SDOF and time-history analyses were also compared in the previous chapter and this comparison confirmed that the SDOF approach as well generates convincing results.

After the determination of the capacity curve and the performance point, the next step is to determine the yield and plastic rotations that the yielding members of the structure experience. Yield and plastic rotations are calculated as given in Equations 2-6 and 2-7. The calculation of the yield rotation is performed manually for each member, whereas the plastic rotations are taken from the SAP2000 [11] output file.

The procedure followed to determine the modification factors for yielding elements is summarized in Figure 3.2.

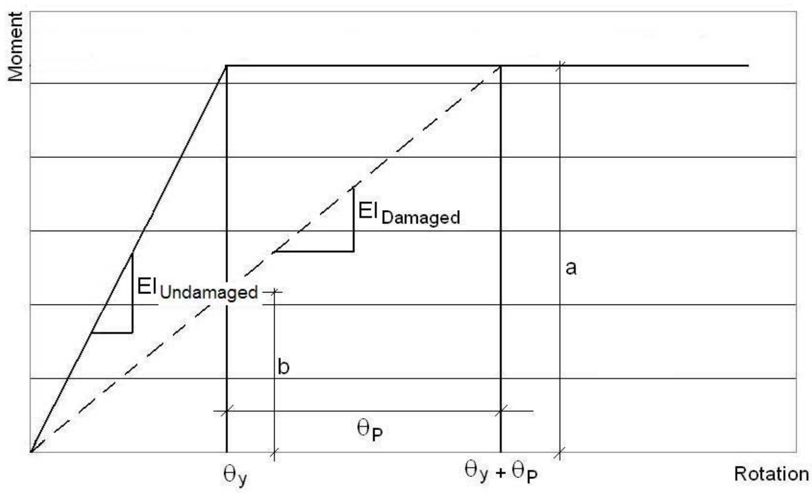

Figure 3.2: Determination of Modification Factors

In Section 2.5.1, it was stated that the strain hardening of the members is ignored therefore the moment–rotation relations will be in the form as presented in Figure 3.2. The solid line in the figure represents the moment–rotation relation of the undamaged member. After an earthquake, the damaged member experiences a plastic rotation of θ_P and thus a total rotation of $\theta_y+\theta_p$. The initial stiffness of the yielding member will be approximated by its secant stiffness, which is plotted as the dashed line in the figure. The modulus of elasticity of the member remains constant therefore the reduction in the initial slope can be attributed to the change in the member's moment of inertia (I). This change can be explained by the loss of cross–section of the member due to cracking occurring after the earthquake. Consequently, if a relation between the slopes of these two curves can be formed and expressed as a ratio, this ratio will also constitute the modification factor by which the element's moment of inertia should be modified. With this explanation made the following relations can be written;

$$EI_{undamaged}=\frac{a}{\theta_y} \quad \text{and} \quad EI_{damaged}=\frac{b}{\theta_y}$$

$$\therefore \quad \frac{EI_{damaged}}{EI_{undamaged}}=\frac{\theta_y}{\theta_y+\theta_p} \qquad 3\text{-}1$$

$\frac{\theta_y}{\theta_y+\theta_p}$ will be the ratio by which the moment of inertia of the yielding elements is modified. The software SAP2000 [11], allows this modification by the modification factor for moment of inertia in the section properties scale dialog box.

After experiencing a plastic deformation of θ_P, the element will have exhausted some of its plastic deformation capability. Therefore the moment rotation relation of this element has to be altered in order to represent this decrease in its plastic rotation capacity. This is achieved by subtracting the amount of plastic deformation imposed on the element from the ultimate rotation of this element which is calculated by Equation 2-8. The ultimate rotation of the damaged element thus becomes;

$$\theta_{u,damaged} = \theta_u - \theta_P \qquad 3\text{-}2$$

The application of this procedure is summarized as follows;

Step 1. Analyze the undamaged structure to obtain its capacity curve.

Step 2. Calculate the performance point and obtain the plastic rotations of elements at this point from the output file. The yield rotation of the element is calculated from its yield curvature and Equation 2-6. Equation 2-8 is used to determine the ultimate rotation.

Step 3. Use Equation 3-1 to compute the modification factor and multiply the moment of inertia of the elements with the modification factor.

Step 4. Determine the ultimate rotation of the damaged element using Equation 3-2.

Step 5. Re-analyze the structure to obtain the capacity curve for the damaged structure.

Step 6. Use the capacity curve obtained in Step 5 to calculate the displacement demand for the earthquake effect considered. Note that the earthquake effect can be represented by the response spectrum if a ground motion record is not available in which case approximate procedures such as the Capacity Spectrum Method [2] or the Displacement Coefficient Method [13] can be used.

In Figures 3.3–3.8, the undamaged and damaged capacity curves are presented together with the maximum top displacement obtained from the SDOF analyses corresponding to each deformation level separately. The curve named as “Capacity Curve” represents the capacity curve of the undamaged structure and the curve named as “Damaged Capacity Curve” stands for the capacity curve of the damaged structure. The vertical line represents the deformation level under consideration. The time-history solutions of the undamaged and damaged structure are as well presented in the graphs by filled and unfilled symbols. It is clearly seen from the time-history analyses results that as the degree of damage due to prior earthquakes increases the deformation due to subsequent earthquakes also increases.

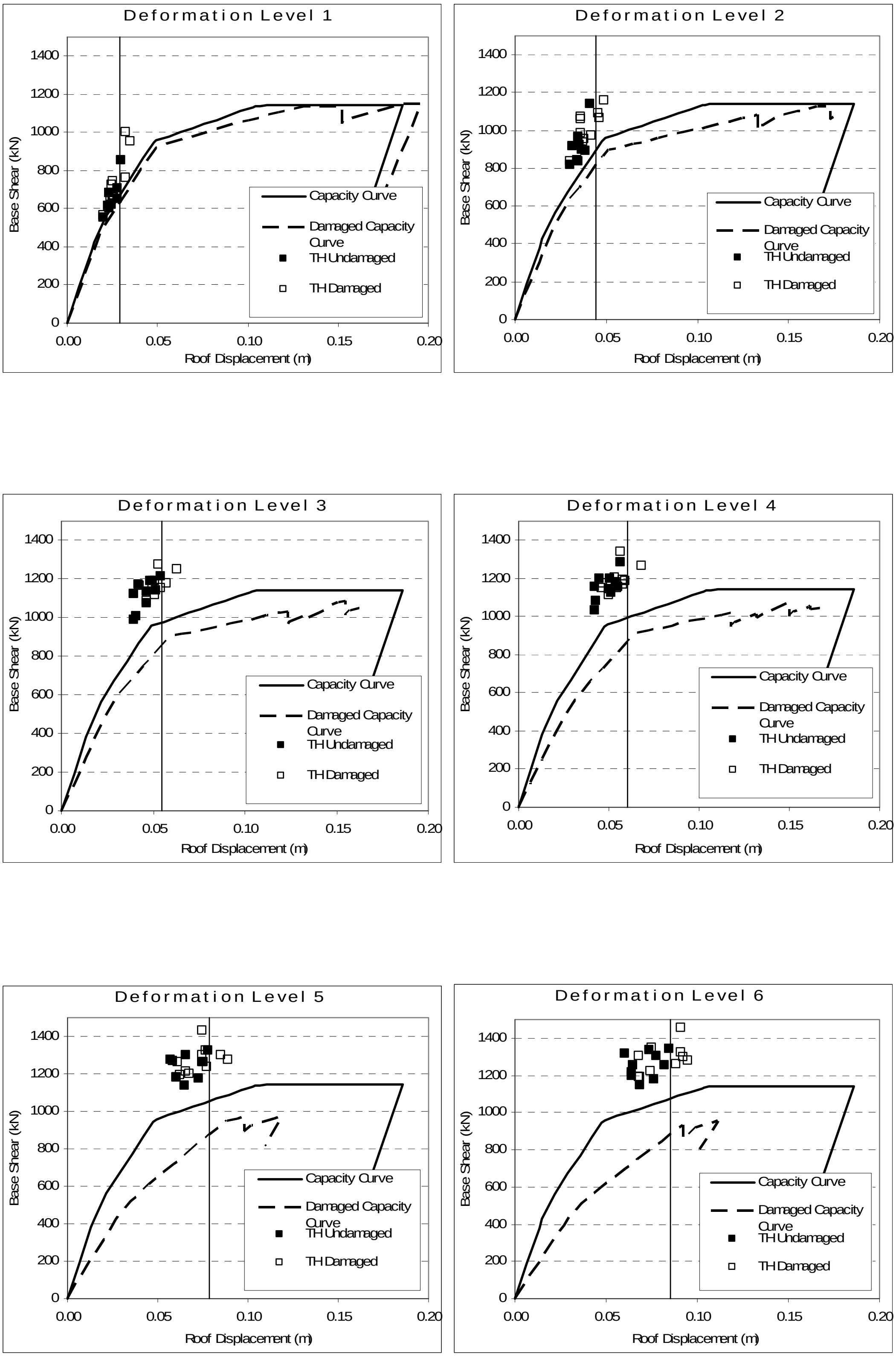

Figure 3.3: Undamaged and Damaged Capacity Curves and Time-History Results of Frame “F2S2B”

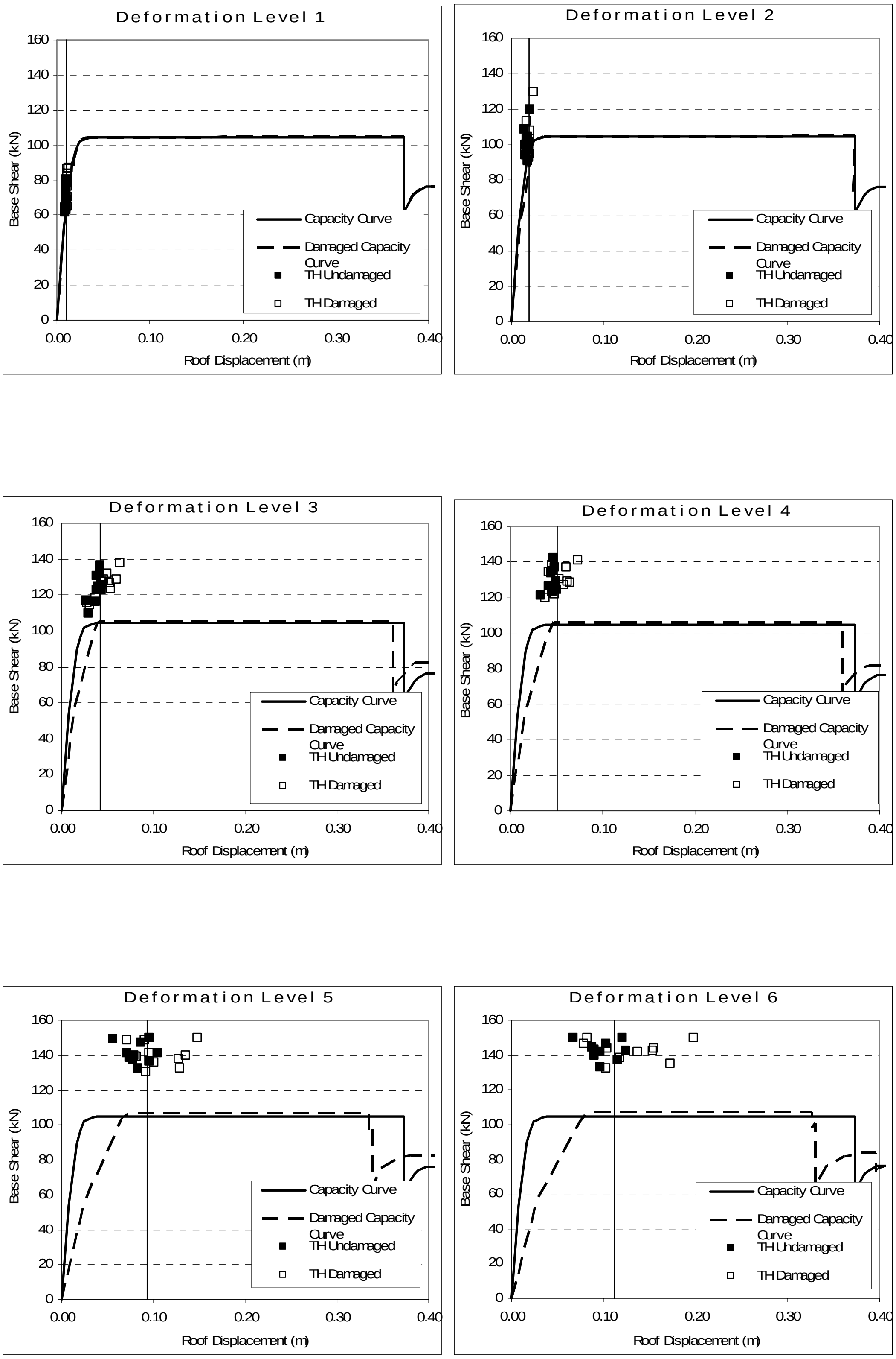

Figure 3.4: Undamaged and Damaged Capacity Curves and Time-History Results of Frame "F4S3B"

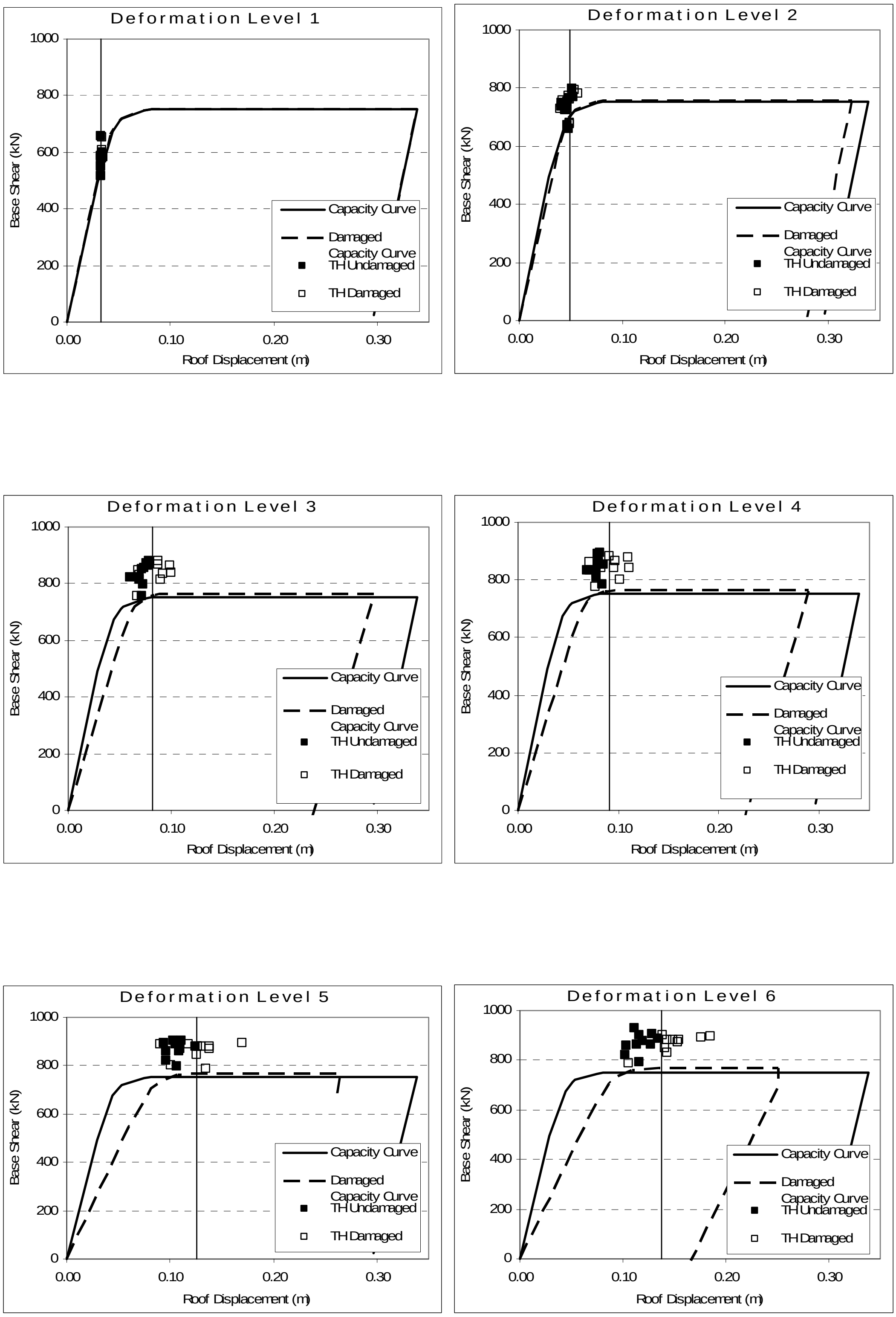

Figure 3.5: Undamaged and Damaged Capacity Curves and Time-History Results of Frame “F5S2B”

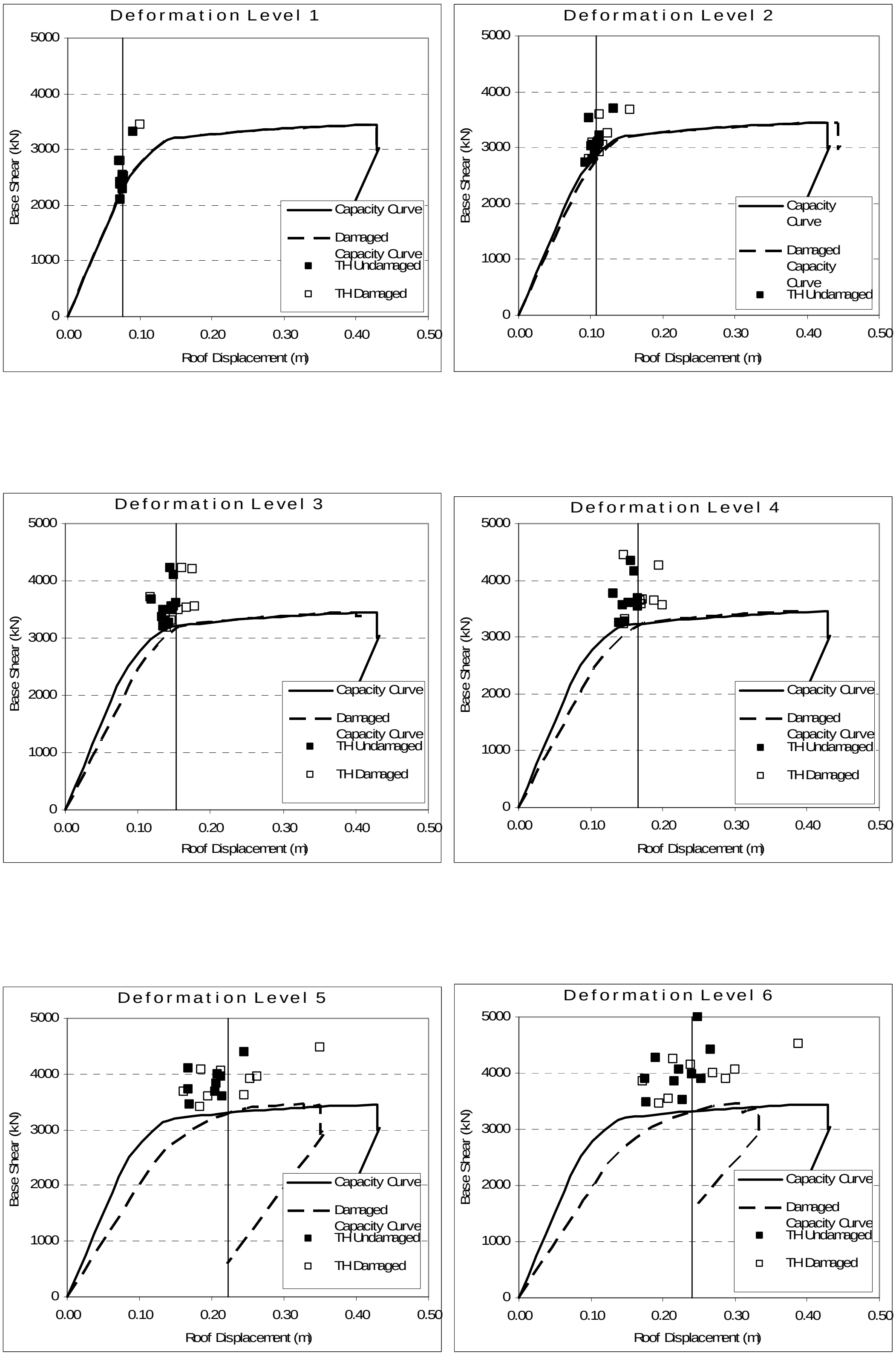

Figure 3.6: Undamaged and Damaged Capacity Curves and Time-History Results of Frame "F5S4B"

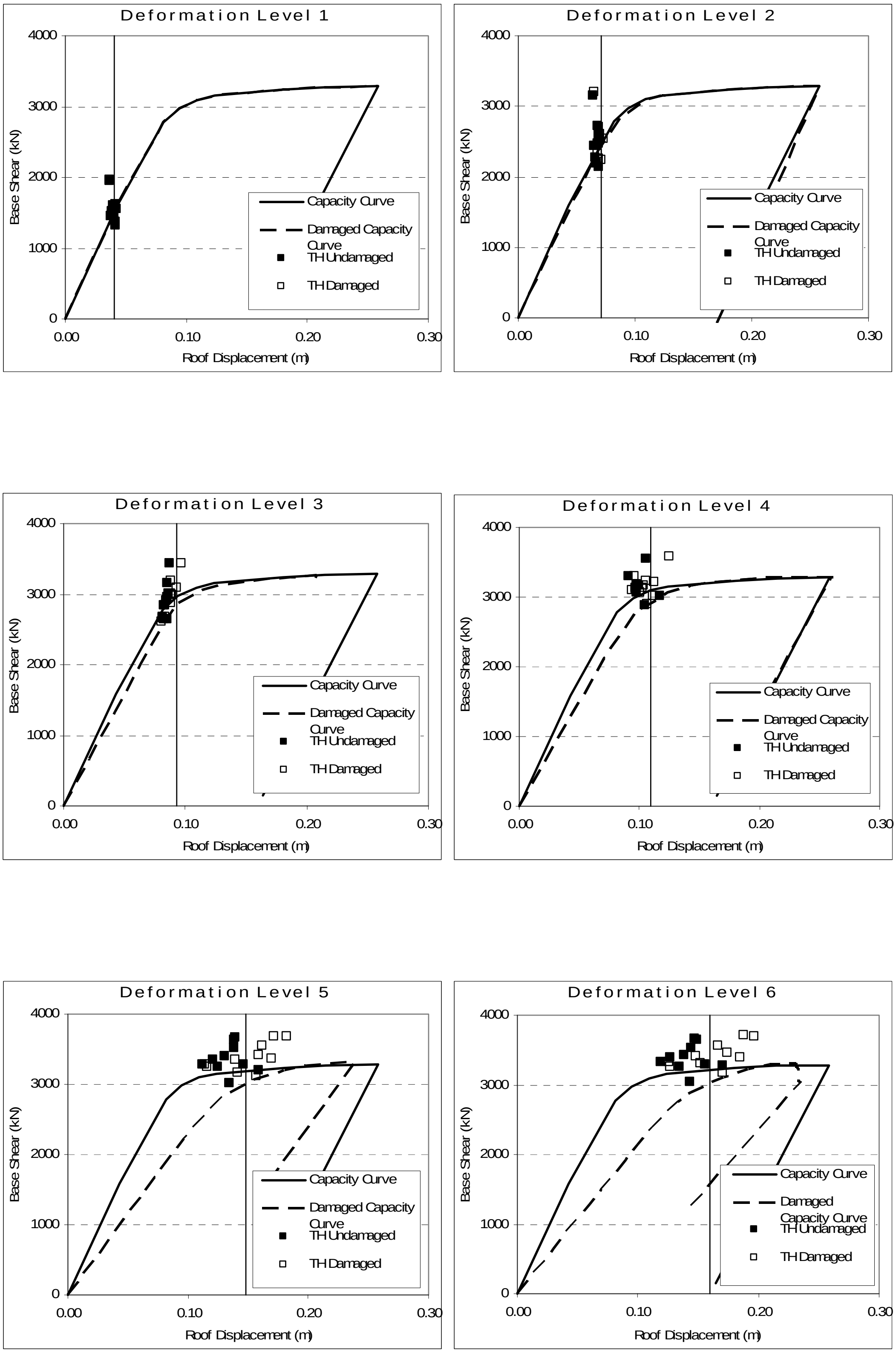

Figure 3.7: Undamaged and Damaged Capacity Curves and Time-History Results of Frame “F5S7B”

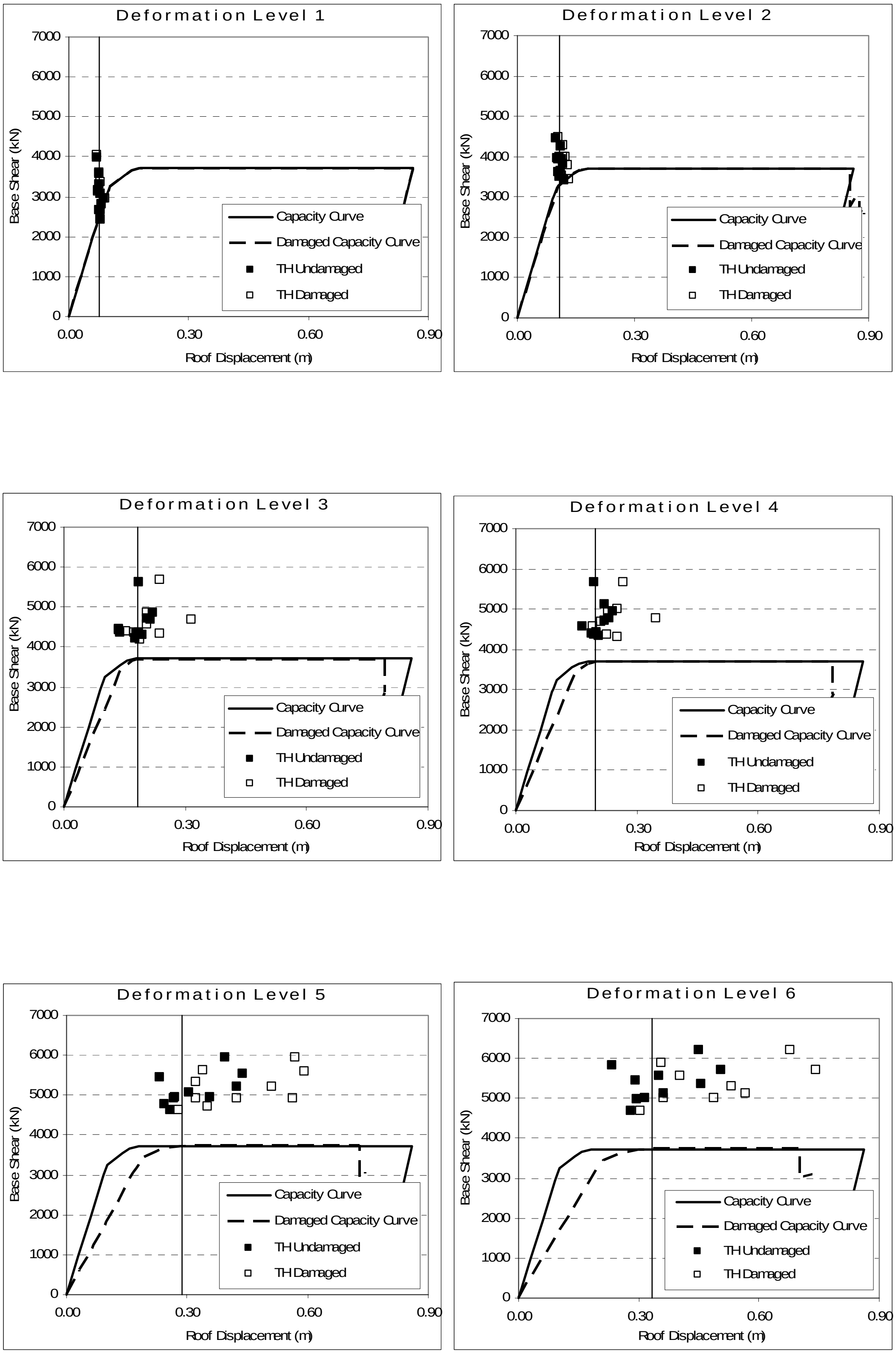

Figure 3.8: Undamaged and Damaged Capacity Curves and Time-History Results of Frame “F8S3B”

Table 3.1 SDOF System – Time-History Analysis Comparison for Damaged Structure

Deformation Level	Düzce																	
	F2S2B			F4S3B			F5S2B			F5S4B			F5S7B			F8S3B		
	Δ_{max} (m)		Error (%)	Δ_{max} (m)		Error (%)	Δ_{max} (m)		Error (%)	Δ_{max} (m)		Error (%)	Δ_{max} (m)		Error (%)	Δ_{max} (m)		Error (%)
	TH	SDOF		TH	SDOF		TH	SDOF		TH	SDOF		TH	SDOF		TH	SDOF	
I	0.020	0.033	69.11	0.011	0.010	11.44	0.033	0.033	2.31	0.075	0.076	1.97	0.040	0.041	1.75	0.072	0.076	5.81
II	0.030	0.043	42.86	0.019	0.017	9.22	0.049	0.052	5.74	0.117	0.104	11.44	0.069	0.074	7.42	0.104	0.105	1.47
III	0.039	0.082	108.34	0.054	0.081	49.88	0.069	0.107	54.62	0.168	0.159	5.56	0.089	0.107	20.83	0.186	0.284	52.91
IV	0.046	0.090	95.40	0.058	0.118	102.15	0.081	0.122	49.93	0.200	0.193	3.67	0.104	0.140	35.50	0.200	0.274	37.31
V	0.062	0.127	104.12	0.092	0.120	30.64	0.125	0.151	20.54	0.246	0.255	3.96	0.158	0.200	26.34	0.279	0.492	76.48
VI	0.068	0.141	108.54	0.103	0.146	41.44	0.141	0.150	6.62	0.287	0.337	17.37	0.174	0.186	7.27	0.303	0.561	85.10

Deformation Level	Elcentro																	
	F2S2B			F4S3B			F5S2B			F5S4B			F5S7B			F8S3B		
	Δ_{max} (m)		Error (%)	Δ_{max} (m)		Error (%)	Δ_{max} (m)		Error (%)	Δ_{max} (m)		Error (%)	Δ_{max} (m)		Error (%)	Δ_{max} (m)		Error (%)
	TH	SDOF		TH	SDOF		TH	SDOF		TH	SDOF		TH	SDOF		TH	SDOF	
I	0.025	0.029	16.88	0.010	0.010	2.81	0.033	0.033	1.15	0.073	0.074	1.41	0.043	0.041	4.49	0.079	0.076	3.56
II	0.037	0.042	11.93	0.016	0.020	26.73	0.049	0.048	1.16	0.097	0.101	3.73	0.073	0.072	2.04	0.122	0.101	17.19
III	0.050	0.063	26.97	0.028	0.029	4.69	0.092	0.082	9.92	0.117	0.177	50.98	0.088	0.111	25.96	0.204	0.202	1.07
IV	0.053	0.066	22.52	0.039	0.039	0.97	0.095	0.103	8.12	0.131	0.210	59.89	0.106	0.142	33.99	0.212	0.210	0.58
V	0.075	0.093	24.04	0.096	0.098	2.61	0.130	0.183	40.02	0.186	0.213	14.72	0.139	0.190	36.51	0.322	0.289	10.33
VI	0.092	0.099	7.20	0.137	0.119	13.12	0.154	0.226	46.57	0.215	0.254	18.15	0.148	0.224	51.55	0.402	0.305	24.17

Deformation Level	Pacoima Dam																	
	F2S2B			F4S3B			F5S2B			F5S4B			F5S7B			F8S3B		
	Δ_{max} (m)		Error (%)	Δ_{max} (m)		Error (%)	Δ_{max} (m)		Error (%)	Δ_{max} (m)		Error (%)	Δ_{max} (m)		Error (%)	Δ_{max} (m)		Error (%)
	TH	SDOF		TH	SDOF		TH	SDOF		TH	SDOF		TH	SDOF		TH	SDOF	
I	0.032	0.027	17.02	0.013	0.012	0.53	0.034	0.035	3.13	0.073	0.075	2.57	0.037	0.041	9.83	0.078	0.078	0.59
II	0.047	0.044	5.18	0.021	0.027	30.16	0.053	0.050	6.82	0.110	0.117	6.37	0.065	0.081	23.25	0.109	0.112	2.60
III	0.053	0.058	9.09	0.046	0.062	34.08	0.099	0.144	45.31	0.178	0.202	13.31	0.097	0.150	54.53	0.189	0.206	9.04
IV	0.056	0.060	6.85	0.041	0.064	55.83	0.109	0.204	86.35	0.189	0.224	18.63	0.125	0.189	50.95	0.227	0.231	1.92
V	0.074	0.097	30.10	0.081	0.105	29.35	0.170	0.230	35.03	0.262	0.363	38.21	0.182	0.344	88.53	0.352	0.402	14.18
VI	0.091	0.132	44.62	0.104	0.124	18.88	0.176	0.242	37.66	0.269	0.377	39.84	0.196	0.375	91.04	0.297	0.452	51.94

Table 3.1 Continued

Deformation Level	Parkfield																	
	F2S2B			F4S3B			F5S2B			F5S4B			F5S7B			F8S3B		
	Δ_{max} (m)		Error (%)	Δ_{max} (m)		Error (%)	Δ_{max} (m)		Error (%)	Δ_{max} (m)		Error (%)	Δ_{max} (m)		Error (%)	Δ_{max} (m)		Error (%)
	TH	SDOF		TH	SDOF		TH	SDOF		TH	SDOF		TH	SDOF		TH	SDOF	
I	0.026	0.032	22.89	0.010	0.010	2.60	0.034	0.033	1.32	0.073	0.072	0.77	0.042	0.042	0.76	0.081	0.076	6.24
II	0.042	0.046	9.53	0.019	0.019	4.11	0.040	0.051	27.73	0.112	0.112	0.01	0.070	0.067	5.21	0.113	0.109	3.41
III	0.051	0.067	31.45	0.037	0.040	7.61	0.087	0.090	3.13	0.149	0.159	6.08	0.088	0.072	17.58	0.205	0.242	18.29
IV	0.054	0.070	27.73	0.048	0.029	39.22	0.097	0.092	5.14	0.169	0.171	1.57	0.103	0.093	9.11	0.229	0.288	26.08
V	0.085	0.126	47.80	0.129	0.163	26.71	0.138	0.096	30.55	0.195	0.236	20.75	0.116	0.112	3.33	0.593	0.471	20.56
VI	0.091	0.140	53.89	0.172	0.179	4.02	0.153	0.107	30.48	0.209	0.260	24.73	0.127	0.127	0.36	0.741	0.582	21.50
Deformation Level	El Centro 79a																	
	F2S2B			F4S3B			F5S2B			F5S4B			F5S7B			F8S3B		
	Δ_{max} (m)		Error (%)	Δ_{max} (m)		Error (%)	Δ_{max} (m)		Error (%)	Δ_{max} (m)		Error (%)	Δ_{max} (m)		Error (%)	Δ_{max} (m)		Error (%)
	TH	SDOF		TH	SDOF		TH	SDOF		TH	SDOF		TH	SDOF		TH	SDOF	
I	0.025	0.032	29.96	0.009	0.010	6.80	0.035	0.035	0.32	0.076	0.075	1.48	0.041	0.041	1.00	0.089	0.079	11.80
II	0.036	0.047	29.77	0.020	0.012	38.66	0.047	0.048	2.80	0.112	0.080	29.03	0.069	0.068	1.46	0.130	0.107	18.09
III	0.043	0.060	40.86	0.050	0.046	7.24	0.069	0.099	42.98	0.146	0.135	7.55	0.082	0.102	25.42	0.136	0.125	7.82
IV	0.047	0.059	25.68	0.060	0.052	13.57	0.083	0.117	39.89	0.147	0.148	0.15	0.100	0.140	40.14	0.253	0.185	26.69
V	0.066	0.073	11.12	0.148	0.182	23.11	0.138	0.123	10.88	0.162	0.166	2.80	0.169	0.140	17.09	0.569	0.289	49.16
VI	0.074	0.077	3.81	0.199	0.209	5.21	0.149	0.131	12.30	0.171	0.171	0.01	0.185	0.143	22.90	0.679	0.384	43.39
Deformation Level	El Centro 79b																	
	F2S2B			F4S3B			F5S2B			F5S4B			F5S7B			F8S3B		
	Δ_{max} (m)		Error (%)	Δ_{max} (m)		Error (%)	Δ_{max} (m)		Error (%)	Δ_{max} (m)		Error (%)	Δ_{max} (m)		Error (%)	Δ_{max} (m)		Error (%)
	TH	SDOF		TH	SDOF		TH	SDOF		TH	SDOF		TH	SDOF		TH	SDOF	
I	0.024	0.032	34.64	0.011	0.010	8.65	0.034	0.033	1.91	0.074	0.076	3.51	0.039	0.041	3.70	0.080	0.078	2.90
II	0.038	0.047	22.85	0.017	0.020	19.55	0.045	0.047	4.90	0.112	0.112	0.24	0.069	0.076	9.59	0.117	0.121	3.01
III	0.047	0.058	23.54	0.060	0.070	16.89	0.087	0.087	0.03	0.176	0.170	2.91	0.088	0.110	24.97	0.314	0.249	20.72
IV	0.050	0.056	12.04	0.065	0.073	12.67	0.091	0.094	3.54	0.195	0.202	3.22	0.096	0.133	38.06	0.347	0.265	23.70
V	0.077	0.081	4.78	0.135	0.101	25.52	0.118	0.129	9.32	0.350	0.375	7.11	0.172	0.179	4.40	0.424	0.313	26.22
VI	0.088	0.089	1.08	0.154	0.112	27.37	0.138	0.139	0.73	0.388	0.390	0.48	0.188	0.195	3.95	0.487	0.344	29.33

Table 3.1 Continued

Chi-Chi

Deformation Level	F2S2B			F4S3B			F5S2B			F5S4B			F5S7B			F8S3B		
	Δ_{max} (m)		Error (%)	Δ_{max} (m)		Error (%)	Δ_{max} (m)		Error (%)	Δ_{max} (m)		Error (%)	Δ_{max} (m)		Error (%)	Δ_{max} (m)		Error (%)
	TH	SDOF		TH	SDOF		TH	SDOF		TH	SDOF		TH	SDOF		TH	SDOF	
I	0.035	0.027	23.67	0.011	0.011	3.01	0.034	0.033	0.69	0.077	0.078	1.33	0.039	0.041	5.21	0.076	0.078	1.37
II	0.049	0.042	15.54	0.020	0.026	30.36	0.057	0.064	11.29	0.103	0.121	17.71	0.069	0.077	10.97	0.111	0.107	3.80
III	0.063	0.047	25.65	0.052	0.057	10.21	0.100	0.102	2.00	0.138	0.176	27.66	0.093	0.104	11.57	0.174	0.219	25.29
IV	0.068	0.052	23.62	0.062	0.070	14.08	0.111	0.118	6.60	0.171	0.197	14.67	0.112	0.124	10.77	0.189	0.244	29.21
V	0.076	0.110	44.11	0.128	0.128	0.20	0.127	0.191	50.24	0.253	0.244	3.89	0.162	0.240	48.39	0.511	0.405	20.80
VI	0.075	0.125	66.47	0.154	0.134	13.29	0.143	0.185	29.71	0.301	0.302	0.45	0.166	0.269	62.24	0.533	0.632	18.58

Northridge-Pacoima

Deformation Level	F2S2B			F4S3B			F5S2B			F5S4B			F5S7B			F8S3B		
	Δ_{max} (m)		Error (%)	Δ_{max} (m)		Error (%)	Δ_{max} (m)		Error (%)	Δ_{max} (m)		Error (%)	Δ_{max} (m)		Error (%)	Δ_{max} (m)		Error (%)
	TH	SDOF		TH	SDOF		TH	SDOF		TH	SDOF		TH	SDOF		TH	SDOF	
I	0.025	0.032	28.54	0.010	0.010	0.40	0.034	0.035	2.29	0.076	0.076	0.19	0.041	0.042	2.29	0.080	0.076	5.15
II	0.036	0.042	14.29	0.020	0.021	7.77	0.048	0.052	9.64	0.111	0.109	1.53	0.068	0.071	4.19	0.132	0.107	19.26
III	0.051	0.066	28.94	0.031	0.048	52.63	0.090	0.095	6.01	0.139	0.145	4.27	0.080	0.090	11.75	0.236	0.173	26.89
IV	0.058	0.076	31.34	0.045	0.069	53.09	0.101	0.103	1.55	0.146	0.148	0.95	0.107	0.113	6.09	0.252	0.184	27.09
V	0.089	0.121	35.79	0.072	0.148	106.10	0.135	0.163	21.19	0.185	0.181	2.07	0.156	0.160	2.13	0.563	0.258	54.13
VI	0.095	0.133	40.11	0.079	0.142	79.29	0.143	0.172	20.43	0.196	0.208	6.28	0.170	0.163	4.07	0.567	0.330	41.83

Cape Mendocino

Deformation Level	F2S2B			F4S3B			F5S2B			F5S4B			F5S7B			F8S3B		
	Δ_{max} (m)		Error (%)	Δ_{max} (m)		Error (%)	Δ_{max} (m)		Error (%)	Δ_{max} (m)		Error (%)	Δ_{max} (m)		Error (%)	Δ_{max} (m)		Error (%)
	TH	SDOF		TH	SDOF		TH	SDOF		TH	SDOF		TH	SDOF		TH	SDOF	
I	0.033	0.028	13.93	0.011	0.010	9.44	0.033	0.032	2.93	0.101	0.076	24.35	0.041	0.041	1.11	0.070	0.076	9.26
II	0.046	0.043	6.42	0.025	0.024	4.74	0.049	0.043	11.52	0.155	0.116	25.55	0.071	0.069	2.06	0.104	0.112	7.57
III	0.054	0.048	10.97	0.064	0.088	37.66	0.067	0.067	0.05	0.161	0.173	7.47	0.083	0.089	6.47	0.238	0.249	4.80
IV	0.058	0.049	14.13	0.073	0.095	29.50	0.077	0.084	10.24	0.147	0.206	40.37	0.111	0.122	9.43	0.266	0.272	2.19
V	0.067	0.065	3.31	0.091	0.138	51.67	0.100	0.113	12.85	0.340	0.477	40.03	0.141	0.189	33.98	0.341	0.335	1.69
VI	0.069	0.067	3.14	0.082	0.126	53.76	0.106	0.131	23.80	0.350	0.488	39.19	0.152	0.200	31.64	0.356	0.337	5.33

Table 3.1 Continued

Deformation Level	Northridge																	
	F2S2B			F4S3B			F5S2B			F5S4B			F5S7B			F8S3B		
	Δ_{max} (m)		Error (%)	Δ_{max} (m)		Error (%)	Δ_{max} (m)		Error (%)	Δ_{max} (m)		Error (%)	Δ_{max} (m)		Error (%)	Δ_{max} (m)		Error (%)
	TH	SDOF		TH	SDOF		TH	SDOF		TH	SDOF		TH	SDOF		TH	SDOF	
I	0.025	0.029	15.99	0.011	0.010	8.93	0.034	0.035	2.15	0.078	0.078	0.17	0.037	0.041	8.34	0.078	0.078	0.22
II	0.036	0.046	26.13	0.017	0.024	34.94	0.042	0.061	46.97	0.123	0.124	0.39	0.066	0.078	18.67	0.117	0.112	4.12
III	0.058	0.062	6.88	0.045	0.073	63.67	0.069	0.159	131.16	0.157	0.151	3.85	0.084	0.090	6.36	0.153	0.228	49.06
IV	0.059	0.070	17.37	0.053	0.090	70.28	0.071	0.145	103.28	0.171	0.189	10.55	0.094	0.107	13.47	0.190	0.245	29.25
V	0.061	0.103	68.99	0.101	0.097	4.18	0.091	0.206	125.69	0.212	0.323	52.37	0.114	0.162	42.77	0.323	0.299	7.33
VI	0.068	0.133	95.49	0.119	0.106	10.40	0.185	0.335	81.16	0.239	0.349	45.99	0.126	0.182	44.30	0.363	0.333	8.45

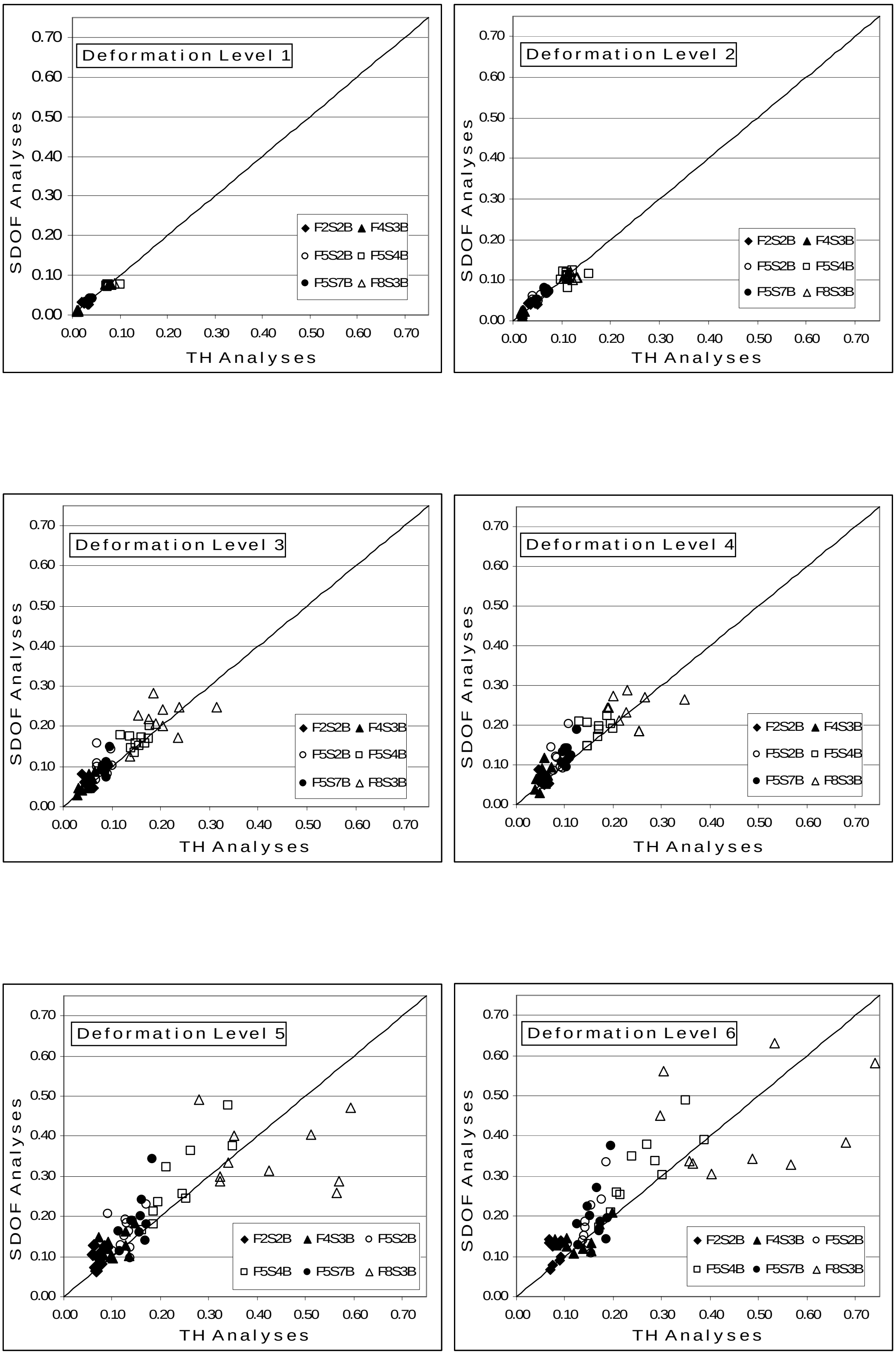

Figure 3.9: SDOF System – Time-History Analysis Comparison

In Figures 3.3-3.8, a clear trend is that the initial stiffness of the structures decreases as the damage level due to prior earthquake increases. This is an expected result because a higher damage level will cause an increase in both the number of yielding elements and the amount of plastic rotation that the elements experience. As the number of elements going into the inelastic range increases, there will be more elements whose moment of inertia is decreased thus leading to a softer structure. Moreover, greater plastic rotations decrease the modification factor leading to smaller moment of inertia and thus a less stiff structure.

Additionally at higher deformation levels there are more elements which have exhausted some of their plastic deformation capacity therefore the damaged structures are not able to deform as much as their undamaged counterparts. This can be observed from the decrease in the ultimate roof displacement for the damaged state capacity curves.

The capacity curve of the damaged structure is expected to converge to that of the undamaged structure at the performance point. In general it can be said that this tendency is achieved in the frames analyzed. In all frames, except frame "F2S2B" the damaged capacity curve merges the undamaged capacity curve in the vicinity of the performance point.

Table 3.1 and Figure 3.9 compare the displacement demands obtained for the damaged structure using time-history analyses and Procedure 1. A large discrepancy for individual earthquakes at high levels of damage is observed. This percentage error is generally within 30 percent when all the results are averaged as shown in Table 3.2 and Figure 3.9. Since all approximate procedures are intended to provide satisfactory results on the average, the observed error margins are considered to be within acceptable limits.

Table 3.2 Mean of Percentage Errors for Damaged Structure

Deformation Level	F2S2B	F4S3B	F5S2B	F5S4B	F5S7B	F8S3B
I	27.26	5.46	1.82	3.77	3.85	4.69
II	18.45	20.62	12.86	9.60	8.49	8.05
III	31.27	28.46	29.52	12.96	20.54	21.59
IV	27.67	39.13	31.46	15.37	24.75	20.40
V	37.42	30.01	35.63	18.59	30.35	28.09
VI	42.43	26.68	28.95	19.25	31.93	32.96

In Procedure 1, the residual displacement and unloading stiffness of the member load-deformation relationships were included through the use of the secant stiffness. This assumption has been tested in Figure 3.10. Firstly the unloading stiffness of the equivalent SDOF system was considered to be equal to its initial stiffness. The ground motions were applied to the undamaged SDOF system and the residual displacement was recorded. This residual displacement was added to the undamaged SDOF maximum displacement. This total displacement was compared with the SDOF results obtained using the capacity curve from Procedure 1. As can be seen from Figure 3.10 and Appendix A5 there is large scatter in the results. The assumption employed in this study assumes a ratio of 1.00 shown by the dashed line. This assumption seems reasonable when compared to the mean of the data computed as 1.05 and shown with the solid line in the figure. Procedure 1 proposed here may be used for a given seismic effect represented by a response spectrum so the inclusion of residual displacement that requires a ground motion record is not possible in this case.

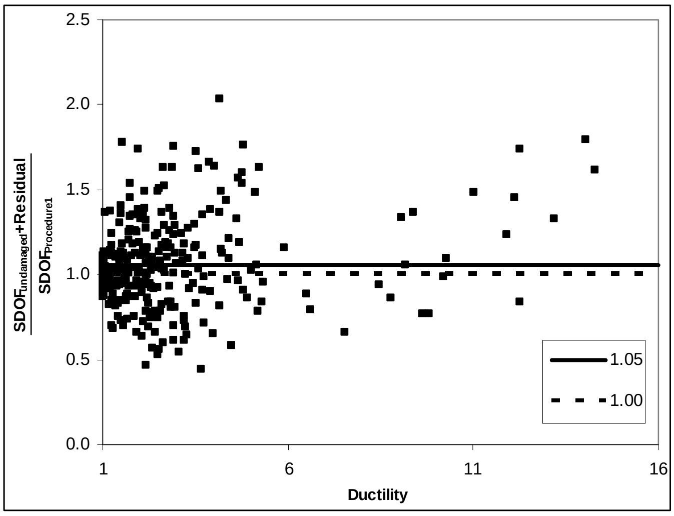

Figure 3.10: Inclusion of Residual Displacement

3.2.2 Procedure 2

The procedure described in the previous section produces quite satisfying results. A disadvantage of this method is that it is not very easy to implement. Determining the yield and plastic rotations and modifying the stiffness of every single yielding element can be very cumbersome especially for large structures, which have a large number of elements. In order to find a simpler procedure, which has a more practical implementation and can thus be used for more general purposes, the results of the analyses presented in the previous sections will be examined now. The rationale of this simplified method relies on the idea that the reduction in the stiffness of the structure experiencing an earthquake should be expressed in relation to the damage level the structure will suffer. Based on this thought the reduction factor will be defined in proportion to the performance point of the structure subjected to the prior earthquake. The displacement demands at the performance point of each frame are normalized by the yield point of the capacity curve of the undamaged structure. To facilitate the coherence of the determination of the yield point of the capacity curve, the bilinear form of the curve will be used. As proposed previously the method utilized in this study is the procedure recommended by FEMA273 [13]. The ratio of the displacement at the performance point to the displacement at the yield point, which can also be termed as the ductility demand, will be used as the normalized displacement in this simplified procedure.

As a next step it has to be determined, given the ductility demand of the performance point, by what proportion has the global stiffness of the structure to be decreased. At this point there are two alternatives available, which are going to be explored next. One alternative is using the secant stiffness at the performance point and modifying the rigidities of all elements of the structure in relation to the ratio of the secant stiffness to the initial stiffness of the capacity curve. In Figure 3.11 the line “Secant Slope” joins the performance point and the origin. In order to attain the curve “Secant Stiffness”, the slope of line ”Secant Slope” is divided by the initial slope of the undamaged capacity curve and the modulus of elasticity of the structure is multiplied by this factor. The capacity curve obtained from the analysis of this structure is the curve “Secant Stiffness”.

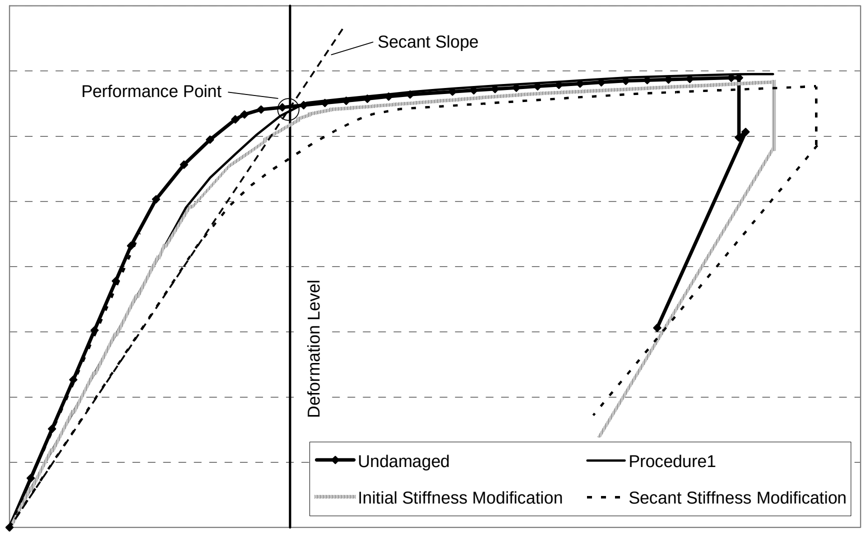

Figure 3.11: Alternatives of Global Stiffness Modification

The second alternative that is going to be investigated is to use the initial slope of the curve obtained from Procedure 1. The resulting curve after the detailed analysis explained in the previous section is the curve named as “Procedure 1” in Figure 3.11. In order to obtain the curve “Initial Stiffness”, in a similar manner to the first alternative, the slope of line ”Procedure 1” is divided by the initial slope of the undamaged capacity curve and the modulus of elasticity of the material of the structure is multiplied by this factor. Again the structure is analyzed after this modification is made and the resulting capacity curve is the curve “Initial Stiffness”.

The curves in Figure 3.11 clearly demonstrate that the initial stiffness alternative produces much better results than the secant stiffness alternative. In order to quantify the difference between these two alternatives, frame “F5S4B” is analyzed by the equivalent SDOF system approach and the resulting displacements are summarized in Table 3.3. The results obtained from the solution of Procedure 1 are the reference values against which the results of the initial stiffness and secant stiffness alternatives are compared because the aim is to find a simplified method which will not require the cumbersome modification of this method.

Table 3.3 Comparison of Alternatives for Procedure 2

Düzce									
Deformation Level	Procedure 1		Initial Stiffness			Secant Stiffness			
	Δ	V_{base}	Δ	V_{base}	Error (%)	Δ	V_{base}	Error	Error (%)
I	0.076	2305.769	0.076	2292.07	0.05	0.076	2265.80	0.000	0.05
II	0.104	2890.210	0.105	2885.60	0.77	0.100	2647.53	0.003	3.10
III	0.159	3207.938	0.167	3116.19	5.64	0.151	3039.92	0.007	4.50
IV	0.193	3246.396	0.198	3127.28	3.00	0.201	3080.95	0.008	4.39
V	0.255	3327.241	0.240	3136.88	6.01	0.303	3101.50	0.048	18.61
VI	0.337	3372.078	0.347	3253.11	2.89	0.482	3291.76	0.145	43.02
Elcentro									
Deformation Level	Procedure 1		Initial Stiffness			Secant Stiffness			
	Δ	V_{base}	Δ	V_{base}	Error (%)	Δ	V_{base}	Error	Error (%)
I	0.074	2224.865	0.074	2211.65	0.05	0.072	2146.55	0.001	1.77
II	0.101	2816.102	0.102	2811.61	0.77	0.106	3093.70	0.005	4.75
III	0.177	3223.126	0.174	3123.63	1.61	0.173	3064.19	0.004	2.37
IV	0.210	3260.389	0.198	3127.28	5.42	0.182	3060.22	0.027	13.09
V	0.213	3293.285	0.214	3108.84	0.41	0.235	2961.09	0.021	10.03
VI	0.254	3287.976	0.268	3175.12	5.67	0.273	3033.76	0.020	7.78
Pacoima Dam									
Deformation Level	Procedure 1		Initial Stiffness			Secant Stiffness			
	Δ	V_{base}	Δ	V_{base}	Error (%)	Δ	V_{base}	Error	Error (%)
I	0.075	2265.317	0.075	2251.86	0.05	0.078	2305.55	0.003	3.62
II	0.117	3139.381	0.118	3111.64	0.77	0.123	3111.49	0.006	5.35
III	0.202	3243.740	0.204	3156.37	0.75	0.232	3130.93	0.030	14.67
IV	0.224	3272.230	0.228	3161.19	1.60	0.252	3137.25	0.028	12.36
V	0.363	3414.254	0.341	3247.64	5.88	0.399	3214.24	0.036	10.04
VI	0.377	3411.502	0.368	3274.26	2.13	0.440	3238.84	0.063	16.73
Parkfield									
Deformation Level	Procedure 1		Initial Stiffness			Secant Stiffness			
	Δ	V_{base}	Δ	V_{base}	Error (%)	Δ	V_{base}	Error	Error (%)
I	0.072	2184.413	0.072	2171.44	0.05	0.072	2146.55	0.000	0.05
II	0.112	3112.534	0.113	3106.06	0.77	0.115	3035.84	0.004	3.17
III	0.159	3207.938	0.159	3107.26	0.57	0.163	3053.57	0.005	3.10
IV	0.171	3229.174	0.176	3101.07	2.39	0.176	3052.81	0.004	2.39
V	0.236	3311.324	0.232	3128.47	1.45	0.339	3143.59	0.103	43.75
VI	0.260	3294.547	0.257	3164.55	1.11	0.398	3187.57	0.138	52.97
El Centro 79a									
Deformation Level	Procedure 1		Initial Stiffness			Secant Stiffness			
	Δ	V_{base}	Δ	V_{base}	Error (%)	Δ	V_{base}	Error	Error (%)
I	0.075	2265.317	0.075	2251.86	0.05	0.071	2106.80	0.004	5.31
II	0.080	2223.239	0.080	2219.69	0.77	0.070	1835.62	0.010	12.66
III	0.135	3188.409	0.134	3078.99	0.57	0.146	3033.86	0.011	8.37
IV	0.148	3209.799	0.149	3070.24	0.70	0.150	2951.81	0.002	1.60
V	0.166	3255.084	0.168	3058.37	1.09	0.132	1970.31	0.034	20.51
VI	0.171	3205.188	0.188	3095.81	9.54	0.146	2017.12	0.025	14.72
El Centro 79b									
Deformation Level	Procedure 1		Initial Stiffness			Secant Stiffness			
	Δ	V_{base}	Δ	V_{base}	Error (%)	Δ	V_{base}	Error	Error (%)
I	0.076	2305.769	0.076	2292.07	0.05	0.078	2305.55	0.001	1.80
II	0.112	3112.534	0.113	3106.06	0.77	0.114	3000.54	0.002	1.97
III	0.170	3217.702	0.172	3120.66	0.63	0.229	3127.90	0.059	34.43
IV	0.202	3253.931	0.212	3142.69	4.92	0.292	3181.69	0.090	44.77
V	0.375	3423.804	0.349	3256.06	6.79	0.373	3184.18	0.001	0.28
VI	0.390	3424.643	0.378	3283.51	3.01	0.386	3172.68	0.004	0.94

Table 3.3 Continued

Chi-Chi									
Deformation Level	Procedure 1		Initial Stiffness			Secant Stiffness			
	Δ	V_{base}	Δ	V_{base}	Error (%)	Δ	V_{base}	Error	Error (%)
I	0.078	2346.221	0.078	2332.28	0.05	0.080	2385.05	0.003	3.50
II	0.121	3143.253	0.122	3115.83	0.77	0.129	3116.97	0.008	6.31
III	0.176	3222.041	0.180	3129.59	2.18	0.174	3065.71	0.002	0.87
IV	0.197	3249.626	0.205	3134.98	4.33	0.228	3110.58	0.031	15.92
V	0.244	3317.691	0.236	3132.67	3.05	0.290	3086.47	0.046	19.09
VI	0.302	3336.598	0.299	3205.53	1.05	0.297	3063.53	0.005	1.50
Northridge-Pacoima									
Deformation Level	Procedure 1		Initial Stiffness			Secant Stiffness			
	Δ	V_{base}	Δ	V_{base}	Error (%)	Δ	V_{base}	Error	Error (%)
I	0.076	2305.769	0.076	2292.07	0.05	0.078	2305.55	0.001	1.80
II	0.109	3038.426	0.110	3033.58	0.77	0.110	2894.64	0.001	0.77
III	0.145	3197.088	0.150	3096.85	3.26	0.131	2741.10	0.014	9.65
IV	0.148	3209.799	0.154	3076.41	4.33	0.145	2846.39	0.003	2.02
V	0.181	3266.756	0.167	3056.96	7.67	0.189	2811.99	0.008	4.40
VI	0.208	3241.982	0.184	3091.85	11.69	0.202	2794.36	0.006	2.66
Cape Mendocino									
Deformation Level	Procedure 1		Initial Stiffness			Secant Stiffness			
	Δ	V_{base}	Δ	V_{base}	Error (%)	Δ	V_{base}	Error	Error (%)
I	0.076	2305.769	0.076	2292.07	0.05	0.076	2265.80	0.000	0.05
II	0.116	3138.090	0.117	3110.25	0.77	0.131	3119.70	0.016	13.51
III	0.173	3219.872	0.166	3114.71	4.00	0.224	3121.83	0.051	29.28
IV	0.206	3257.160	0.206	3136.53	0.30	0.268	3155.02	0.062	30.26
V	0.477	3506.573	0.456	3372.43	4.42	0.479	3307.44	0.002	0.43
VI	0.488	3523.200	0.493	3397.19	1.12	0.516	3333.11	0.028	5.79
Northridge									
Deformation Level	Procedure 1		Initial Stiffness			Secant Stiffness			
	Δ	V_{base}	Δ	V_{base}	Error (%)	Δ	V_{base}	Error	Error (%)
I	0.078	2346.221	0.078	2332.28	0.05	0.082	2424.81	0.004	5.22
II	0.124	3145.835	0.125	3118.62	0.77	0.126	3114.23	0.002	1.86
III	0.151	3201.428	0.149	3095.36	1.25	0.154	3042.96	0.003	2.30
IV	0.189	3243.167	0.176	3101.07	6.92	0.182	3060.22	0.006	3.37
V	0.323	3382.420	0.313	3216.80	3.18	0.371	3181.17	0.047	14.67
VI	0.349	3383.905	0.348	3254.43	0.19	0.399	3189.22	0.050	14.40

The error in percentage column in Table 3.3 represents the ratio of the difference in absolute terms to the displacement obtained from Procedure 1. The results in this table verify the conclusion of Figure 3.11 that the initial stiffness alternative is a better approximation to Procedure 1.

Another problem arises because the modification factors obtained from the initial stiffness approach are achieved by using the initial slope of the curve resulting from Procedure 1. This means that all steps of Procedure 1 have to be performed in order to utilize this alternative which of course is not rational. In order to come up with a more practical solution, the results of the analyses of the six frames that are summarized in Table 3.4 and plotted in Figure 3.12 are used.

Table 3.4 Analyses Results for Procudre1

Deformation Level	F2S2B			F4S3B			F5S2B		
	Δ_y= 0.043			Δ_y= 0.014			Δ_y= 0.043		
	Δ_{PP}	Δ_{PP}/Δ_y	K_e/K_i	Δ_{PP}	Δ_{PP}/Δ_y	K_e/K_i	Δ_{PP}	Δ_{PP}/Δ_y	K_e/K_i
I	0.029	0.677	0.900	0.010	0.699	0.978	0.033	0.770	0.998
II	0.044	1.016	0.805	0.019	1.310	0.830	0.049	1.125	0.912
III	0.055	1.262	0.716	0.042	2.970	0.573	0.082	1.894	0.691
IV	0.060	1.385	0.669	0.051	3.581	0.507	0.091	2.102	0.651
V	0.079	1.816	0.549	0.094	6.551	0.332	0.126	2.901	0.529
VI	0.086	1.970	0.517	0.111	7.774	0.290	0.137	3.167	0.498
Deformation Level	F5S4B			F5S7B			F8S3B		
	Δ_y= 0.103			Δ_y= 0.083			Δ_y= 0.111		
	Δ_{PP}	Δ_{PP}/Δ_y	K_e/K_i	Δ_{PP}	Δ_{PP}/Δ_y	K_e/K_i	Δ_{PP}	Δ_{PP}/Δ_y	K_e/K_i
I	0.076	0.742	0.997	0.041	0.489	1.000	0.076	0.686	1.000
II	0.107	1.042	0.919	0.071	0.856	0.939	0.109	0.977	0.961
III	0.153	1.485	0.814	0.093	1.116	0.851	0.182	1.638	0.747
IV	0.165	1.602	0.783	0.109	1.315	0.806	0.197	1.777	0.712
V	0.222	2.162	0.666	0.148	1.789	0.620	0.289	2.602	0.559
VI	0.240	2.331	0.638	0.160	1.926	0.575	0.334	3.009	0.506

In Table 3.4, the yield displacement of the idealized capacity curve (Δ_y), the displacement at the performance point (Δ_{PP}) and the ratio of these two values are presented. K_e/K_i is the ratio of the initial slope of the curve obtained through Procedure 1 to initial slope of the capacity curve of the undamaged structure. Figure 3.12 plots the K_e/K_i vs Δ_{PP}/Δ_y values.

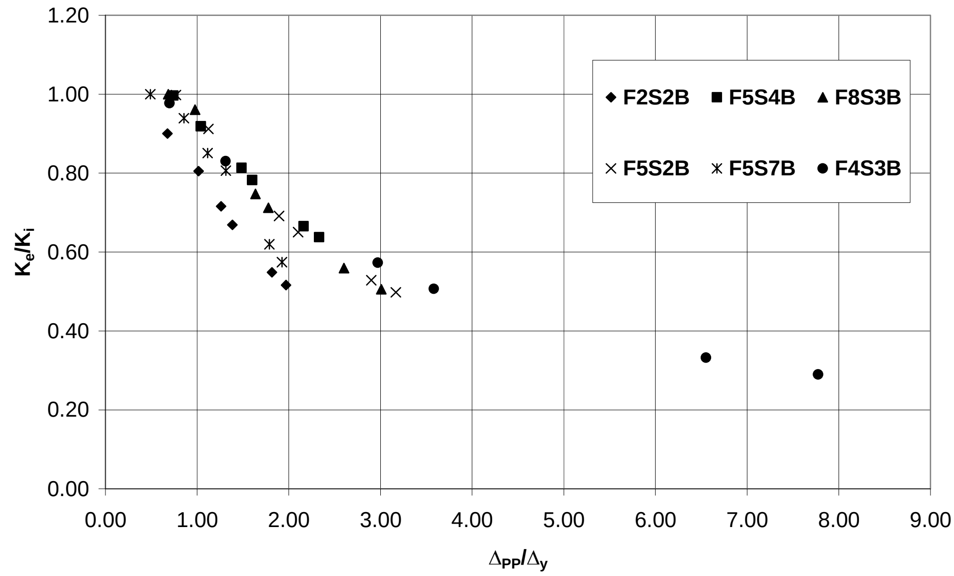

Figure 3.12: K_e/K_i vs Δ_{PP}/Δ_y Values for Frames Analyzed

It is evident that the last two K_e/K_i and Δ_{PP}/Δ_y pairs for Frame "F4S3B" correspond to very high ductility ratios. These pairs are clear outliers and therefore discarded from the analysis. The remaining pairs are re-plotted in Figure 3.13 together with the least sum of squares regression line.

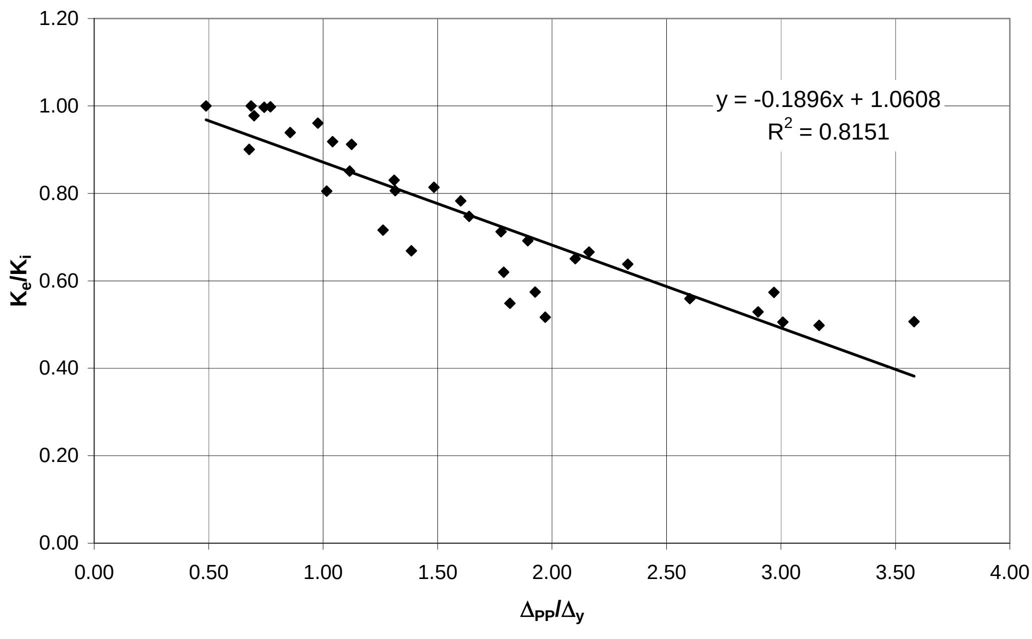

Figure 3.13: Best Fit for K_e/K_i vs Δ_{PP}/Δ_y values for Frames Analyzed

The regression analysis of these data yields the best fit trend line;

$$\frac{K_e}{K_i} = -0.1896\frac{\Delta_{PP}}{\Delta_y} + 1.0608$$

$$R^2 = 0.8151 \qquad 3\text{-}3$$

In this equation the ductility ratio (Δ_{PP}/Δ_y) is input as the abscissa and the ordinate yields the modification factor (K_e/K_i) by which the global stiffness has to be modified.

R^2 in Equation 3-3 is the coefficient of determination, which gives in percentage terms the total variation in the dependent variable that can be explained by the regression model. This means that 81.51% of the variation in the ordinate (K_e/K_i) can be explained by this regression model, which indicates that the model is very successful in estimating the reduction factor used to alter the stiffness of the structure.

This equation is valid for ductility ratios of approximately up to 3.5. The performance points selected in the analyses of this study were in the Immediate Occupancy–Life Safety performance state range, therefore the proposed equation also addresses to displacements in this range.

Procedure 2 is implemented by the following steps;

Step 1. Analyze the undamaged structure to obtain its capacity curve.

Step 2. Calculate the performance point and yield displacement using the curve obtained in Step 1.

Step 3. Use Equation 3-3 to compute the modification factor and multiply the modulus of elasticity of the undamaged structure with the modification factor to determine the modulus of elasticity of the damaged structure.

Step 4. Re-analyze the structure to obtain the capacity curve for the damaged structure.

Step 5. Use this capacity curve to determine the displacement demand under the presumed earthquake effect.

The proposed regression equation will next be applied to the frames to test the applicability of this easy to implement procedure (Procedure 2) and the results will be compared to those obtained by Procedure 1.

The modification factors obtained through Procedure 2 are given in Table 3.5.

Table 3.5 Modification Factors for Procedure 2

Deformation Level	F2S2B				F4S3B				F5S2B			
	Δ_y= 0.043		E_i= 28730.456		Δ_y= 0.014		E_i= 27400.093		Δ_y= 0.043		E_i= 28534.442	
	Δ_{PP}	Δ_{PP}/Δ_y	K_e/K_i	E_e	Δ_{PP}	Δ_{PP}/Δ_y	K_e/K_i	E_e	Δ_{PP}	Δ_{PP}/Δ_y	K_e/K_i	E_e
I	0.029	0.677	0.932	26787.683	0.010	0.699	0.928	25435.690	0.033	0.770	0.915	26105.575
II	0.044	1.016	0.868	24942.891	0.019	1.310	0.812	22259.153	0.049	1.125	0.848	24183.840
III	0.055	1.262	0.821	23601.223	0.042	2.970	0.498	13637.122	0.082	1.894	0.702	20020.079
IV	0.060	1.385	0.798	22930.390	0.051	3.581	0.382	10460.585	0.091	2.102	0.662	18899.067
V	0.079	1.816	0.716	20582.472	0.094	6.551			0.126	2.901	0.511	14575.161
VI	0.086	1.970	0.687	19743.930	0.111	7.774			0.137	3.167	0.460	13133.860
Deformation Level	F5S4B				F5S7B				F8S3B			
	Δ_y= 0.043		E_i= 27792.769		Δ_y= 0.043		E_i= 28534.442		Δ_y= 0.043		E_i= 27792.769	
	Δ_{PP}	Δ_{PP}/Δ_y	K_e/K_i	E_e	Δ_{PP}	Δ_{PP}/Δ_y	K_e/K_i	E_e	Δ_{PP}	Δ_{PP}/Δ_y	K_e/K_i	E_e
I	0.076	0.742	0.920	25571.262	0.041	0.489	0.968	27622.489	0.076	0.686	0.931	25870.257
II	0.107	1.042	0.863	23993.015	0.071	0.856	0.898	25637.354	0.109	0.977	0.875	24331.679
III	0.153	1.485	0.779	21659.954	0.093	1.116	0.849	24231.216	0.182	1.638	0.750	20853.155
IV	0.165	1.602	0.757	21042.379	0.109	1.315	0.812	23155.935	0.197	1.777	0.724	20117.314
V	0.222	2.162	0.651	18091.743	0.148	1.789	0.722	20591.802	0.289	2.602	0.567	15769.159
VI	0.240	2.331	0.619	17199.691	0.160	1.926	0.696	19847.376	0.334	3.009	0.490	13628.530

The last two deformation levels of F4S3B were excluded from the analysis due to their high ductility ratios. The proposed regression model is valid for ductility ratios up to 3.5 therefore these two levels are not applicable to the regression equation that is proposed.

In Figure 3.14, the capacity curves obtained by Procedure 1 and Procedure 2 are compared for each deformation level and Table 3.6 explores differences in the SDOF solution of the two procedures in order to quantify the differences of the results displayed in Figure 3.13. These comparisons were made only for frame F5S4B because the graphical representation of the capacity curves of the other frames illustrate similar results.

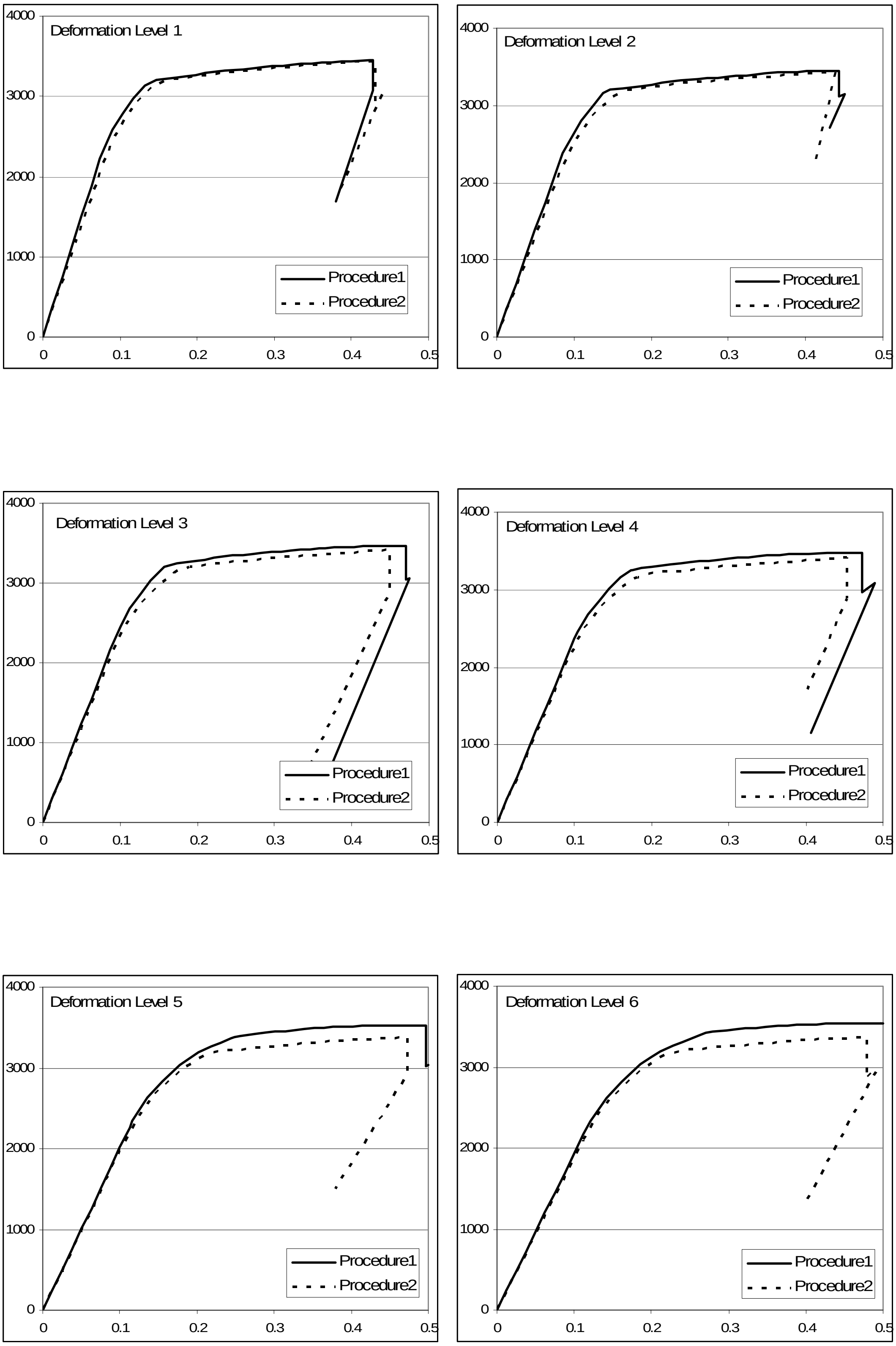

Figure 3.14: Graphical Comparison of Procedure 1 and Procedure 2

Table 3.6 Comparison of Procedure 1 and Procedure 2

Düzce

Deformation Level	Procedure 1		Procedure 2		Error (%)
	Δ_{max} (m)	Vmax (kN)	Δ_{max} (m)	Vmax (kN)	
I	0.076	2305.769	0.075	2095.839	1.71
II	0.104	2890.210	0.100	2645.565	3.10
III	0.159	3207.938	0.155	3106.649	1.97
IV	0.193	3246.396	0.193	3140.730	0.21
V	0.255	3327.241	0.253	3167.450	0.82
VI	0.337	3372.078	0.348	3246.373	3.29

Elcentro

Deformation Level	Procedure 1		Procedure 2		Error (%)
	Δ_{max} (m)	Vmax (kN)	Δ_{max} (m)	Vmax (kN)	
I	0.074	2224.865	0.071	1983.562	3.59
II	0.101	2816.102	0.106	2786.662	4.75
III	0.177	3223.126	0.184	3136.130	3.68
IV	0.210	3260.389	0.208	3155.991	0.95
V	0.213	3293.285	0.224	3138.453	4.84
VI	0.254	3287.976	0.267	3165.823	5.14

Pacoima Dam

Deformation Level	Procedure 1		Procedure 2		Error (%)
	Δ_{max} (m)	Vmax (kN)	Δ_{max} (m)	Vmax (kN)	
I	0.075	2265.317	0.082	2282.967	8.98
II	0.117	3139.381	0.123	3086.860	5.35
III	0.202	3243.740	0.212	3165.612	4.73
IV	0.224	3272.230	0.229	3178.189	2.20
V	0.363	3414.254	0.354	3266.304	2.48
VI	0.377	3411.502	0.371	3268.822	1.42

Parkfield

Deformation Level	Procedure 1		Procedure 2		Error (%)
	Δ_{max} (m)	Vmax (kN)	Δ_{max} (m)	Vmax (kN)	
I	0.072	2184.413	0.075	2095.839	3.75
II	0.112	3112.534	0.115	3033.581	3.17
III	0.159	3207.938	0.162	3113.668	2.26
IV	0.171	3229.174	0.174	3121.307	1.60
V	0.236	3311.324	0.240	3154.269	1.76
VI	0.260	3294.547	0.260	3159.220	0.08

El Centro 79a

Deformation Level	Procedure 1		Procedure 2		Error (%)
	Δ_{max} (m)	Vmax (kN)	Δ_{max} (m)	Vmax (kN)	
I	0.075	2265.317	0.060	1684.156	19.61
II	0.080	2223.239	0.068	1798.984	14.34
III	0.135	3188.409	0.141	3091.206	4.40
IV	0.148	3209.799	0.150	3096.334	1.60
V	0.166	3255.084	0.178	3093.639	7.16
VI	0.171	3205.188	0.185	3085.272	7.97

El Centro 79b

Deformation Level	Procedure 1		Procedure 2		Error (%)
	Δ_{max} (m)	Vmax (kN)	Δ_{max} (m)	Vmax (kN)	
I	0.076	2305.769	0.079	2208.116	3.56
II	0.112	3112.534	0.115	3033.581	3.17
III	0.170	3217.702	0.178	3130.515	4.56
IV	0.202	3253.931	0.216	3164.315	6.92
V	0.375	3423.804	0.366	3278.166	2.32
VI	0.390	3424.643	0.385	3282.027	1.29

Table 3.6 Continued

Deformation Level	Procedure 1		Procedure 2		Error (%)
Chi-Chi					
	Δ_{max} (m)	Vmax (kN)	Δ_{max} (m)	Vmax (kN)	
I	0.078	2346.221	0.086	2395.244	10.40
II	0.121	3143.253	0.129	3092.719	6.31
III	0.176	3222.041	0.178	3130.515	1.41
IV	0.197	3249.626	0.201	3149.054	2.29
V	0.244	3317.691	0.247	3160.859	1.23
VI	0.302	3336.598	0.300	3198.835	0.61
Northridge-Pacoima					
Deformation Level	Procedure 1		Procedure 2		Error (%)
	Δ_{max} (m)	Vmax (kN)	Δ_{max} (m)	Vmax (kN)	
I	0.076	2305.769	0.076	2133.264	0.05
II	0.109	3038.426	0.110	2892.485	0.77
III	0.145	3197.088	0.146	3096.822	0.49
IV	0.148	3209.799	0.151	3097.721	2.51
V	0.181	3266.756	0.174	3089.684	3.61
VI	0.208	3241.982	0.192	3091.874	7.82
Cape Mendocino					
Deformation Level	Procedure 1		Procedure 2		Error (%)
	Δ_{max} (m)	Vmax (kN)	Δ_{max} (m)	Vmax (kN)	
I	0.076	2305.769	0.083	2320.393	8.82
II	0.116	3138.090	0.131	3095.648	13.51
III	0.173	3219.872	0.185	3137.534	6.83
IV	0.206	3257.160	0.210	3158.766	2.26
V	0.477	3506.573	0.474	3384.929	0.48
VI	0.488	3523.200	0.496	3391.629	1.67
Northridge					
Deformation Level	Procedure 1		Procedure 2		Error (%)
	Δ_{max} (m)	Vmax (kN)	Δ_{max} (m)	Vmax (kN)	
I	0.078	2346.221	0.087	2432.670	12.12
II	0.124	3145.835	0.126	3089.790	1.86
III	0.151	3201.428	0.163	3115.072	8.53
IV	0.189	3243.167	0.188	3135.181	0.53
V	0.323	3382.420	0.322	3234.671	0.57
VI	0.349	3383.905	0.351	3249.014	0.58

In order to visualize the error distribution in a better way results of Procedure 1 are plotted against that of Procedure 2. Figure 3.15 clearly demonstrates that the SDOF solutions for the two procedures produce very close results.

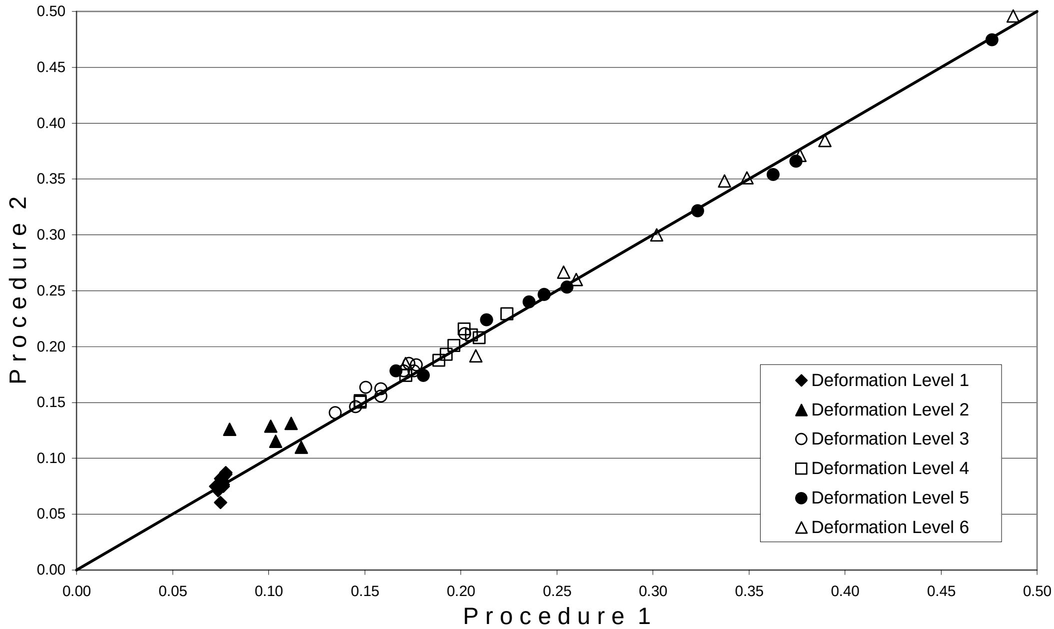

Figure 3.15: Comparison of Procedure 1 and Procedure 2

3.3 APPLICATION TO A CASE STUDY BUILDING

The above described procedures will now be applied to a real 3D building. The building will be analyzed for three differently scaled versions of the Düzce ground motion record. These scales correspond to performance points in the Immediate Occupancy – Life Safety performance levels as was the case for the previously analyzed frames. The building will at first be analyzed by the detailed procedure defined as "Procedure 1" in Section 3.1.1. Next the building is analyzed by the simplified method proposed in Section 3.1.2 and termed as "Procedure 2". The results of these two procedures will be compared in order to test the validity of the simplified procedure.

3.3.1 Description of the Building

The building is a real structure located in the city of Bursa in Turkey. It is a residential building and serves as an employee housing for a state agency. The building was designed and built in the 80s according to the 1975 Turkish Seismic

Code Specifications for Buildings to be Constructed in Disaster Areas. It is a five story building possessing a story height of 2.80 m, seven bays in the East-West (longitudinal) and three bays in the North-South (transverse) directions. Plan views of this building are presented in Figures 3.16 and 3.17.

The structure possesses 9 different column sections which are named S1 – S9. These columns are located as shown in the Figures 3.15-3.16. The reason for presenting the 1^{st} and 2 – 5^{th} story plans separately is that there is a reduction in cross sections of columns located at joints C2, C3, and C4. Columns S4, S5, and S6 of Story 1 change sections to become columns S8, S2, and S9 respectively in upper stories. All beams of the building are comprised of the same cross section. A detailed plot of the section properties of the columns and beams is presented in Appendix A6.

The material properties for this building, determined by the survey team investigating the as-built properties are as given below;

E = 23750 MPa, f_y = 220 MPa, f_c = 9 MPa,

The calculated natural period of vibration for this structure is;

T_n = 0.7772 sec.

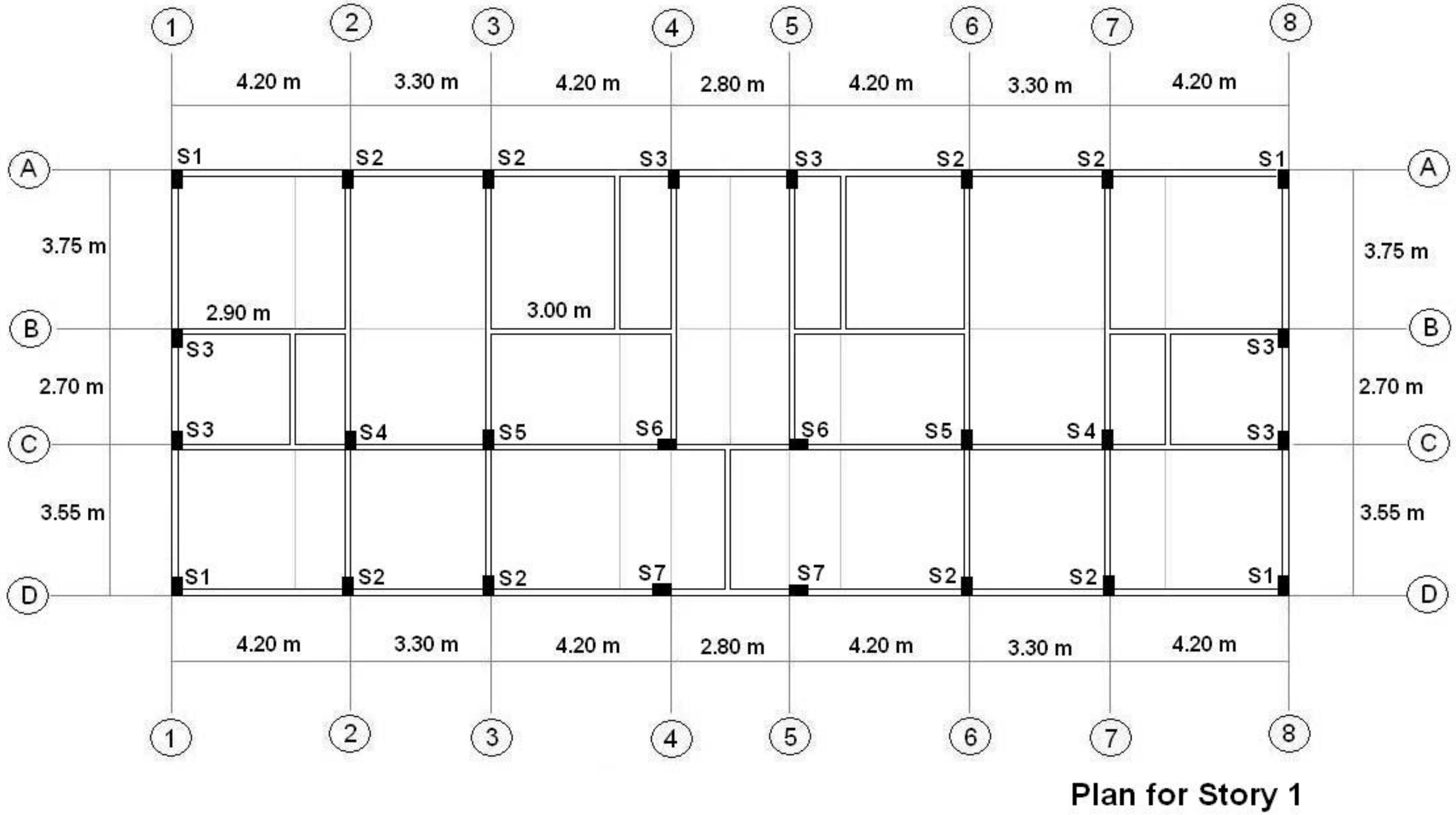

Figure 3.16: Story Plan for 1st Story

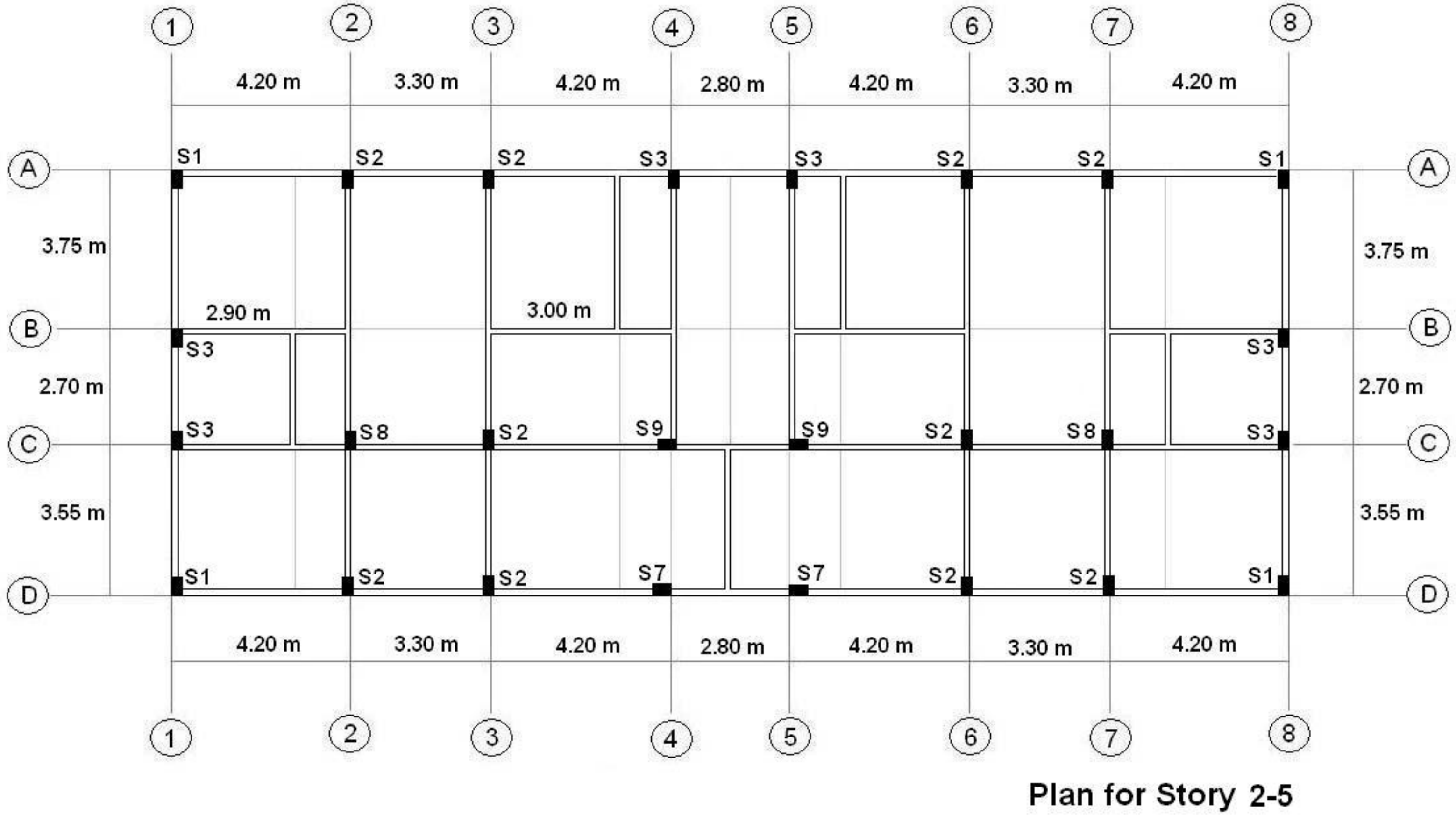

Figure 3.17: Story Plan for 2-5th Stories

The building was analyzed by the software SAP2000 [11] under the same modeling rules and assumptions given in Section 2.5.1 for the previously analyzed frames. For 3D structures, SAP2000 permits the definition of three dimensional interaction diagrams so that the axial load of the columns which is not constant can be updated. This is achieved by the definition of five axial force-moment interaction curves equally spaced at angles of 0°, 22.5°, 45°, 67.5°, and 90°. The curve at angle 0° corresponds to the minor moment (M2), whereas angle 90° corresponds to the major moment (M3). The curves in between are obtained by utilizing the following relation proposed by Parme et al. [18];

$$\left(\frac{Mux}{Mux_0}\right)^{\frac{\log 0.5}{\log\beta}}+\left(\frac{Muy}{Muy_0}\right)^{\frac{\log 0.5}{\log\beta}}=1 \qquad 3\text{-}4$$

where, Mux_o : Uniaxial flexural strength about the x-axis

Mux : Component of biaxial flexural strength on the x-axis at the required inclination.

Muy_o : Uniaxial flexural strength about the y-axis

Muy : Component of biaxial flexural strength on the y-axis at the required inclination.

β : Parameter dictating the shape of the interaction surface. This parameter takes a value of 0.7 for the ground, first, and second floor columns, and a value of 0.6 for the other columns of the structures in this study.

The values Mux_0 and Muy_0 correspond to the moments occurring at 0°, and 90°, or in other words to the minor and major moments respectively. The relation between M_{ux} and M_{uy} is as follows;

$$M_{uy} = M_{ux} \times \mathrm{Tan}(\alpha) \qquad 3\text{-}5$$

where, α : the angle of the interaction surface under consideration.

The equation given above is iterated for each angle and Mux_o and Muy_o values and the three dimensional interaction surfaces shown in Figure 3.18 are determined in this fashion.

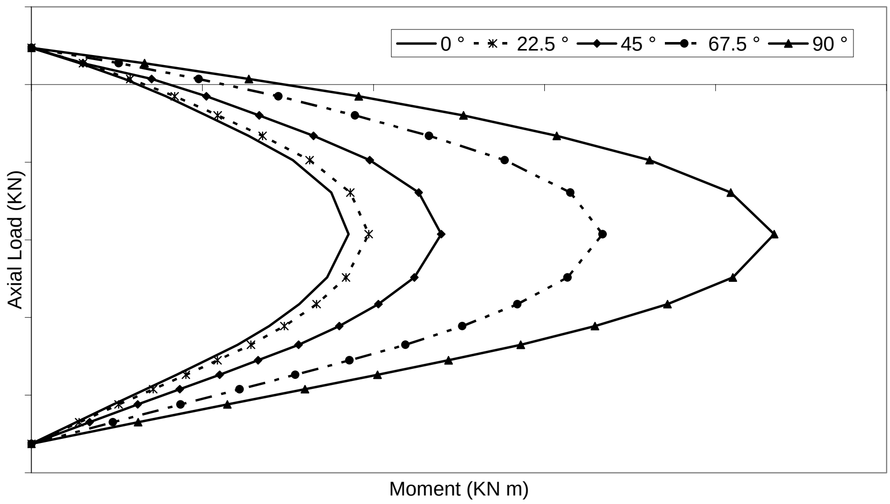

Figure 3.18: Interaction Surfaces for Columns

The nonlinear static analysis of the building in the x-direction produced the capacity curve shown in Figure 3.19. In this figure the chosen deformation levels are as well presented. Table 3.7 shows the earthquake scale factors corresponding to these deformation levels.

Table 3.7 Ground Motion Scale Factors Corresponding to the Deformation Levels Considered

Deformation Level	Düzce
I	0.05
II	0.13
III	0.21

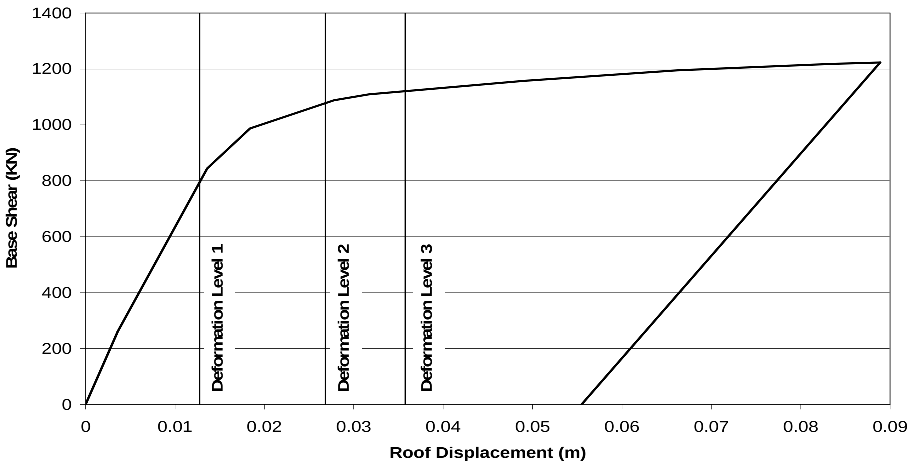

Figure 3.19: Capacity Curve of Undamaged Building and Deformation Levels

3.3.2 Interpretation of Results

3.3.2.1 Procedure 1

The application of the detailed procedure yielded the capacity curves given in Figure 3.20. In a similar manner as in Section 3.2.1, the solid and dashed lines represent the capacity curve of the undamaged and damaged structures respectively. In each graph the damaged capacity curves that stand for the deformation level specified by the vertical line are plotted.

The graphs in Figure 3.20 reveal similar results as those of the previously analyzed frames. The capacity curve shifts to the right as the degree of prior earthquake damage increases and intersects the initial capacity curve approximately at the performance point.

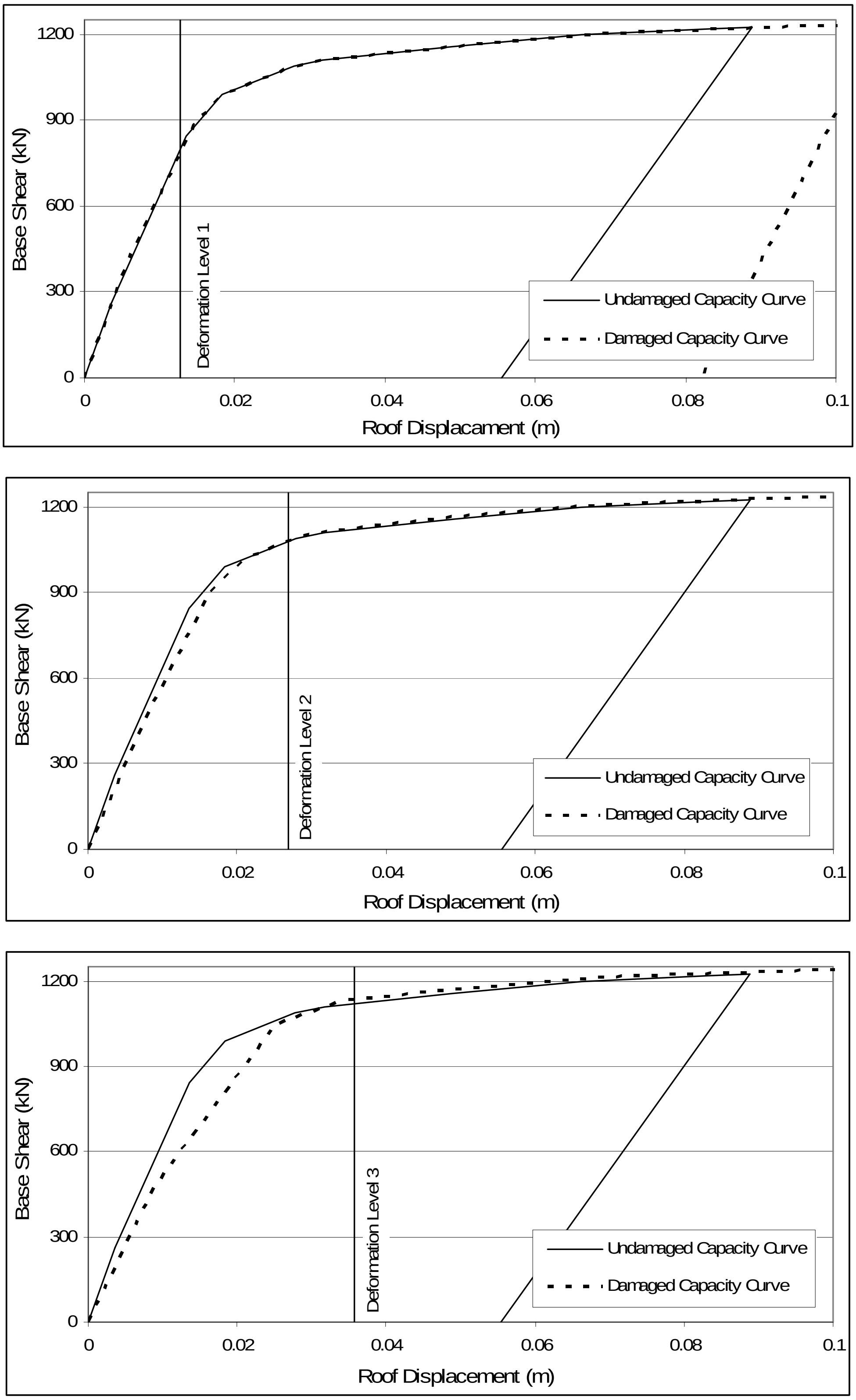

Figure 3.20: Undamaged and Damaged Capacity Curves of Case Building using Procedure 1

3.3.2.2 Procedure 2

In this section the simplified method proposed in Section 3.1.2 will be used to determine the change in building capacity during the three applied earthquakes. The regression equation used to determine the post earthquake stiffness is repeated in Equation 3-6;

$$\frac{K_e}{K_i} = -0.1896\frac{\Delta_{PP}}{\Delta_y} + 1.0608 \qquad \text{3-6}$$

This ratio will be used to identify the new modulus of elasticity of the whole structure as given in Equation 3-7;

$$E_e = E_i \times \frac{K_e}{K_i} \qquad \text{3-7}$$

The values used for the application of this procedure are summarized in Table 3.8.

Table 3.8 Application of Procedure 2

Deformation Level	Δ_y= 0.0168		E_i= 23750000	
	Δ_{PP}	Δ_{PP}/Δ_y	K_e/K_i	E_e
I	0.0128	0.7601	0.917	21771349
II	0.0268	1.5962	0.758	18006433
III	0.0358	2.1282	0.657	15610577

Results are visualized in Figure 3.21 in a similar manner as that for Procedure 1 in the previous section.

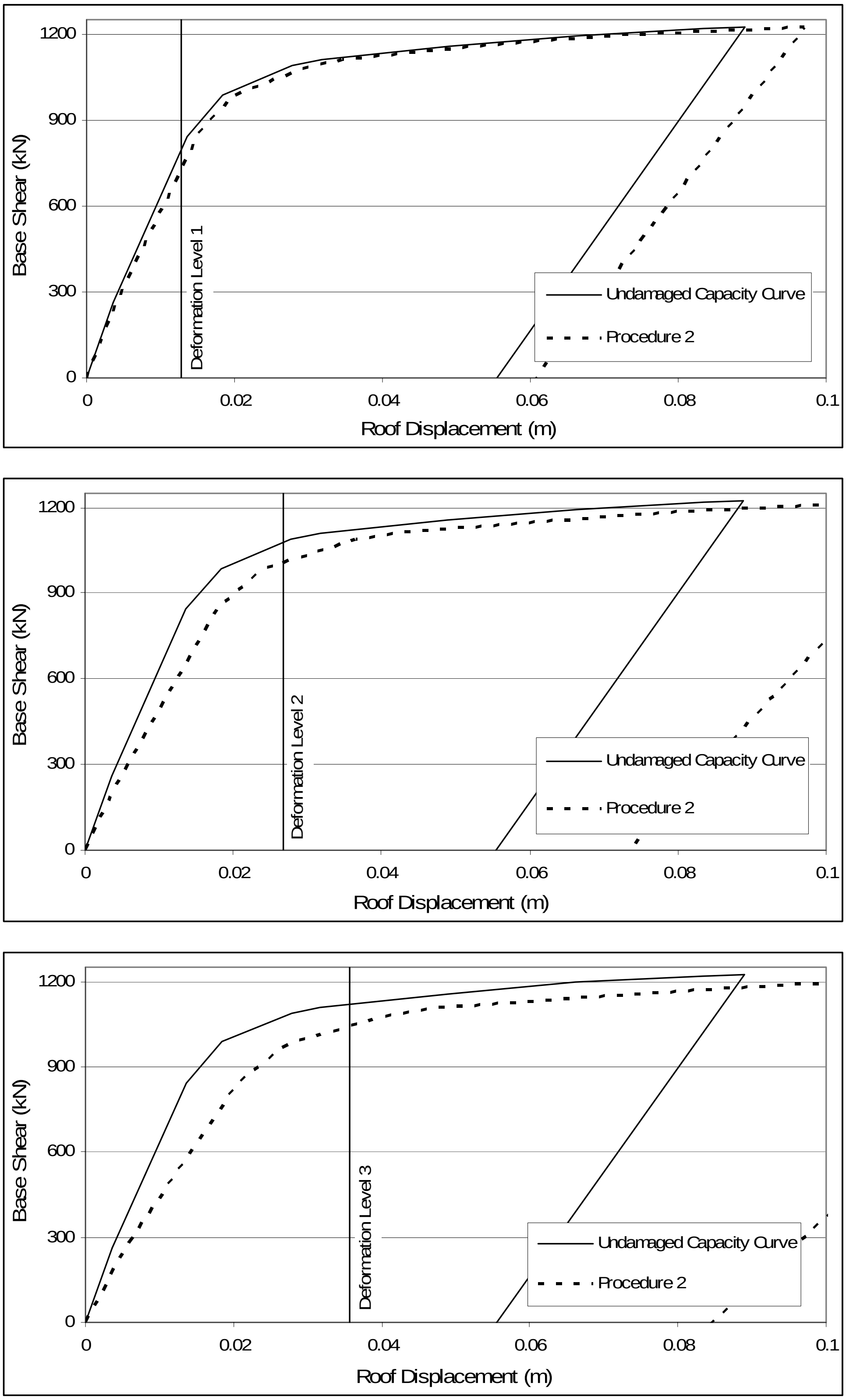

Figure 3.21: Undamaged and Damaged Capacity Curves of Case Building using Procedure 2

3.3.3 Comparison of Results

To test the validity of the simplified procedure on this 3D building the comparisons of results will be presented in this part of the study. This comparison will include Procedure 1 and Procedure 2 as well as the capacity curves by modifying the undamaged capacity curve based on the initial stiffness of the curve obtained in Procedure 1 in a similar manner as done in Section 3.2.2. This comparison has to be done because Procedure 2 is in fact an approximation of this curve. Comparisons will include graphical representations of the capacity curves identified by each method for each deformation level. The results are further explored by performing SDOF analyses of the building by using the bilinear representation of the capacity curves obtained through each method. Figure 3.22 visualizes the capacity curves obtained by each of the analysis methods separately for each scale. These graphs indicate that Procedure 2 approximates Procedure 1 quite well with no need for the detailed calculations performed. In fact Procedure 2 is the approximation for the dashed curve ”Initial Stiffness Procedure 1” which is obtained by changing the rigidity of the building by the ratio of the initial slope of the curve “Procedure1” to the initial slope of the “Undamaged Capacity Curve”. On the whole, in all cases the simplified procedure gives satisfying results. The base shear capacity appears to decrease when the simplified procedure is applied. This behavior is not anticipated and is believed to be due to the modifications in the stiffness of members leading to changes in the order of occurrence of plastic hinges. It can be seen that in all cases the graphs obtained through the simplified Procedure 2 form a lower bound therefore this method can be used as an alternative with confidence. In Table 3.9 the SDOF system properties defined for each method are given. Equivalent SDOF system representations of the building are characterized by these properties and analyzed to yield the results presented in Table 3.10. Finally in Table 3.11 the accuracy of Procedure 2 is compared against Procedure 1. The error term is calculated as given in Equation 3-8. Since Procedure 2 is the simplified method, results obtained through Procedure 1 form the reference values of this comparison.

$$\text{Error (\%)}=\frac{\left|\Delta_{\text{Procedure 2}}-\Delta_{\text{Procedure 1}}\right|}{\Delta_{\text{Procedure 1}}}\times 100 \qquad 3\text{-}8$$

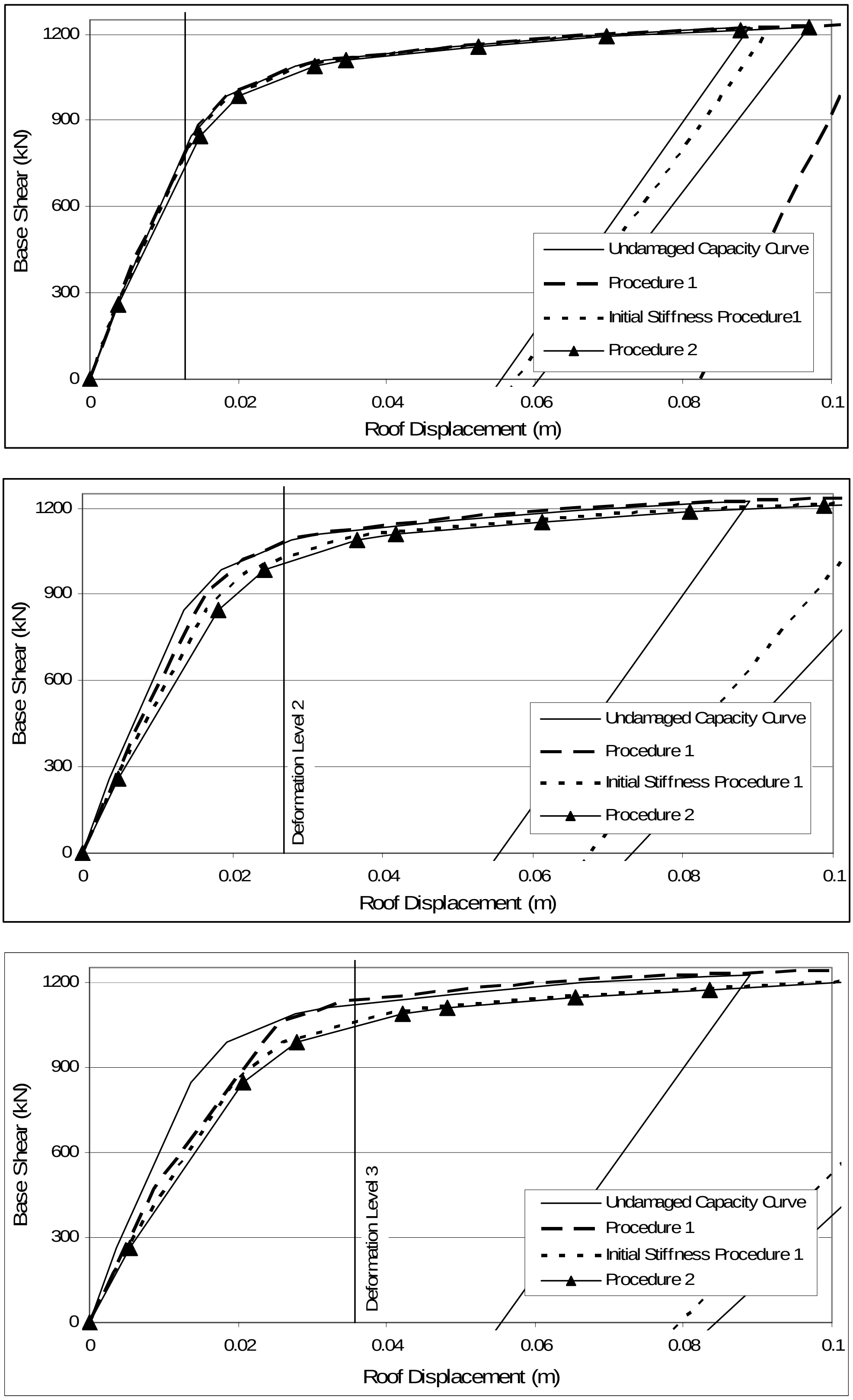

Figure 3.22: Comparison of Analysis Methods

Table 3.9 Force Displacement Relationships of SDOF System Representations of Analysis Methods

Deformation Level		T_{eff}(sec)	m*(ton)	k_1(kN/m)	k_2(kN/m)	F_y(kN)
	Undamaged	0.840	1436.61	80416.72	2924.76	1058
I	Procedure 1	0.844	1440.94	79863.19	1856.421	1105
	Initial Stiffness Procedure 1	0.851	1436.61	78304.21	2683.48	1067
	Procedure 2	0.879	1436.61	73458.28	2494.283	1070
II	Procedure 1	0.907	1460.11	70048.73	1095.476	1144
	Initial Stiffness Procedure 1	0.920	1436.61	66944.44	2389.944	1059
	Procedure 2	0.966	1436.61	60812.04	2165.971	1062
III	Procedure 1	1.009	1479.73	57395.26	597.426	1180
	Initial Stiffness Procedure 1	1.002	1436.61	56459.67	1900.406	1070
	Procedure 2	1.031	1436.61	53330.96	1840.806	1065

Table 3.10 Peak Roof Displacements and Base Shear Obtained by TH Analysis of Equivalent SDOF Systems

Deformation Level	Method	Δ_{max} (m)	V_{base} (kN)
I	Undamaged Curve	0.01277	804.17
	Procedure 1	0.01272	798.63
	Initial Stiffness Procedure 1	0.01277	783.04
	Procedure 2	0.01405	808.04
II	Undamaged Curve	0.02682	1080.94
	Procedure 1	0.03138	1153.50
	Initial Stiffness Procedure 1	0.03065	1078.55
	Procedure 2	0.03320	1080.49
III	Undamaged Curve	0.03575	1101.41
	Procedure 1	0.04358	1188.63
	Initial Stiffness Procedure 1	0.04597	1102.40
	Procedure 2	0.04469	1092.67

Table 3.11 Roof Displacement Comparison for Procedure 1 and Procedure 2

Deformation Level	Δ_{max} (m)		Error (%)
	Procedure 1	Procedure 2	
I	0.01272	0.01405	10.42
II	0.03138	0.03320	5.80
III	0.04358	0.04469	2.55

The structural damage is directly related to the inter-story drift ratio therefore the accurate estimation of the displacement profile and inter-story drift ratio together with its distribution along the height of the structure are very crucial for seismic performance evaluation purposes. Figure 3.23 plots the displacement profiles of the case building for the above mentioned methods and in Table 3.12 the inter-story drift ratios are presented.

Table 3.12 Inter Story Drift Ratios

Deformation Level 1				
h(m)	Undamaged	Procedure1	Initital Stiffness Procedure 1	Procedure2
0.00				
3.00	0.0009	0.0009	0.0009	0.0009
5.80	0.0023	0.0023	0.0023	0.0023
8.60	0.0034	0.0034	0.0034	0.0034
11.40	0.0042	0.0042	0.0042	0.0042
14.20	0.0046	0.0046	0.0046	0.0046
Deformation Level 2				
h(m)	Undamaged	Procedure1	Initital Stiffness Procedure 1	Procedure2
0.00				
3.00	0.0022	0.0022	0.0021	0.0021
5.80	0.0054	0.0054	0.0053	0.0052
8.60	0.0078	0.0078	0.0076	0.0075
11.40	0.0090	0.0090	0.0089	0.0089
14.20	0.0096	0.0096	0.0096	0.0096
Deformation Level 3				
h(m)	Undamaged	Procedure1	Initital Stiffness Procedure 1	Procedure2
0.00				
3.00	0.0033	0.0032	0.0029	0.0029
5.80	0.0076	0.0076	0.0071	0.0071
8.60	0.0106	0.0107	0.0103	0.0102
11.40	0.0122	0.0122	0.0120	0.0120
14.20	0.0128	0.0128	0.0128	0.0128

These data repeat the conclusion that Procedure 1 and Procedure 2 produce comparable results.

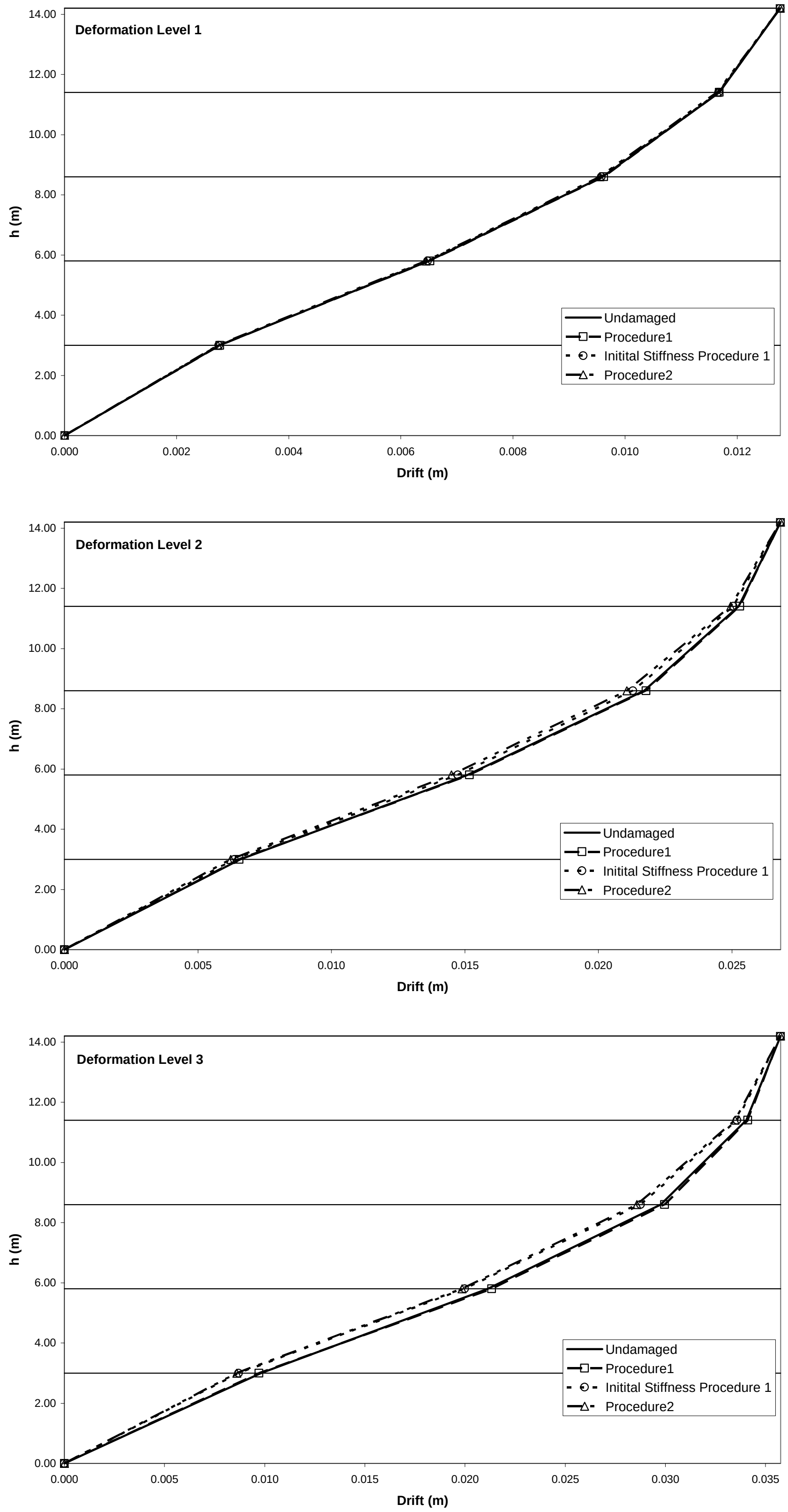

Figure 3.23: Displacement Profiles

CHAPTER 4

CONCLUSIONS AND RECOMMENDATIONS

4.1 SUMMARY

The aim of this study was to determine a procedure that can be used to assess the change in building capacity after experiencing an earthquake so that the probable damage of a second earthquake that hits the structure can be estimated. Six frames and ten randomly selected earthquakes were used for this aim. Initially the selected frames were analyzed by two widely accepted methods; the time-history analysis and the nonlinear static procedure, to identify the prior earthquake capacities of these frames. The base shear-roof displacement pairs obtained by the time-history analyses are compared with the capacity curve obtained by the nonlinear static procedure to confirm the reliability of the pushover procedure. The pushover procedure was performed with the aid of two software; DRAIN-2DX and SAP2000 in order to compare these two software.

After the verification of the analyses procedures and tools, a new method by which the post earthquake capacity of structures can be determined is proposed. This method was named Procedure 1 and in this method, the rigidities of the elements of the structure that go into post elastic states are altered with respect to the plastic deformation that they experience. After this modification the structure is re-analyzed to produce the capacity curve of the damaged structure.

Finally, based on the results of Procedure 1, a regression equation is derived, by which the rigidity of the whole structure is modified in accordance with the ductility ratio that the damaging earthquake implies on the structure. In this procedure, entitled as Procedure 2, the ratio of the performance point of the damaging earthquake to the yield displacement is entered as the independent variable to calculate the dependent variable which is the ratio of the rigidity of the damaged structure to the undamaged one.

4.2 CONCLUSIONS

The analyses procedures and software used throughout this study provided good opportunities to compare these procedures and software to come up with conclusions for the widely implemented nonlinear analyses methods. The procedures developed are intended to be used in the assessment of buildings subjected to prior earthquakes. The following set of conclusions can be drawn from the results of this study;

- The comparison of the capacity curves obtained by the two software DRAIN-2DX and SAP2000 showed that if identical hinge properties and element descriptions are used, these two software produce identical results. A drawback of DRAIN-2DX is that the deformation limits of single elements cannot be identified thus the capacity curve obtained by this software extends up to infinite displacements. If the maximum displacement that the structure can attain is of importance for the user, as was the case in this study, SAP2000 is a better analyses tool to be implemented.
- For the determination of the equivalent SDOF system that corresponds to the first mode shape of the original MDOF system it is required to approximate the capacity curve of the original building with a bilinear curve. The comparison of the three most widely used methods for this approximation; FEMA 273 Approach [13], Initial Stiffness Approach, and Secant Stiffness Approach, revealed the conclusion that using the Initial Stiffness Approach results in the most accurate representation when the base shear-top displacement pairs resulting from the time-history analyses of the MDOF system and SDOF system are compared.

- From the inspection of the time-history analyses results and the pushover curve obtained by nonlinear static analyses it can be concluded that the pushover curve results a lower bound to the exact solution indicating that this method is conservative.
- The SDOF analyses of the structure produce almost identical results with the time-history procedure at deformation levels in the elastic range or in close neighborhood to the yield point of the structure but this accuracy diminishes at points of higher ductility ratios. There could be no clear trend attributed to the amount of change in error because the error distribution seems to be dependent on the characteristics of the structure analyzed as well as on the damaging ground motion itself. But as a general trend, the examination of the mean error distribution designates that the error increases at higher deformation levels.
- The pushover curve of the damaged structure can be obtained by determining the amount of plastic rotation that elements of the undamaged structure will suffer and modifying the rigidity of each yielding member as outlined in this study.
- If the cumbersome calculations involved in Procedure 1 are not wanted to be undertaken, an approximate method based on the regression analysis performed in this study can be used. In this method, named as Procedure 2 in this study, the ductility ratio that the prior earthquake introduces on the structure is used to establish the modification factor by which the modulus of elasticity of the structure needs to be altered. The following equation gives the relationship proposed for the modification of the member rigidities

  $$\frac{K_e}{K_i}=-0.1896\frac{\Delta_{PP}}{\Delta_y}+1.0608$$

4.3 RECOMMENDATIONS FOR FUTURE STUDIES

The analyses in this study were limited to six frames and ten earthquakes. Although the results obtained and comparisons made showed satisfying results the analyses should be broadened to include more frames and ground motion data especially for the regression analysis performed. This study mainly stressed mid rise reinforced concrete buildings therefore future studies could be made to include low and high rise structures as well as steel and masonry buildings and walls.

REFERENCES

[1] Antoniou, S., Pinho, R., 2002, *Seismo Signal*, Seismo Soft Company.

[2] ATC, 1996, *Seismic Evaluation and Retrofit of Concrete Buildings, Applied Technology Council (ATC-40 Report)*, Vol. I, Redwood City, California

[3] ATC, 1998a, *Evaluation of Earthquake Damaged Concrete and Masonry Wall Buildings, Basic Procedures Manual, Applied Technology Council (ATC-43 Project)*, Federal Emergency Management Agency, Report No. FEMA-306, Washington D.C.

[4] ATC, 1998b, *Evaluation of Earthquake Damaged Concrete and Masonry Wall Buildings, Technical Resources, Applied Technology Council (ATC-43 Project)*, Federal Emergency Management Agency, Report No. FEMA-307, Washington D.C.

[5] Araki, H., Shimazu, T., and Ohta, K., 1990, *On Residual Deformation of Structures After Earthquakes, Proceedings of the Eight Japan Earthquake Engineering Symposium-1990*, Tokyo, Vol. 2, pp. 1581-1586. (In Japanese with English abstract)

[6] Aschheim, M., Black, E., 1999, *Effects of Prior Earthquake Damage on Response of Simple Stiffness-Degrading Structures*, Earthquake Spectra, Vol. 15, No. 1, pp. 1-24.

[7] Bazzurro, P., Cornell, A., Menun, C., Luco, N., Motahari, M., 2004, *Advanced Seismic Assessment Guidelines*, Pacific Gas & Electric (PG&E)/PEER Lifelines Program Task 507

[8] Bentz, E.C., 2000, *Sectional Analysis of Reinforced Concrete*, Ph.D. Thesis, Department of Civil Engineering, University of Toronto.

[9] Charney, F.A., *Nonlinear Dynamic Time History Analysis of Single Degree of Freedom Systems (NONLIN)*, Advanced Structural Concepts, Golden, Colorado and Schnabel Engineering, Denver, Colorado.

[10] Chopra, A.K., 1995, *Dynamics of Structures –Theory and Application to Earthquake Engineering*, Prentice Hall, New Jersey.

[11] Computers and Structures Inc. (CSI), 1998, *SAP2000 Three Dimensional Static and Dynamic Finite Element Analysis and Design of Structures V7.40*, Berkeley, California.

[12] Çeçen, H., 1979, *Response of Ten-Story Reinforced Concrete Model Frames to Simulated Earthquakes*, Ph.D. Thesis, Department of Civil Engineering, University of Illinois at Urbana.

[13] Federal Emergancy Management Agency (FEMA), 1997, *NEHRP Guidelines for the Seismic Rehabilitation of Buildings*, FEMA-273.

[14] Gülkan, P., Sözen, M.A., 1974, *Inelastic Response of Reinforced Concrete Structures to Earthquake Ground Motions*, Journal of the American Concrete Institute, Vol. 71, pp. 601-609.

[15] Hanson, R.D., 1996, *The Evaluation of Reinforced Concrete Members Damaged by Earthquakes*, Earthquake Spectra, Vol. 12, No. 3, Earthquake Engineering Research Institute, Oakland, California.

[16] International Conference on Building Officials (ICBO), 1982, *Uniform Building Code*, Whittier, CA.

[17] Park, R., Paulay, T., 1975, *Reinforced Concrete Structures*, John Wiley and sons, Inc, pp. 769.

[18] Parme, A.L., Nieves, J.M., Gouwens, A., 1966, *Capacity of Reinforced Rectangular Columns Subject to Biaxial Bending*, Journal of the American Concrete Institute, Vol. 63, pp. 911-923.

[19] Powell, G.H., 1993, *Drain-2DX Element Description and User Guide for Elements*, Structural Engineering Mechanics and Materials Report No. 93/18, University of California, California

[20] Prakash, V., Powell, G.H., Campbell, S., 1993, *Drain-2DX Base Program Description and User Guide*, Structural Engineering Mechanics and Materials Report No. 93/17, University of California, California.

[21] Saidii, M., Sözen, M.A., 1981, *Simple Nonlinear Seismic Response of R/C Structures*, Journal of Structural Division, ASCE, Vol. 107, pp. 937-952.

[22] Sözen, M.A., 2000, *Measured Ground Shaking and Observed Damage: Do Recent Events Confirm a Direct Connection?*, Earthquake Engineering Frontiers in the Millennium, Proceedings of the China-US Millennium Symposium on Earthquake Engineering, 8-11 November 2000, Beijing, China, pp. 43-56.

[23] *Turkish Earthquake Code: Specifications for the Buildings to be Constructed in Earthquake Areas*, 1998, Ministry of Public Works and Settlement, Ankara, Turkey.

[24] Turkish Standards Institute, 2000, *TS500 – Requirements for Design and Construction of Reinforced Concrete Structures*, Ankara, Turkey.

[25] Wolschlag, C., 1993, *Experimental Investigation of the Response of R/C Structural Walls Subjected to Static and Dynamic Loading*, Ph.D. Thesis, Department of Civil Engineering, University of Illinois at Urbana.

APPENDIX

A.1 DESCRIPTION OF FRAMES

A.1.1 F2S2B

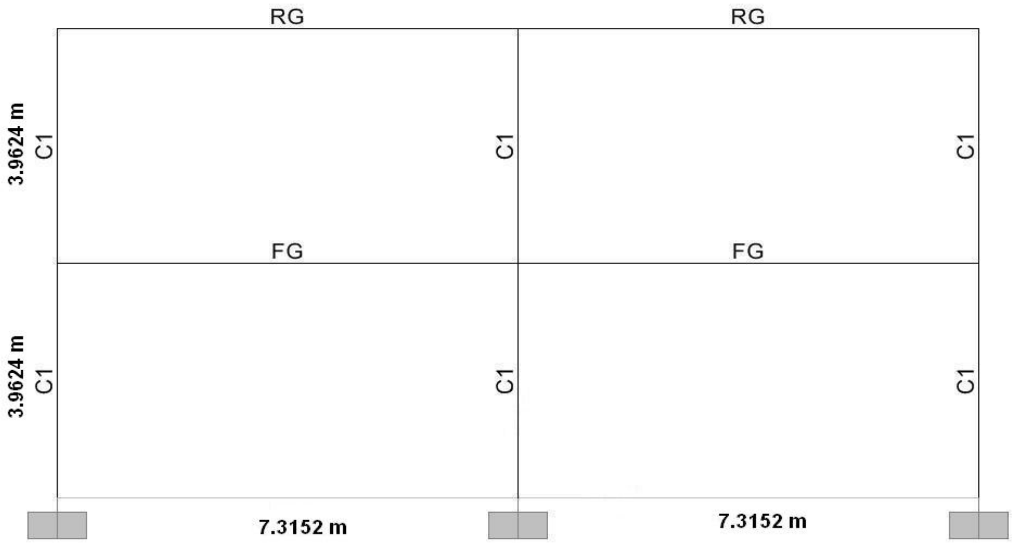

Figure A.1: F2S2B

E = 28730 MPa, f_y = 494 MPa, f_c = 26 MPa, T_n = 0.4879 s.

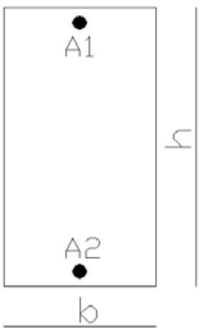

Beam Properties:

FG

b = 305 mm, h = 556 mm, A1 = 1342 mm^2, A2=3148 mm^2

clear cover = 56 mm

RG

b = 305 mm, h = 508 mm, A1 = 1342 mm^2, A2=2503 mm^2

clear cover = 51 mm

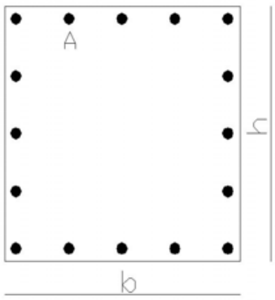

Column Properties:

C1

b = 609.6 mm, h = 609.6 mm, A = 645.2 mm^2

clear cover = 61 mm

Modal Properties

T_1 (s)	T_2 (s)	ω_1 (rad/s)	ω_2 (rad/s)
0.4879	0.1481	12.87802	42.42529

Damping Coefficients α= 0.98767 s^{-1} β= 0.00181 s

Column Hinge Properties

	P_{yc} (kN)	P_{yt} (kN)	M_y^+ (kNm)	M_y^- (kNm)	P_A (kN)	M_A (kNm)	P_B (kN)	M_B (kNm)
C1	13805.60	5098.50	1193.70	1193.70	3244.32	1468.25	3244.32	1468.25

Beam Hinge Properties

FG		RG	
M_y^+ (kNm)	M_y^- (kNm)	M_y^+ (kNm)	M_y^- (kNm)
677.00	307.00	498.00	278.00

Story Masses (ton)

Story		
	1	177.7014
	2	97.5535

Beam Loading

FG		RG	
DL (kN/m) :	24.71	DL (kN/m) :	19.23
LL (kN/m) :	1.95	LL (kN/m) :	0.98
M (kNm) :	111.36	M (kNm) :	86.85
V (kN) :	91.34	V (kN) :	71.23

A.1.2 F4S3B

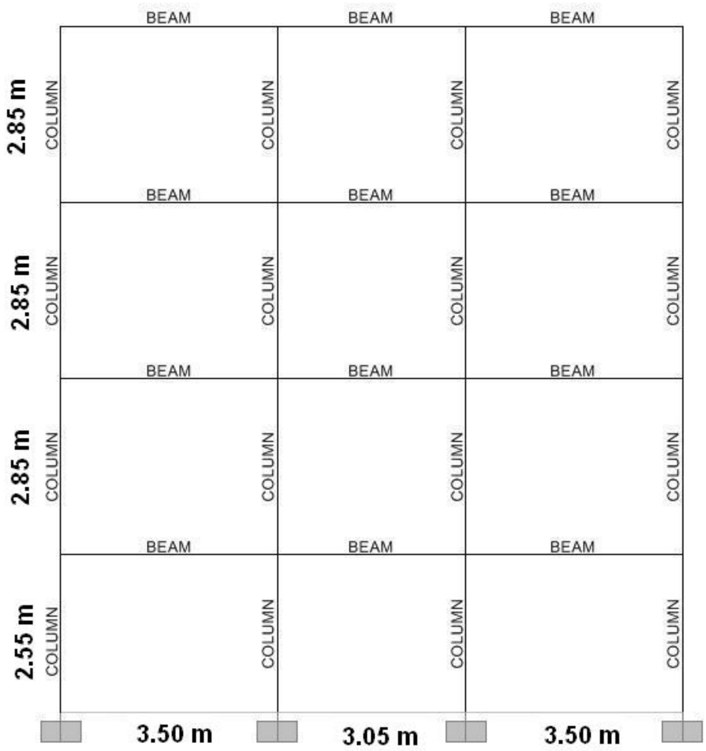

Figure A.2: F4S3B

E = 27400 MPa, f_y = 220 MPa, f_c = 17 MPa, T_n = 0.8375 s.

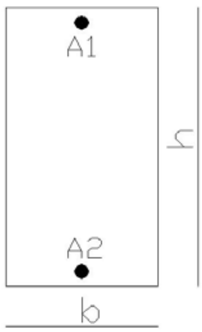

Beam Properties:

BEAM

b = 200 mm, h = 400 mm, A1 = 550 mm^2, A2 = 350 mm^2

clear cover = 50 mm

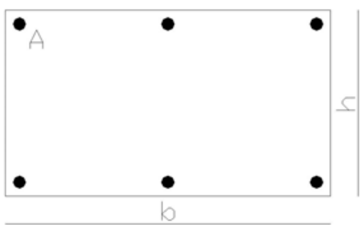

Column Properties:

C

b = 350 mm, h = 200 mm, A = 154 mm^2

clear cover = 50 mm

Modal Properties

T_1 (s)	T_2 (s)	T_3 (s)	ω_1 (rad/s)	ω_2 (rad/s)	ω_3 (rad/s)
0.8375	0.2671	0.1545	7.5023	23.5237	40.6679
T_4 (s)			ω_4 (rad/s)		
0.1159			54.2121		

Damping Coefficients α= 0.63831 s^{-1} β= 0.00207 s

Column Hinge Properties

	P_{yc} (kN)	P_{yt} (kN)	M_y^+ (kNm)	M_y^- (kNm)	P_A (kN)	M_A (kNm)	P_B (kN)	M_B (kNm)
Clmn	1377.53	203.28	37.6	37.6	618.51	71.816	618.51	71.816

Beam Hinge Properties

BEAM	
M_y^+ (kNm)	M_y^- (kNm)
27.61	39.69

Story Masses (ton)

Story	
1	45.127
2	45.127
3	45.127
4	53.744

Beam Loading

BEAM (L=3.5m)		BEAM(L=3.05m)	
DL (kN/m) :	18.00	DL (kN/m) :	16.00
LL (kN/m) :	4.50	LL (kN/m) :	3.25
M (kNm) :	19.52	M (kNm) :	14.83
V (kN) :	33.47	V (kN) :	29.17
BEAM (Top Floor) L=3.5m		BEAM (Top Floor) L=3.05m	
DL (kN/m) :	18.00	DL (kN/m) :	16.00
LL (kN/m) :	4.50	LL (kN/m) :	3.25
M (kNm) :	17.16	M (kNm) :	13.03
V (kN) :	29.42	V (kN) :	25.64

A.1.3 F5S2B

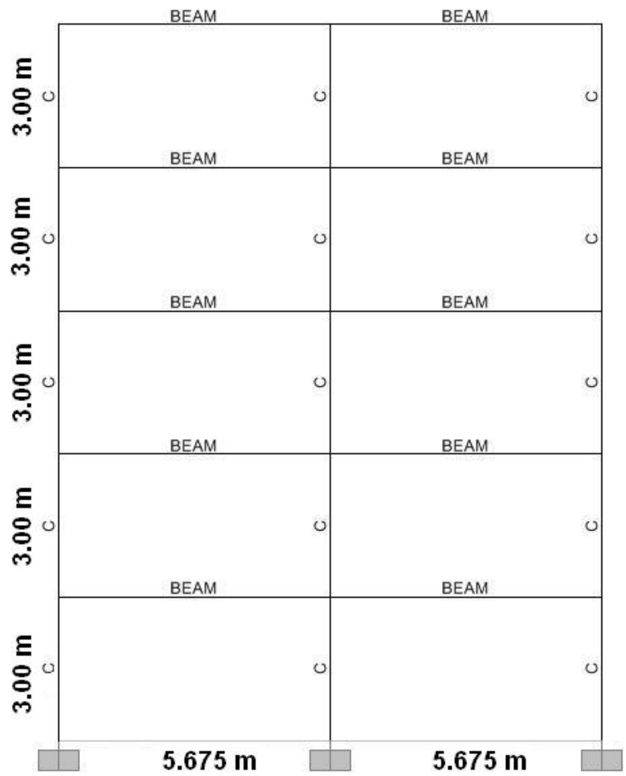

Figure A.3: F5S2B

E = 28534 MPa, f_y = 420 MPa, f_c = 20 MPa, T_n = 0.6150 s.

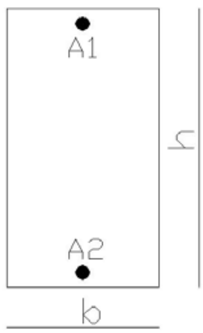

Beam Properties:

BEAM

b = 250 mm, h = 600 mm, A1 = 2500 mm^2, A2 = 1650 mm^2

clear cover = 50 mm

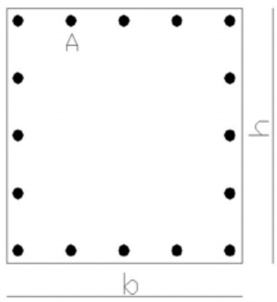

Column Properties:

C

b = 600 mm, h = 600 mm, A = 254 mm^2

clear cover = 50 mm

Modal Properties

T_1 (s)	T_2 (s)	T_3 (s)	ω_1 (rad/s)	ω_2 (rad/s)	ω_3 (rad/s)
0.615	0.1809	0.0896	10.2166	34.7329	70.1248
T_4 (s)	T_5 (s)		ω_4 (rad/s)	ω_5 (rad/s)	
0.0547	0.0408		114.8663	153.9996	

Damping Coefficients α= 0.84112 s^{-1} β= 0.00137 s

Column Hinge Properties

	P_{yc} (kN)	P_{yt} (kN)	M_y^+ (kNm)	M_y^- (kNm)	P_A (kN)	M_A (kNm)	P_B (kN)	M_B (kNm)
C	8670	1710.53	485	485	2835.09	746.9	2835.09	746.9

Beam Hinge Properties

BEAM	
M_y^+ (kNm)	M_y^- (kNm)
334.39	496.76

Story Masses (ton)

Story	Mass
1	47.505
2	52.177
3	52.177
4	52.177
5	56.14

Beam Loading

BEAM		BEAM (Top Floor)	
DL (kN/m) :	20.00	DL (kN/m) :	20.00
LL (kN/m) :	5.00	LL (kN/m) :	3.50
M (kNm) :	57.03	M (kNm) :	56.02
V (kN) :	60.3	V (kN) :	59.23

A.1.4 F5S4B

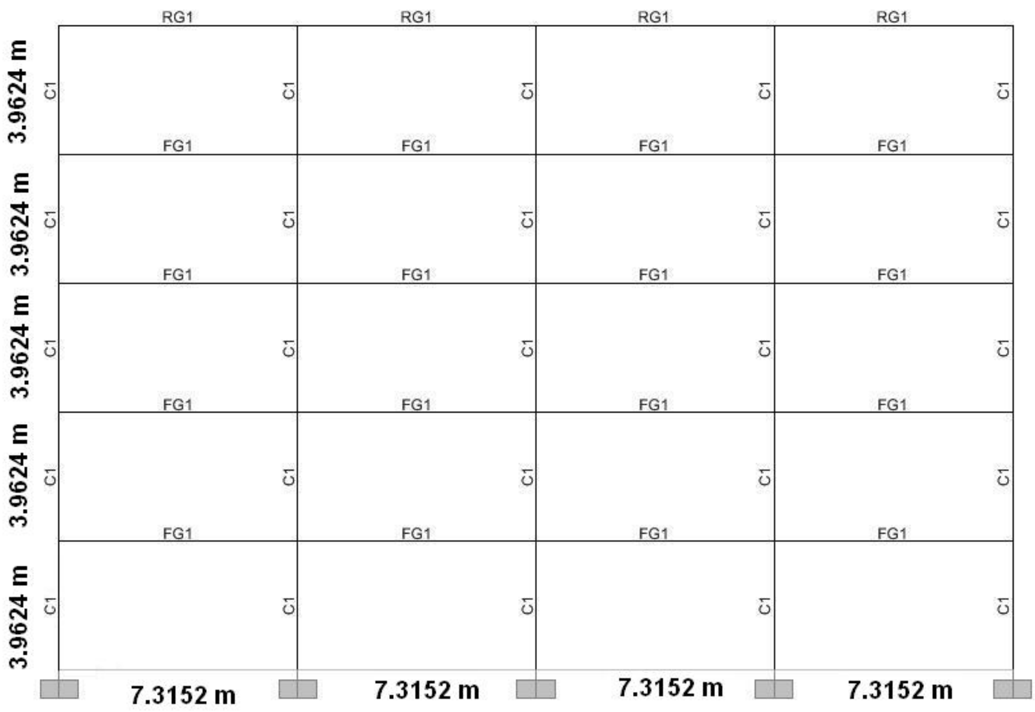

Figure A.4: FS4B

E = 27793 MPa, f_y = 459 MPa, f_c = 28 MPa, T_n = 0.8872 s.

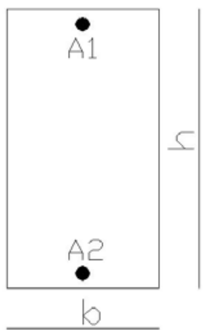

Beam Properties:

FG1

b = 406 mm, h = 660 mm, A1 = 5080 mm^2, A2=3150 mm^2

clear cover = 66 mm

RG1

b = 305 mm, h = 508 mm, A1 = 3790 mm^2, A2=2500 mm^2

clear cover = 51 mm

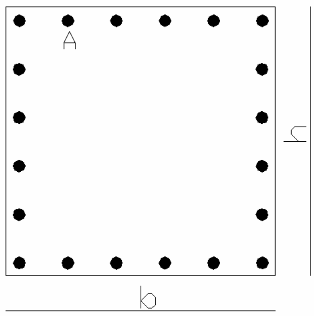

Column Properties:

C1

b = 711 mm, h = 711 mm, A = 885.8 mm^2

clear cover = 46 mm

Modal Properties

T_1 (s)	T_2 (s)	T_3 (s)	ω_1 (rad/s)	ω_2 (rad/s)	ω_3 (rad/s)
0.8872	0.2849	0.1513	7.0820	22.0540	41.5280
T_4 (s)	**T_5 (s)**		**ω_4 (rad/s)**	**ω_5 (rad/s)**	
0.0944	0.0700		66.5592	89.7598	

Damping Coefficients $\alpha=$ 0.68272 s^{-1} $\beta=$ 0.00094 s

Column Hinge Properties

	P_{yc} (kN)	P_{yt} (kN)	M_y^+ (kNm)	M_y^- (kNm)	P_A (kN)	M_A (kNm)	P_B (kN)	M_B (kNm)
C1	20810.3	8133.5	2345.2	2345.2	4911.23	2790.79	4911.23	2790.788

Beam Hinge Properties

FG		RG	
M_y^+ (kNm)	M_y^- (kNm)	M_y^+ (kNm)	M_y^- (kNm)
782	1226	474	699

Beam Loading

FG		RG	
DL (kN/m) :	20.49	**DL (kN/m) :**	15.64
LL (kN/m) :	1.31	**LL (kN/m) :**	0.53
M (kNm) :	92.83	**M (kNm) :**	70.34
V (kN) :	76.14	**V (kN) :**	57.69

Story Masses (ton)

Story	
1	212.43
2	212.43
3	212.43
4	212.43
5	157.40

A.1.5 F5S7B

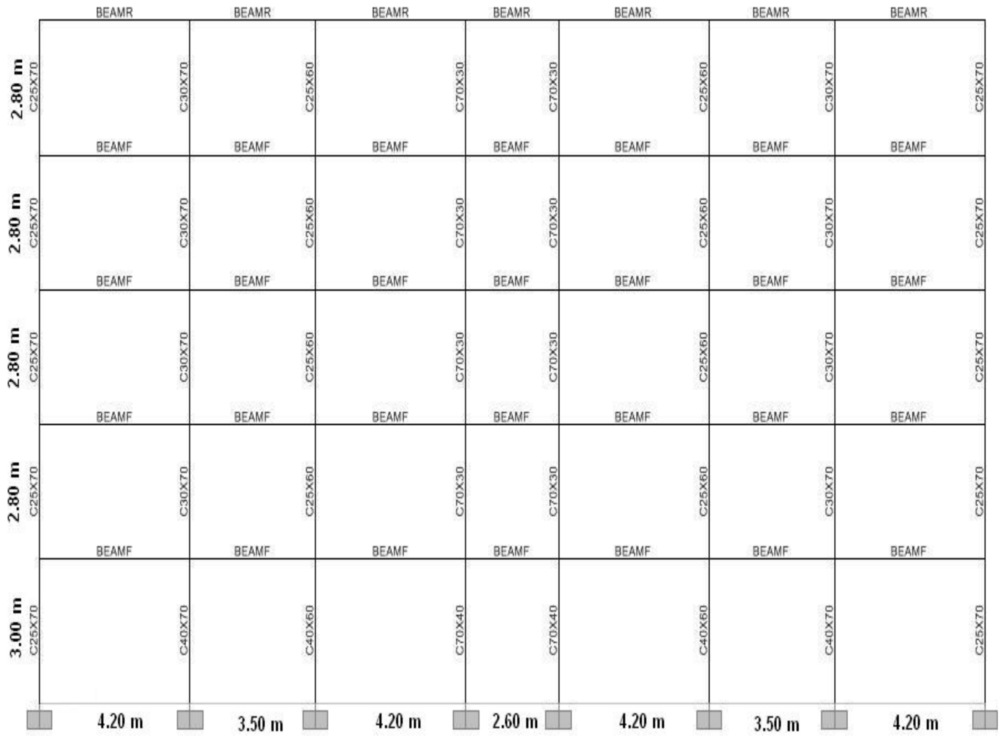

Figure A.5: 5S7B

E = 28534 MPa, f_y = 420 MPa, f_c = 20 MPa, T_n = 0.7232 s.

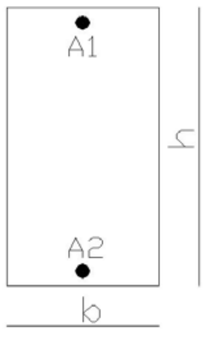

Beam Properties:

BEAMF

b = 200 mm, h = 600 mm, A1 = 4000 mm^2, A2 = 2500 mm^2

clear cover = 50 mm

BEAMR

b = 200 mm, h = 600 mm, A1 = 2500 mm^2, A2 = 1500 mm^2

clear cover = 50 mm

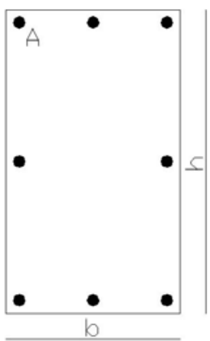

Column Properties:

C25x70

b = 250 mm, h = 700 mm, A = 1125 mm^2

clear cover = 50 mm

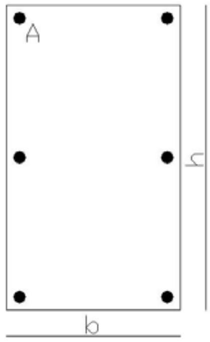

Column Properties:

C40x70

b = 400 mm, h = 700 mm, A = 1330 mm^2

clear cover = 50 mm

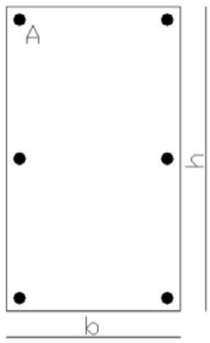

Column Properties:

C30x70

b = 300 mm, h = 700 mm, A = 1370 mm^2

clear cover = 50 mm

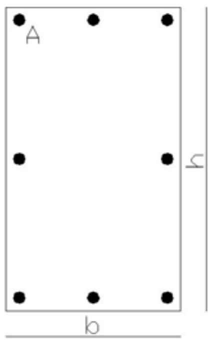

Column Properties:

C40x60

b = 400 mm, h = 600 mm, A = 1330 mm^2

clear cover = 50 mm

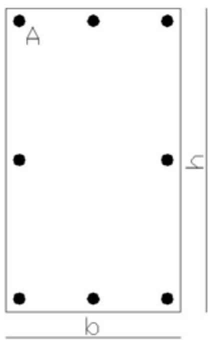

Column Properties:

C25x60

b = 250 mm, h = 600 mm, A = 1330 mm^2

clear cover = 50 mm

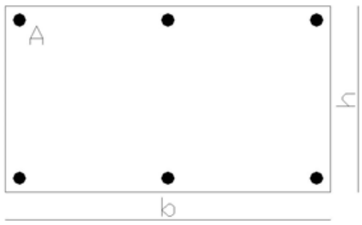

Column Properties:

C70x40

b = 700 mm, h = 400 mm, A = 2370 mm^2

clear cover = 50 mm

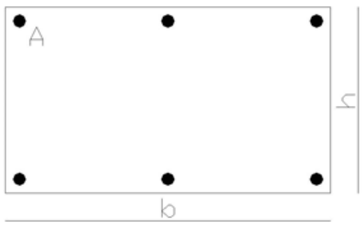

Column Properties:

C70x30

b = 700 mm, h = 300 mm, A = 2370 mm^2

clear cover = 50 mm

Modal Properties

T_1 (s)	T_2 (s)	T_3 (s)	ω_1 (rad/s)	ω_2 (rad/s)	ω_3 (rad/s)
0.7232	0.2305	0.1291	8.6880	27.2589	48.6691
T_4 (s)	**T_5 (s)**		**ω_4 (rad/s)**	**ω_5 (rad/s)**	
0.0888	0.0715		70.7566	87.8767	

Damping Coefficients α= 0.73197 s^{-1} β= 0.00205 s

Column Hinge Properties

	P_{yc} (kN)	P_{yt} (kN)	M_y^+ (kNm)	M_y^- (kNm)	P_A (kN)	M_A (kNm)	P_B (kN)	M_B (kNm)
C25x70	8133.87	3780.00	286.41	286.41	1285.15	320.78	1285.15	320.78
C40x70	10545.57	3351.60	513.61	513.61	2341.12	785.82	2341.12	785.82
C30x70	8778.44	3452.40	356.06	356.06	1685.46	487.80	1685.46	487.80
C40x60	10466.59	4468.80	762.89	762.89	1852.59	884.95	1852.59	884.95
C25x60	8095.53	4468.80	317.13	317.13	955.27	339.33	955.27	339.33
C70x40	12966.55	5972.40	1597.24	1597.24	1983.88	1725.02	1983.88	1725.02
C70x30	11068.22	5979.35	1531.68	1531.68	1317.12	1577.63	1317.12	1577.63

Beam Hinge Properties

BEAMF		BEAMR	
M_y^+ (kNm)	M_y^- (kNm)	M_y^+ (kNm)	M_y^- (KNm)
528.93	822.27	320.12	522.47

Beam Loading

BEAMF (L=4.2m)		BEAMF (L=3.5m)	
DL (kN/m) :	16.84	DL (kN/m) :	22.79
LL (kN/m) :	4.10	LL (kN/m) :	4.40
M (kNm) :	25.38	M (kNm) :	24.39
V (kN) :	36.26	V (kN) :	41.81

Story Masses (ton)

Story	
1	150.81
2	148.08
3	148.08
4	148.08
5	174.07

	BEAMF (L=4.2m)		BEAMF (L=2.6m)		
	DL (kN/m) :	22.02	DL (kN/m) :	24.01	
	LL (KN/m) :	5.40	LL (kN/m) :	6.43	
	M (kNm) :	34.35	M (kNm) :	14.42	
	V (kN) :	49.08	V (kN) :	33.27	
	BEAMR (L=4.2m)		BEAMR (L=3.5m)		
	DL (kN/m) :	16.32	DL (kN/m) :	17.30	
	LL (kN/m) :	3.16	LL (kN/m) :	3.30	
	M (kNm) :	25.12	M (kNm) :	18.50	
	V (kN) :	35.88	V (kN) :	31.72	
	BEAMR (L=4.2m)		BEAMR (L=2.6m)		
	DL (kN/m) :	20.56	DL (kN/m) :	19.06	
	LL (kN/m) :	4.05	LL (kN/m) :	3.71	
	M (kNm) :	31.71	M (kNm) :	11.26	
	V (kN) :	45.30	V (kN) :	25.98	

A.1.6 F8S3B

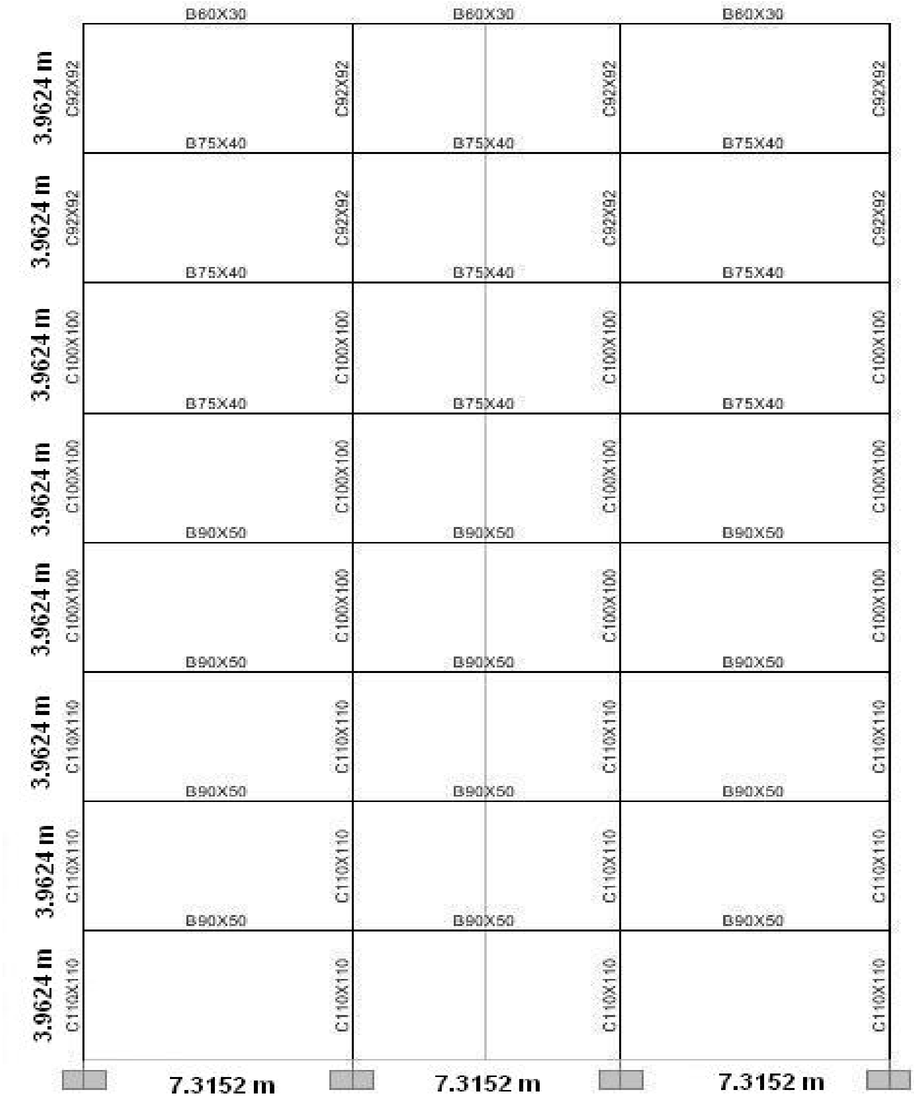

Figure A.6: F8S3B

E = 27793 MPa, f_y = 459 MPa, f_c = 28 MPa, T_n = 1.0642 s.

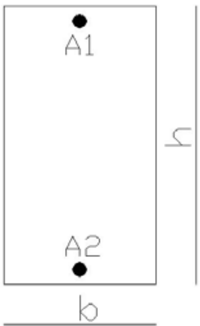

Beam Properties:

B90x50

b = 900 mm, h = 500 mm, A1 = 5400 mm^2, A2 = 4800 mm^2

clear cover = 50 mm

B75x40

b = 750 mm, h = 400 mm, A1 = 4500 mm^2, A2=3600 mm^2

clear cover = 50 mm

B60x30

b = 600 mm, h = 300 mm, A1 = 1800 mm^2, A2=1125 mm^2

clear cover = 50 mm

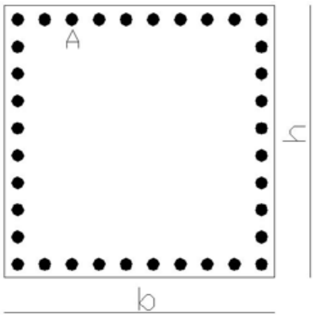

Column Properties:

C110x110

b = 1100 mm, h = 1100 mm, A = 510 mm^2

clear cover = 50 mm

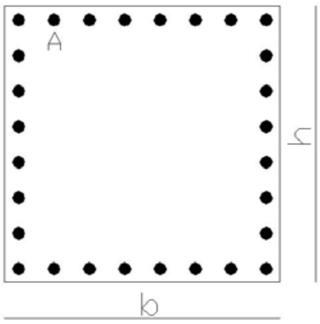

Column Properties:

C100x100

b = 1000 mm, h = 1000 mm, A = 510 mm^2

clear cover = 50 mm

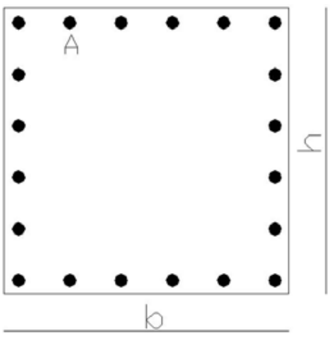

Column Properties:

C92x92

b = 920 mm, h = 920 mm, A = 510 mm^2

clear cover = 50 mm

Modal Properties

T_1 (s)	T_2 (s)	T_3 (s)	T_4 (s)	ω_1 (rad/s)	ω_2 (rad/s)	ω_3 (rad/s)	ω_4 (rad/s)
1.0642	0.3743	0.1924	0.1175	5.904	16.786	32.657	53.474
T_5 (s)	**T_6 (s)**	**T_7 (s)**	**T_8 (s)**	**ω_5 (rad/s)**	**ω_6 (rad/s)**	**ω_7 (rad/s)**	**ω_8 (rad/s)**
0.0786	0.0578	0.0454	0.0371	79.939	108.706	138.396	169.358

Damping Coefficients α= 0.54982 s^{-1} β= 0.00116 s

Column Hinge Properties

	P_{yc} (kN)	P_{yt} (kN)	M_y^+ (kNm)	M_y^- (kNm)	P_A (kN)	M_A (kNm)	P_B (KN)	M_B (kNm)
C110x110	40055.1	8429.5	4020.71	4020.71	14099.4	6955.83	14099.4	6955.828
C100x100	32765.2	6555.89	2839.51	2839.51	11631.6	5054.33	11631.6	5054.328
C92x92	27012.7	4684.78	1885.82	1885.82	9778.6	3696.21	9778.6	3696.207

Beam Hinge Properties

B90x50		B75x40	
M_y^+ (kNm)	M_y^- (kNm)	M_y^+ (kNm)	M_y^- (kNm)
1770	1980	1072	1340
B60x30			
M_y^+ (kNm)	M_y^- (kNm)		
265	419		

Story Masses (ton)

Story	Mass
1	230.45
2	230.45
3	230.45
4	230.45
5	230.45
6	230.45
7	230.45
8	202.92

Beam Loading

B90x50		B75x40	
DL (kN/m) :	18.64	DL (kN/m) :	18.64
LL (kN/m) :	1.21	LL (kN/m) :	1.21
M (kNm) :	84.47	M (kNm) :	84.47
V (kN) :	69.28	V (kN) :	69.28
B60x30			
DL (KN/m) :	14.55		
LL (kN/m) :	0.49		
M (kNm) :	65.43		
V (kN) :	53.67		

A.2 PEAK ROOF DISPLACEMENT AND BASE SHEAR RESULTS FOR TH ANALYSES OF UNDAMAGED STRUCTURE

Deformation Level	Düzce											
	F2S2B		F4S3B		F5S2B		F5S4B		F5S7B		F8S3B	
	Δ_{max} (m)	V_{max} (kN)	Δ_{max} (m)	V_{max} (kN)	Δ_{max} (m)	V_{max} (kN)	Δ_{max} (m)	V_{max} (kN)	Δ_{max} (m)	V_{max} (kN)	Δ_{max} (m)	V_{max} (kN)
I	0.020	550.430	0.010	66.821	0.032	586.490	0.075	2371.100	0.040	1496.500	0.073	3163.600
II	0.030	815.530	0.016	93.983	0.047	751.790	0.106	2924.600	0.068	2475.500	0.101	3968.600
III	0.047	1074.500	0.044	122.840	0.060	822.290	0.148	3498.900	0.086	2930.500	0.186	4363.900
IV	0.051	1122.200	0.050	124.330	0.068	832.270	0.165	3530.900	0.097	3117.100	0.199	4418.500
V	0.061	1179.700	0.084	132.660	0.096	862.120	0.204	3687.200	0.130	3396.800	0.259	4637.600
VI	0.064	1214.000	0.097	132.890	0.104	860.210	0.253	3893.000	0.138	3434.700	0.280	4685.500
Deformation Level	El Centro											
	F2S2B		F4S3B		F5S2B		F5S4B		F5S7B		F8S3B	
	Δ_{max} (m)	V_{max} (kN)	Δ_{max} (m)	V_{max} (kN)	Δ_{max} (m)	V_{max} (kN)	Δ_{max} (m)	V_{max} (kN)	Δ_{max} (m)	V_{max} (kN)	Δ_{max} (m)	V_{max} (kN)
I	0.023	617.310	0.010	65.703	0.033	549.150	0.073	2103.300	0.041	1547.700	0.077	3309.200
II	0.031	916.470	0.016	96.926	0.048	660.150	0.092	2737.700	0.070	2522.800	0.108	4000.800
III	0.042	1173.200	0.027	116.610	0.068	820.660	0.120	3669.700	0.084	2847.100	0.206	4721.400
IV	0.045	1197.600	0.033	121.030	0.072	833.960	0.131	3767.800	0.098	3181.400	0.220	4724.500
V	0.057	1272.100	0.071	141.220	0.106	888.950	0.169	4095.400	0.121	3353.800	0.305	5074.000
VI	0.065	1251.700	0.097	141.680	0.127	863.960	0.191	4276.600	0.127	3393.800	0.351	5575.700
Deformation Level	Pacoima Dam											
	F2S2B		F4S3B		F5S2B		F5S4B		F5S7B		F8S3B	
	Δ_{max} (m)	V_{max} (kN)	Δ_{max} (m)	V_{max} (kN)	Δ_{max} (m)	V_{max} (kN)	Δ_{max} (m)	V_{max} (kN)	Δ_{max} (m)	V_{max} (kN)	Δ_{max} (m)	V_{max} (kN)
I	0.028	652.490	0.011	78.476	0.033	656.680	0.073	2409.200	0.037	1957.000	0.078	2673.700
II	0.038	891.880	0.017	104.570	0.051	796.280	0.102	3023.100	0.064	3146.800	0.106	3611.300
III	0.054	1215.000	0.038	130.440	0.076	873.350	0.147	3545.900	0.087	3432.600	0.175	4208.500
IV	0.057	1281.800	0.045	135.260	0.080	891.540	0.153	3598.100	0.105	3554.400	0.194	4358.500
V	0.066	1300.300	0.074	138.660	0.111	904.190	0.206	3832.200	0.140	3660.900	0.244	4784.000
VI	0.074	1334.700	0.088	144.420	0.116	902.600	0.217	3862.600	0.149	3641.400	0.292	5455.600

A2 Continued

Deformation Level	Parkfield											
	F2S2B		F4S3B		F5S2B		F5S4B		F5S7B		F8S3B	
	Δ_{max} (m)	V_{max} (kN)	Δ_{max} (m)	V_{max} (kN)	Δ_{max} (m)	V_{max} (kN)	Δ_{max} (m)	V_{max} (kN)	Δ_{max} (m)	V_{max} (kN)	Δ_{max} (m)	V_{max} (kN)
I	0.025	618.530	0.010	68.692	0.033	590.570	0.073	2383.100	0.042	1615.200	0.081	2818.900
II	0.034	836.430	0.019	101.290	0.041	735.890	0.109	3087.100	0.069	2570.100	0.108	3490.000
III	0.041	1006.900	0.037	116.110	0.074	856.430	0.154	3608.500	0.085	2952.300	0.220	4867.900
IV	0.043	1084.000	0.045	123.060	0.081	862.260	0.166	3678.400	0.097	3132.000	0.239	4937.200
V	0.078	1326.200	0.095	136.250	0.110	869.770	0.215	3596.300	0.125	3245.100	0.439	5533.300
VI	0.085	1342.700	0.116	136.920	0.120	876.130	0.227	3524.800	0.134	3253.100	0.506	5711.500
Deformation Level	El Centro 79a											
	F2S2B		F4S3B		F5S2B		F5S4B		F5S7B		F8S3B	
	Δ_{max} (m)	V_{max} (kN)	Δ_{max} (m)	V_{max} (kN)	Δ_{max} (m)	V_{max} (kN)	Δ_{max} (m)	V_{max} (kN)	Δ_{max} (m)	V_{max} (kN)	Δ_{max} (m)	V_{max} (kN)
I	0.023	680.900	0.009	61.582	0.034	578.430	0.076	2295.500	0.041	1369.700	0.087	2958.400
II	0.035	969.110	0.018	90.369	0.046	724.390	0.103	2790.100	0.067	2191.400	0.118	3816.700
III	0.046	1136.700	0.042	131.730	0.069	812.580	0.144	3256.600	0.082	2636.800	0.137	4424.000
IV	0.050	1145.500	0.048	137.060	0.079	825.680	0.148	3281.400	0.097	3060.600	0.220	5121.500
V	0.060	1183.900	0.095	149.760	0.108	859.310	0.168	3718.700	0.146	3288.800	0.394	5955.300
VI	0.064	1200.100	0.121	149.850	0.114	862.570	0.175	3895.300	0.155	3293.900	0.451	6211.000
Deformation Level	El Centro 79b											
	F2S2B		F4S3B		F5S2B		F5S4B		F5S7B		F8S3B	
	Δ_{max} (m)	V_{max} (kN)	Δ_{max} (m)	V_{max} (kN)	Δ_{max} (m)	V_{max} (kN)	Δ_{max} (m)	V_{max} (kN)	Δ_{max} (m)	V_{max} (kN)	Δ_{max} (m)	V_{max} (kN)
I	0.024	603.400	0.010	79.272	0.034	597.570	0.072	2800.200	0.039	1595.200	0.080	3089.100
II	0.034	845.530	0.014	108.730	0.044	737.660	0.098	3539.400	0.068	2716.600	0.113	3945.100
III	0.040	990.490	0.040	124.830	0.078	880.910	0.150	4107.800	0.085	3160.700	0.215	4675.800
IV	0.043	1033.300	0.042	126.420	0.082	894.520	0.160	4165.100	0.091	3296.500	0.231	4779.300
V	0.075	1262.800	0.079	140.020	0.103	905.180	0.246	4386.700	0.138	3630.500	0.266	4909.500
VI	0.082	1254.000	0.090	143.310	0.112	929.940	0.267	4406.900	0.147	3664.000	0.296	4969.600

A2 Continued

Deformation Level	Chi-Chi											
	F2S2B		F4S3B		F5S2B		F5S4B		F5S7B		F8S3B	
	Δ_{max} (m)	V_{max} (kN)	Δ_{max} (m)	V_{max} (kN)	Δ_{max} (m)	V_{max} (kN)	Δ_{max} (m)	V_{max} (kN)	Δ_{max} (m)	V_{max} (kN)	Δ_{max} (m)	V_{max} (kN)
I	0.030	854.410	0.011	74.499	0.033	579.090	0.076	2520.500	0.039	1513.100	0.076	2659.900
II	0.041	1137.500	0.017	103.050	0.053	769.100	0.102	3048.900	0.069	2601.200	0.107	3629.100
III	0.048	1187.900	0.043	125.350	0.079	865.210	0.134	3370.600	0.086	3005.700	0.179	4348.000
IV	0.050	1195.800	0.049	128.890	0.086	852.470	0.164	3594.100	0.100	3172.000	0.189	4389.200
V	0.059	1266.400	0.104	140.860	0.125	879.180	0.213	3949.700	0.139	3520.000	0.423	5210.600
VI	0.060	1317.000	0.125	142.340	0.134	887.730	0.241	3984.900	0.144	3535.700	0.456	5371.200
Deformation Level	Northridge-Pacoima											
	F2S2B		F4S3B		F5S2B		F5S4B		F5S7B		F8S3B	
	Δ_{max} (m)	V_{max} (kN)	Δ_{max} (m)	V_{max} (kN)	Δ_{max} (m)	V_{max} (kN)	Δ_{max} (m)	V_{max} (kN)	Δ_{max} (m)	V_{max} (kN)	Δ_{max} (m)	V_{max} (kN)
I	0.023	683.690	0.010	62.794	0.034	584.460	0.076	2449.000	0.041	1469.200	0.080	2418.200
II	0.037	897.580	0.017	91.245	0.048	765.850	0.108	2986.200	0.066	2273.800	0.120	3425.500
III	0.051	1143.000	0.029	109.720	0.073	796.420	0.135	3207.000	0.082	2675.400	0.195	4293.300
IV	0.055	1156.200	0.044	133.650	0.078	810.410	0.140	3241.700	0.105	2885.500	0.205	4333.600
V	0.073	1174.400	0.087	147.190	0.096	822.550	0.169	3450.000	0.135	3015.900	0.356	4940.400
VI	0.076	1177.700	0.103	146.760	0.102	819.560	0.177	3482.400	0.143	3035.500	0.361	5116.600
Deformation Level	Cape Mendocino											
	F2S2B		F4S3B		F5S2B		F5S4B		F5S7B		F8S3B	
	Δ_{max} (m)	V_{max} (kN)	Δ_{max} (m)	V_{max} (kN)	Δ_{max} (m)	V_{max} (kN)	Δ_{max} (m)	V_{max} (kN)	Δ_{max} (m)	V_{max} (kN)	Δ_{max} (m)	V_{max} (kN)
I	0.028	709.470	0.010	80.140	0.033	515.450	0.091	3315.700	0.041	1329.600	0.069	3972.600
II	0.035	960.230	0.020	119.550	0.047	671.530	0.131	3691.500	0.069	2135.100	0.098	4468.900
III	0.039	1125.300	0.042	136.560	0.072	755.970	0.145	4231.100	0.085	2652.600	0.186	5623.800
IV	0.042	1157.600	0.047	142.130	0.084	783.330	0.155	4348.700	0.117	3012.900	0.195	5674.200
V	0.065	1138.800	0.056	148.970	0.107	795.980	0.243	5014.700	0.159	3192.700	0.232	5444.700
VI	0.068	1149.800	0.067	149.910	0.116	790.670	0.249	5004.600	0.170	3280.000	0.235	5814.500

A2 Continued

Deformation Level	Northridge											
	F2S2B		F4S3B		F5S2B		F5S4B		F5S7B		F8S3B	
	Δ_{max} (m)	V_{max} (kN)	Δ_{max} (m)	V_{max} (kN)	Δ_{max} (m)	V_{max} (kN)	Δ_{max} (m)	V_{max} (kN)	Δ_{max} (m)	V_{max} (kN)	Δ_{max} (m)	V_{max} (kN)
I	0.023	615.080	0.010	63.683	0.034	577.750	0.077	2515.000	0.037	1453.500	0.077	3576.100
II	0.035	921.340	0.015	99.590	0.041	750.770	0.112	3213.400	0.065	2438.000	0.111	4250.000
III	0.050	1190.100	0.038	122.960	0.072	851.470	0.136	3489.500	0.082	2835.700	0.139	4364.100
IV	0.054	1182.200	0.045	125.240	0.079	853.100	0.144	3554.800	0.097	3123.200	0.164	4578.700
V	0.074	1261.200	0.078	137.460	0.094	895.530	0.208	4001.600	0.112	3276.500	0.271	4945.200
VI	0.078	1301.800	0.090	140.020	0.128	906.150	0.223	4070.600	0.119	3327.000	0.315	5012.400

A.3 PEAK ROOF DISPLACEMENT AND BASE SHEAR RESULTS FOR IDEALIZATION METHODS USED FOR F2S2B

Deformation Level	Düzce						El Centro 79b					
	FEMA		Initial Stiffness		Major Yield		FEMA		Initial Stiffness		Major Yield	
	Δ_{max} (m)	Vmax (kN)	Δ_{max} (m)	Vmax (kN)	Δ_{max} (m)	Vmax (kN)	Δ_{max} (m)	Vmax (kN)	Δ_{max} (m)	Vmax (kN)	Δ_{max} (m)	Vmax (kN)
I	0.029	707.804	0.020	570.102	0.039	772.179	0.029	707.804	0.023	646.115	0.036	718.926
II	0.044	1045.474	0.029	836.149	0.057	1102.665	0.044	1045.474	0.035	988.176	0.056	1102.253
III	0.055	1052.775	0.039	1026.170	0.080	1109.673	0.055	1052.775	0.044	1030.390	0.069	1106.375
IV	0.060	1056.425	0.041	1028.280	0.087	1111.734	0.060	1056.425	0.048	1033.554	0.072	1107.199
V	0.079	1069.202	0.053	1037.774	0.103	1116.680	0.079	1069.202	0.071	1051.487	0.095	1114.207
VI	0.086	1073.765	0.059	1041.993	0.104	1117.093	0.086	1073.765	0.076	1055.706	0.100	1115.856

Deformation Level	El Centro						Chi-Chi					
	FEMA		Initial Stiffness		Major Yield		FEMA		Initial Stiffness		Major Yield	
	Δ_{max} (m)	Vmax (kN)	Δ_{max} (m)	Vmax (kN)	Δ_{max} (m)	Vmax (kN)	Δ_{max} (m)	Vmax (kN)	Δ_{max} (m)	Vmax (kN)	Δ_{max} (m)	Vmax (kN)
I	0.029	707.804	0.025	722.129	0.031	612.418	0.029	707.804	0.032	912.163	0.027	532.537
II	0.044	1045.474	0.037	1025.115	0.047	931.941	0.044	1045.474	0.049	1034.609	0.039	772.179
III	0.055	1052.775	0.047	1032.499	0.063	1104.314	0.055	1052.775	0.057	1040.938	0.047	931.941
IV	0.060	1056.425	0.048	1028.280	0.068	1105.963	0.060	1056.425	0.060	1043.048	0.049	985.194
V	0.079	1069.202	0.067	1048.322	0.088	1112.146	0.079	1069.202	0.061	1044.103	0.059	1103.077
VI	0.086	1073.765	0.072	1052.541	0.092	1113.383	0.086	1073.765	0.063	1045.158	0.073	1107.612

Deformation Level	Pacoima Dam						Northridge-Pacoima					
	FEMA		Initial Stiffness		Major Yield		FEMA		Initial Stiffness		Major Yield	
	Δ_{max} (m)	Vmax (kN)	Δ_{max} (m)	Vmax (kN)	Δ_{max} (m)	Vmax (kN)	Δ_{max} (m)	Vmax (kN)	Δ_{max} (m)	Vmax (kN)	Δ_{max} (m)	Vmax (kN)
I	0.029	707.804	0.032	912.163	0.021	426.030	0.029	707.804	0.027	760.136	0.035	692.299
II	0.044	1045.474	0.044	1030.390	0.032	639.045	0.044	1045.474	0.037	1025.115	0.051	1011.821
III	0.055	1052.775	0.061	1044.103	0.052	1101.016	0.055	1052.775	0.049	1034.609	0.063	1104.314
IV	0.060	1056.425	0.061	1044.103	0.057	1102.665	0.060	1056.425	0.055	1038.828	0.067	1105.551
V	0.079	1069.202	0.072	1052.541	0.073	1107.612	0.079	1069.202	0.072	1052.541	0.087	1111.734
VI	0.086	1073.765	0.082	1059.925	0.080	1109.673	0.086	1073.765	0.077	1056.761	0.094	1113.795

A3 Continued

Deformation Level	Parkfield						Cape Mendocino					
	FEMA		Initial Stiffness		Major Yield		FEMA		Initial Stiffness		Major Yield	
	Δ_{max} (m)	Vmax (kN)	Δ_{max} (m)	Vmax (kN)	Δ_{max} (m)	Vmax (kN)	Δ_{max} (m)	Vmax (kN)	Δ_{max} (m)	Vmax (kN)	Δ_{max} (m)	Vmax (kN)
I	0.029	707.804	0.024	684.122	0.037	745.552	0.029	707.804	0.031	874.156	0.027	532.537
II	0.044	1045.474	0.037	1025.115	0.057	1102.665	0.044	1045.474	0.045	1031.445	0.039	772.179
III	0.056	1053.687	0.048	1033.554	0.064	1104.726	0.055	1052.775	0.051	1035.664	0.048	958.567
IV	0.061	1057.338	0.053	1037.774	0.069	1106.375	0.060	1056.425	0.049	1034.609	0.052	1038.448
V	0.079	1069.202	0.067	1048.322	0.094	1113.795	0.079	1069.202	0.075	1054.651	0.069	1106.375
VI	0.086	1073.765	0.073	1053.596	0.102	1116.268	0.086	1073.765	0.076	1055.706	0.073	1107.612

Deformation Level	El Centro 79a						Northridge					
	FEMA		Initial Stiffness		Major Yield		FEMA		Initial Stiffness		Major Yield	
	Δ_{max} (m)	Vmax (kN)	Δ_{max} (m)	Vmax (kN)	Δ_{max} (m)	Vmax (kN)	Δ_{max} (m)	Vmax (kN)	Δ_{max} (m)	Vmax (kN)	Δ_{max} (m)	Vmax (kN)
I	0.029	707.804	0.025	722.129	0.032	639.045	0.029	707.804	0.025	722.129	0.029	585.791
II	0.044	1045.474	0.039	1026.170	0.048	958.567	0.044	1045.474	0.039	1026.170	0.044	878.687
III	0.055	1052.775	0.044	1030.390	0.057	1102.665	0.055	1052.775	0.053	1037.774	0.067	1105.551
IV	0.060	1056.425	0.045	1031.445	0.061	1103.902	0.060	1056.425	0.052	1036.719	0.061	1103.902
V	0.077	1068.289	0.059	1041.993	0.077	1108.848	0.079	1069.202	0.061	1044.103	0.088	1112.146
VI	0.086	1073.765	0.067	1048.322	0.083	1110.497	0.086	1073.765	0.072	1052.541	0.103	1116.680

A.4 PEAK ROOF DISPLACEMENT AND BASE SHEAR RESULTS FOR TH ANALYSES OF DAMAGED STRUCTURE

Deformation Level	Düzce											
	F2S2B		F4S3B		F5S2B		F5S4B		F5S7B		F8S3B	
	Δ_{max} (m)	V_{max} (kN)	Δ_{max} (m)	V_{max} (kN)	Δ_{max} (m)	V_{max} (kN)	Δ_{max} (m)	V_{max} (kN)	Δ_{max} (m)	V_{max} (kN)	Δ_{max} (m)	V_{max} (kN)
I	0.020	566.830	0.011	70.426	0.033	587.150	0.075	2373.200	0.040	1496.400	0.072	3130.000
II	0.030	839.350	0.019	97.467	0.049	759.440	0.117	3036.300	0.069	2477.900	0.104	3925.900
III	0.039	1123.200	0.054	123.570	0.069	829.310	0.168	3530.800	0.089	2997.400	0.186	4355.300
IV	0.046	1151.100	0.058	127.010	0.081	852.960	0.200	3568.600	0.104	3160.900	0.200	4408.200
V	0.062	1192.000	0.092	130.280	0.125	845.990	0.246	3620.200	0.158	3419.100	0.279	4639.900
VI	0.068	1192.900	0.103	132.540	0.141	846.920	0.287	3896.000	0.174	3466.900	0.303	4693.600

Deformation Level	El Centro											
	F2S2B		F4S3B		F5S2B		F5S4B		F5S7B		F8S3B	
	Δ_{max} (m)	V_{max} (kN)	Δ_{max} (m)	V_{max} (kN)	Δ_{max} (m)	V_{max} (kN)	Δ_{max} (m)	V_{max} (kN)	Δ_{max} (m)	V_{max} (kN)	Δ_{max} (m)	V_{max} (kN)
I	0.025	656.340	0.010	68.987	0.033	549.880	0.073	2108.400	0.043	1557.700	0.079	3359.200
II	0.037	938.010	0.016	95.471	0.049	675.540	0.097	2784.200	0.073	2539.200	0.122	4000.700
III	0.050	1170.900	0.028	115.540	0.092	835.370	0.117	3720.600	0.088	2876.800	0.204	4576.000
IV	0.053	1204.200	0.039	120.060	0.095	841.360	0.131	3773.000	0.106	3226.400	0.212	4695.300
V	0.075	1300.800	0.096	141.060	0.130	878.340	0.186	4073.000	0.139	3347.100	0.322	5345.100
VI	0.092	1296.300	0.137	141.670	0.154	880.120	0.215	4245.700	0.148	3410.700	0.402	5564.000

Deformation Level	Pacoima Dam											
	F2S2B		F4S3B		F5S2B		F5S4B		F5S7B		F8S3B	
	Δ_{max} (m)	V_{max} (kN)	Δ_{max} (m)	V_{max} (kN)	Δ_{max} (m)	V_{max} (kN)	Δ_{max} (m)	V_{max} (kN)	Δ_{max} (m)	V_{max} (kN)	Δ_{max} (m)	V_{max} (kN)
I	0.032	764.210	0.013	86.804	0.034	654.230	0.073	2415.400	0.037	1967.600	0.078	2665.700
II	0.047	1063.400	0.021	107.950	0.053	795.350	0.110	3118.000	0.065	3209.100	0.109	3629.900
III	0.053	1272.400	0.046	128.480	0.099	863.310	0.178	3545.100	0.097	3443.700	0.189	4173.800
IV	0.056	1338.600	0.041	134.250	0.109	879.270	0.189	3646.600	0.125	3578.400	0.227	4356.100
V	0.074	1434.300	0.081	138.930	0.170	895.040	0.262	3948.900	0.182	3690.700	0.352	4702.900
VI	0.091	1454.200	0.104	144.090	0.176	893.510	0.269	3999.400	0.196	3695.800	0.297	8438.500

A4 Continued

Deformation Level	Parkfield											
	F2S2B		F4S3B		F5S2B		F5S4B		F5S7B		F8S3B	
	Δ_{max} (m)	V_{max} (kN)	Δ_{max} (m)	V_{max} (kN)	Δ_{max} (m)	V_{max} (kN)	Δ_{max} (m)	V_{max} (kN)	Δ_{max} (m)	V_{max} (kN)	Δ_{max} (m)	V_{max} (kN)
I	0.026	662.880	0.010	70.676	0.034	589.810	0.073	2380.700	0.042	1614.900	0.081	2818.900
II	0.042	975.310	0.019	99.737	0.040	727.640	0.112	3115.400	0.070	2612.200	0.113	3531.600
III	0.051	1115.200	0.037	118.090	0.087	868.880	0.149	3557.600	0.088	3010.500	0.205	4859.800
IV	0.054	1151.300	0.048	122.090	0.097	867.790	0.169	3641.900	0.103	3135.200	0.229	4919.700
V	0.085	1301.000	0.129	132.700	0.138	868.010	0.195	3590.600	0.116	3247.900	0.593	5600.200
VI	0.091	1322.700	0.172	135.050	0.153	872.930	0.209	3550.100	0.127	3257.200	0.741	5699.100

Deformation Level	El Centro 79a											
	F2S2B		F4S3B		F5S2B		F5S4B		F5S7B		F8S3B	
	Δ_{max} (m)	V_{max} (kN)	Δ_{max} (m)	V_{max} (kN)	Δ_{max} (m)	V_{max} (kN)	Δ_{max} (m)	V_{max} (kN)	Δ_{max} (m)	V_{max} (kN)	Δ_{max} (m)	V_{max} (kN)
I	0.025	724.290	0.009	64.196	0.035	580.780	0.076	2297.500	0.041	1369.300	0.089	2963.700
II	0.036	1057.600	0.020	94.350	0.047	728.390	0.112	2914.800	0.069	2252.300	0.130	3775.300
III	0.043	1163.700	0.050	131.770	0.069	817.680	0.146	3315.500	0.082	2659.800	0.136	4461.100
IV	0.047	1172.500	0.060	137.040	0.083	840.770	0.147	3302.700	0.100	3069.200	0.253	5005.300
V	0.066	1213.100	0.148	149.770	0.138	878.650	0.162	3681.900	0.169	3374.900	0.569	5958.800
VI	0.074	1220.700	0.199	149.860	0.149	880.710	0.171	3857.400	0.185	3388.800	0.679	6212.800

Deformation Level	El Centro 79b											
	F2S2B		F4S3B		F5S2B		F5S4B		F5S7B		F8S3B	
	Δ_{max} (m)	V_{max} (kN)	Δ_{max} (m)	V_{max} (kN)	Δ_{max} (m)	V_{max} (kN)	Δ_{max} (m)	V_{max} (kN)	Δ_{max} (m)	V_{max} (kN)	Δ_{max} (m)	V_{max} (kN)
I	0.024	644.290	0.011	83.576	0.034	606.870	0.074	2801.100	0.039	1595.400	0.080	3078.900
II	0.038	953.920	0.017	113.190	0.045	722.710	0.112	3585.900	0.069	2710.900	0.117	3978.300
III	0.047	1087.100	0.060	128.780	0.087	879.800	0.176	4196.400	0.088	3196.300	0.314	4671.800
IV	0.050	1115.000	0.065	128.310	0.091	883.540	0.195	4252.500	0.096	3303.600	0.347	4783.800
V	0.077	1236.800	0.135	139.700	0.118	889.180	0.350	4480.000	0.172	3675.100	0.424	4933.500
VI	0.088	1263.300	0.154	143.680	0.138	899.710	0.388	4511.700	0.188	3721.000	0.487	4995.000

A4 Continued

Deformation Level	Chi-Chi											
	F2S2B		F4S3B		F5S2B		F5S4B		F5S7B		F8S3B	
	Δ_{max} (m)	V_{max} (kN)	Δ_{max} (m)	V_{max} (kN)	Δ_{max} (m)	V_{max} (kN)	Δ_{max} (m)	V_{max} (kN)	Δ_{max} (m)	V_{max} (kN)	Δ_{max} (m)	V_{max} (kN)
I	0.035	950.980	0.011	76.537	0.034	583.660	0.077	2541.000	0.039	1513.100	0.076	2659.900
II	0.049	1160.800	0.020	103.300	0.057	779.970	0.103	3093.400	0.069	2603.200	0.111	3651.400
III	0.063	1248.400	0.052	126.490	0.100	837.330	0.138	3424.500	0.093	3095.700	0.174	4354.800
IV	0.068	1268.700	0.062	129.000	0.111	842.760	0.171	3661.600	0.112	3212.100	0.189	4390.000
V	0.076	1325.300	0.128	138.060	0.127	879.510	0.253	3921.200	0.162	3542.900	0.511	5198.900
VI	0.075	1346.300	0.154	142.370	0.143	883.920	0.301	4061.200	0.166	3563.400	0.533	5301.500
Deformation Level	Northridge-Pacoima											
	F2S2B		F4S3B		F5S2B		F5S4B		F5S7B		F8S3B	
	Δ_{max} (m)	V_{max} (kN)	Δ_{max} (m)	V_{max} (kN)	Δ_{max} (m)	V_{max} (kN)	Δ_{max} (m)	V_{max} (kN)	Δ_{max} (m)	V_{max} (kN)	Δ_{max} (m)	V_{max} (kN)
I	0.025	741.570	0.010	64.416	0.034	586.390	0.076	2453.300	0.041	1469.800	0.080	2418.500
II	0.036	1074.700	0.020	92.820	0.048	772.540	0.111	3089.600	0.068	2330.500	0.132	3444.800
III	0.051	1189.600	0.031	114.470	0.090	816.100	0.139	3186.800	0.080	2612.900	0.236	4327.100
IV	0.058	1192.900	0.045	138.440	0.101	801.720	0.146	3224.300	0.107	2894.200	0.252	4298.400
V	0.089	1274.000	0.072	148.320	0.135	786.790	0.185	3412.800	0.156	3111.600	0.563	4920.500
VI	0.095	1278.800	0.079	146.810	0.143	830.570	0.196	3451.900	0.170	3173.800	0.567	5117.100
Deformation Level	Cape Mendocino											
	F2S2B		F4S3B		F5S2B		F5S4B		F5S7B		F8S3B	
	Δ_{max} (m)	V_{max} (kN)	Δ_{max} (m)	V_{max} (kN)	Δ_{max} (m)	V_{max} (kN)	Δ_{max} (m)	V_{max} (kN)	Δ_{max} (m)	V_{max} (kN)	Δ_{max} (m)	V_{max} (kN)
I	0.033	802.360	0.011	86.198	0.033	515.510	0.101	3446.100	0.041	1329.000	0.070	4032.800
II	0.046	1089.700	0.025	129.500	0.049	680.420	0.155	3682.600	0.071	2232.800	0.104	4496.000
III	0.054	1151.400	0.064	137.910	0.067	754.470	0.161	4221.800	0.083	2674.200	0.238	5688.700
IV	0.058	1166.900	0.073	140.870	0.077	776.060	0.147	4443.400	0.111	3011.800	0.266	5664.300
V	0.067	1199.500	0.091	148.890	0.100	801.050	0.340	5096.800	0.141	3159.100	0.341	5631.100
VI	0.069	1192.500	0.082	149.810	0.106	785.810	0.350	5124.200	0.152	3308.200	0.356	5884.900

A4 Continued

Deformation Level	Northridge											
	F2S2B		F4S3B		F5S2B		F5S4B		F5S7B		F8S3B	
	Δ_{max} (m)	V_{max} (kN)	Δ_{max} (m)	V_{max} (kN)	Δ_{max} (m)	V_{max} (kN)	Δ_{max} (m)	V_{max} (kN)	Δ_{max} (m)	V_{max} (kN)	Δ_{max} (m)	V_{max} (kN)
I	0.025	672.390	0.011	64.848	0.034	583.640	0.078	2524.800	0.037	1453.400	0.078	3599.200
II	0.036	986.260	0.017	102.660	0.042	757.440	0.123	3265.000	0.066	2446.000	0.117	4273.000
III	0.058	1177.600	0.045	127.440	0.069	845.190	0.157	3497.600	0.084	2904.400	0.153	4389.400
IV	0.059	1186.000	0.053	130.230	0.071	860.950	0.171	3586.000	0.094	3092.900	0.190	4558.700
V	0.061	1261.300	0.101	135.660	0.091	890.720	0.212	4051.100	0.114	3279.800	0.323	4911.600
VI	0.068	1304.700	0.119	138.150	0.185	896.010	0.239	4147.800	0.126	3332.400	0.363	5003.600

A.5 DETERMINATION OF EFFECT OF RESIDUAL DISPLACEMENT ON SDOF RESPONSE

Deformation Level	Düzce																	
	F2S2B						F4S3B						F5S2B					
	Δ (m)				Δ_y=	0.043	Δ (m)				Δ_y=	0.014	Δ (m)				Δ_y=	0.043
	SDOF undamaged	Residual	Undamaged + Residual	SDOF Procedure1	Ductility	Ratio	SDOF undamaged	Residual	Undamaged + Residual	SDOF Procedure1	Ductility	Ratio	SDOF undamaged	Residual	Undamaged + Residual	SDOF Procedure1	Ductility	Ratio
I	0.029	0.000	0.030	0.033	1.000	0.887	0.010	0.000	0.010	0.010	1.000	1.015	0.033	0.000	0.034	0.033	1.000	1.012
II	0.044	-0.001	0.045	0.043	1.028	1.042	0.019	0.000	0.019	0.017	1.340	1.106	0.049	0.002	0.051	0.052	1.175	0.976
III	0.055	0.001	0.056	0.082	1.284	0.683	0.042	0.001	0.044	0.081	3.046	0.541	0.082	0.036	0.118	0.107	2.726	1.101
IV	0.060	0.005	0.065	0.090	1.506	0.729	0.051	0.001	0.052	0.118	3.665	0.445	0.091	0.046	0.137	0.122	3.152	1.125
V	0.079	0.020	0.099	0.127	2.281	0.777	0.094	0.001	0.095	0.120	6.628	0.792	0.126	0.075	0.201	0.151	4.627	1.331
VI	0.086	0.026	0.111	0.141	2.565	0.788	0.111	-0.014	0.126	0.146	8.787	0.863	0.137	0.085	0.222	0.150	5.118	1.480

Deformation Level	Elcentro																	
	F2S2B						F4S3B						F5S2B					
	Δ_{max} (m)						Δ_{max} (m)						Δ_{max} (m)					
	SDOF undamaged	Residual	Undamaged + Residual	SDOF Procedure1	Ductility	Ratio	SDOF undamaged	Residual	Undamaged + Residual	SDOF Procedure1	Ductility	Ratio	SDOF undamaged	Residual	Undamaged + Residual	SDOF Procedure1	Ductility	Ratio
I	0.029	0.000	0.030	0.029	1.000	1.013	0.010	0.000	0.010	0.010	1.000	1.015	0.033	0.000	0.034	0.033	1.000	1.004
II	0.044	-0.001	0.045	0.042	1.038	1.085	0.019	0.000	0.019	0.020	1.319	0.952	0.049	0.006	0.054	0.048	1.252	1.122
III	0.055	0.001	0.056	0.063	1.284	0.886	0.042	-0.017	0.060	0.029	4.175	2.038	0.082	-0.030	0.113	0.082	2.596	1.367
IV	0.060	0.001	0.061	0.066	1.407	0.932	0.051	-0.017	0.068	0.039	4.787	1.761	0.091	-0.036	0.127	0.103	2.928	1.233
V	0.079	-0.023	0.102	0.093	2.352	1.099	0.094	-0.041	0.134	0.098	9.390	1.368	0.126	0.001	0.127	0.183	2.925	0.695
VI	0.086	-0.032	0.117	0.099	2.697	1.187	0.111	-0.062	0.174	0.119	12.142	1.455	0.137	-0.001	0.139	0.226	3.197	0.613

A5 Continued

Deformation Level	Pacoima																	
	F2S2B						F4S3B						F5S2B					
	Δ_{max} (m)						Δ_{max} (m)						Δ_{max} (m)					
	SDOF undamaged	Residual	Undamaged + Residual	SDOF Procedure1	Ductility	Ratio	SDOF undamaged	Residual	Undamaged + Residual	SDOF Procedure1	Ductility	Ratio	SDOF undamaged	Residual	Undamaged + Residual	SDOF Procedure1	Ductility	Ratio
I	0.029	0.000	0.030	0.027	1.000	1.109	0.011	0.000	0.011	0.012	1.000	0.912	0.033	0.001	0.034	0.035	1.000	0.989
II	0.044	0.000	0.044	0.044	1.016	0.998	0.020	0.001	0.020	0.027	1.433	0.753	0.049	0.006	0.055	0.050	1.273	1.112
III	0.055	0.008	0.063	0.058	1.447	1.091	0.040	0.016	0.056	0.062	3.931	0.903	0.081	0.039	0.120	0.144	2.768	0.836
IV	0.060	0.016	0.076	0.060	1.752	1.264	0.050	0.013	0.063	0.064	4.376	0.972	0.091	0.049	0.140	0.204	3.235	0.690
V	0.079	0.031	0.110	0.097	2.525	1.131	0.092	-0.001	0.093	0.105	6.505	0.883	0.126	0.082	0.208	0.230	4.801	0.906
VI	0.086	0.037	0.123	0.132	2.826	0.930	0.112	-0.019	0.131	0.124	9.163	1.056	0.137	0.093	0.231	0.242	5.319	0.953

Deformation Level	Parkfield																	
	F2S2B						F4S3B						F5S2B					
	Δ_{max} (m)						Δ_{max} (m)						Δ_{max} (m)					
	SDOF undamaged	Residual	Undamaged + Residual	SDOF Procedure1	Ductility	Ratio	SDOF undamaged	Residual	Undamaged + Residual	SDOF Procedure1	Ductility	Ratio	SDOF undamaged	Residual	Undamaged + Residual	SDOF Procedure1	Ductility	Ratio
I	0.029	0.000	0.029	0.032	1.000	0.916	0.010	0.000	0.010	0.010	1.000	1.015	0.033	0.000	0.033	0.033	1.000	1.000
II	0.044	0.000	0.044	0.046	1.019	0.972	0.019	0.001	0.019	0.019	1.354	1.043	0.048	0.004	0.052	0.051	1.196	1.018
III	0.056	-0.007	0.063	0.067	1.453	0.943	0.042	0.000	0.043	0.040	2.992	1.062	0.082	-0.004	0.086	0.090	1.980	0.956
IV	0.061	-0.010	0.071	0.070	1.641	1.024	0.050	0.000	0.050	0.029	3.511	1.722	0.090	-0.008	0.098	0.092	2.256	1.066
V	0.079	0.005	0.084	0.126	1.924	0.663	0.092	-0.015	0.108	0.163	7.538	0.662	0.127	-0.029	0.156	0.096	3.591	1.621
VI	0.086	0.004	0.089	0.140	2.054	0.637	0.110	-0.028	0.138	0.179	9.626	0.769	0.139	-0.035	0.174	0.107	4.014	1.635

A5 Continued

Deformation Level	El Centro 79a																	
	F2S2B						F4S3B						F5S2B					
	Δ_{max} (m)						Δ_{max} (m)						Δ_{max} (m)					
	SDOF undamaged	Residual	Undamaged + Residual	SDOF Procedure1	Ductility	Ratio	SDOF undamaged	Residual	Undamaged + Residual	SDOF Procedure1	Ductility	Ratio	SDOF undamaged	Residual	Undamaged + Residual	SDOF Procedure1	Ductility	Ratio
I	0.029	0.001	0.031	0.032	1.000	0.957	0.010	0.000	0.010	0.010	1.000	1.028	0.033	0.000	0.034	0.035	1.000	0.971
II	0.044	0.001	0.045	0.047	1.038	0.961	0.019	0.003	0.022	0.012	1.537	1.776	0.049	-0.002	0.050	0.048	1.160	1.040
III	0.055	0.009	0.064	0.060	1.478	1.065	0.042	0.004	0.046	0.046	3.249	1.002	0.082	0.012	0.094	0.099	2.161	0.950
IV	0.060	0.013	0.073	0.059	1.693	1.249	0.051	0.012	0.063	0.052	4.411	1.208	0.091	0.017	0.108	0.117	2.486	0.925
V	0.077	0.031	0.108	0.073	2.500	1.487	0.094	0.047	0.140	0.182	9.818	0.771	0.127	0.043	0.170	0.123	3.910	1.381
VI	0.086	0.040	0.126	0.077	2.900	1.629	0.111	0.064	0.175	0.209	12.264	0.840	0.137	0.051	0.188	0.131	4.337	1.439

Deformation Level	El Centro 79b																	
	F2S2B						F4S3B						F5S2B					
	Δ_{max} (m)						Δ_{max} (m)						Δ_{max} (m)					
	SDOF undamaged	Residual	Undamaged + Residual	SDOF Procedure1	Ductility	Ratio	SDOF undamaged	Residual	Undamaged + Residual	SDOF Procedure1	Ductility	Ratio	SDOF undamaged	Residual	Undamaged + Residual	SDOF Procedure1	Ductility	Ratio
I	0.029	0.000	0.030	0.032	1.000	0.928	0.010	0.000	0.010	0.010	1.000	1.028	0.033	-0.001	0.034	0.033	1.000	1.027
II	0.044	0.000	0.044	0.047	1.022	0.947	0.019	0.004	0.022	0.020	1.564	1.129	0.049	0.004	0.052	0.047	1.208	1.112
III	0.055	0.010	0.065	0.058	1.499	1.131	0.044	-0.030	0.074	0.070	5.154	1.059	0.082	-0.027	0.109	0.087	2.510	1.246
IV	0.060	0.015	0.075	0.056	1.733	1.340	0.049	-0.036	0.084	0.073	5.905	1.159	0.091	-0.035	0.126	0.094	2.913	1.340
V	0.079	0.015	0.094	0.081	2.164	1.161	0.095	-0.080	0.175	0.101	12.255	1.742	0.127	-0.075	0.203	0.129	4.668	1.571
VI	0.086	0.009	0.095	0.089	2.189	1.064	0.114	-0.087	0.201	0.112	14.055	1.792	0.139	-0.089	0.227	0.139	5.239	1.633

A5 Continued

Deformation Level	Chi-Chi																	
	F2S2B						F4S3B						F5S2B					
	Δ_{max} (m)						Δ_{max} (m)						Δ_{max} (m)					
	SDOF undamaged	Residual	Undamaged + Residual	SDOF Procedure1	Ductility	Ratio	SDOF undamaged	Residual	Undamaged + Residual	SDOF Procedure1	Ductility	Ratio	SDOF undamaged	Residual	Undamaged + Residual	SDOF Procedure1	Ductility	Ratio
I	0.029	0.000	0.029	0.027	1.000	1.099	0.011	0.000	0.011	0.011	1.000	1.003	0.033	0.000	0.033	0.033	1.000	1.000
II	0.044	0.000	0.044	0.042	1.025	1.072	0.020	0.004	0.024	0.026	1.695	0.932	0.049	0.005	0.054	0.064	1.240	0.845
III	0.055	0.011	0.066	0.047	1.515	1.404	0.042	-0.020	0.063	0.057	4.402	1.097	0.081	0.038	0.118	0.102	2.729	1.156
IV	0.060	0.016	0.076	0.052	1.749	1.456	0.050	-0.022	0.072	0.070	5.031	1.021	0.091	0.048	0.139	0.118	3.197	1.177
V	0.079	0.034	0.113	0.110	2.611	1.029	0.094	0.027	0.121	0.128	8.447	0.943	0.126	0.013	0.139	0.191	3.200	0.727
VI	0.086	0.041	0.126	0.125	2.912	1.009	0.111	0.036	0.147	0.134	10.264	1.098	0.137	0.002	0.139	0.185	3.212	0.752
Deformation Level	Northridge-Pacoima																	
	F2S2B						F4S3B						F5S2B					
	Δ_{max} (m)						Δ_{max} (m)						Δ_{max} (m)					
	SDOF undamaged	Residual	Undamaged + Residual	SDOF Procedure1	Ductility	Ratio	SDOF undamaged	Residual	Undamaged + Residual	SDOF Procedure1	Ductility	Ratio	SDOF undamaged	Residual	Undamaged + Residual	SDOF Procedure1	Ductility	Ratio
I	0.029	0.000	0.029	0.032	1.000	0.916	0.010	0.000	0.010	0.010	1.000	1.003	0.033	0.000	0.034	0.035	1.000	0.967
II	0.044	0.000	0.044	0.042	1.022	1.069	0.019	-0.003	0.022	0.021	1.511	1.027	0.049	0.003	0.051	0.052	1.184	0.984
III	0.055	-0.001	0.056	0.066	1.293	0.856	0.042	-0.010	0.053	0.048	3.704	1.112	0.081	-0.021	0.102	0.095	2.350	1.074
IV	0.060	-0.004	0.064	0.076	1.481	0.843	0.051	-0.015	0.066	0.069	4.647	0.960	0.091	-0.029	0.120	0.103	2.759	1.162
V	0.079	-0.015	0.094	0.121	2.174	0.781	0.094	-0.052	0.146	0.148	10.203	0.983	0.126	-0.057	0.183	0.163	4.221	1.123
VI	0.086	-0.019	0.104	0.133	2.405	0.783	0.111	-0.078	0.189	0.142	13.207	1.330	0.137	-0.067	0.205	0.172	4.712	1.190

A5 Continued

Deformation Level	Cape Mendocino																	
	F2S2B						F4S3B						F5S2B					
	Δ_{max} (m)						Δ_{max} (m)						Δ_{max} (m)					
	SDOF undamaged	Residual	Undamaged + Residual	SDOF Procedure1	Ductility	Ratio	SDOF undamaged	Residual	Undamaged + Residual	SDOF Procedure1	Ductility	Ratio	SDOF undamaged	Residual	Undamaged + Residual	SDOF Procedure1	Ductility	Ratio
I	0.029	0.000	0.029	0.028	1.000	1.047	0.010	0.000	0.010	0.010	1.000	1.028	0.033	0.000	0.033	0.032	1.000	1.040
II	0.044	0.000	0.044	0.043	1.025	1.039	0.019	0.000	0.019	0.024	1.338	0.814	0.049	-0.005	0.054	0.043	1.240	1.242
III	0.055	-0.011	0.066	0.048	1.512	1.362	0.044	0.013	0.057	0.088	3.992	0.649	0.082	0.009	0.092	0.067	2.111	1.358
IV	0.060	-0.016	0.076	0.049	1.752	1.537	0.051	0.023	0.074	0.095	5.197	0.784	0.091	-0.004	0.095	0.084	2.190	1.126
V	0.079	0.003	0.082	0.065	1.881	1.256	0.094	0.076	0.170	0.138	11.897	1.236	0.126	0.002	0.128	0.113	2.939	1.127
VI	0.086	0.007	0.093	0.067	2.134	1.390	0.111	0.093	0.204	0.126	14.299	1.616	0.137	0.006	0.143	0.131	3.306	1.097

Deformation Level	Northridge																	
	F2S2B						F4S3B						F5S2B					
	Δ_{max} (m)						Δ_{max} (m)						Δ_{max} (m)					
	SDOF undamaged	Residual	Undamaged + Residual	SDOF Procedure1	Ductility	Ratio	SDOF undamaged	Residual	Undamaged + Residual	SDOF Procedure1	Ductility	Ratio	SDOF undamaged	Residual	Undamaged + Residual	SDOF Procedure1	Ductility	Ratio
I	0.029	0.000	0.030	0.029	1.000	1.008	0.010	0.000	0.010	0.010	1.000	1.015	0.033	0.000	0.033	0.035	1.000	0.963
II	0.044	-0.002	0.046	0.046	1.053	1.004	0.019	0.005	0.023	0.024	1.642	0.999	0.048	0.003	0.050	0.061	1.163	0.825
III	0.055	-0.009	0.064	0.062	1.481	1.044	0.042	-0.017	0.060	0.073	4.175	0.815	0.082	-0.023	0.105	0.159	2.421	0.662
IV	0.060	-0.017	0.077	0.070	1.773	1.107	0.051	-0.024	0.076	0.090	5.293	0.842	0.090	-0.018	0.108	0.145	2.492	0.745
V	0.079	-0.019	0.097	0.103	2.244	0.941	0.094	-0.036	0.130	0.097	9.067	1.337	0.126	0.000	0.126	0.206	2.904	0.613
VI	0.086	-0.014	0.100	0.133	2.297	0.748	0.112	-0.045	0.158	0.106	11.032	1.485	0.139	-0.056	0.195	0.335	4.482	0.580

A5 Continued

Deformation Level	Düzce																	
	F5S4B						F5S7B						F8S3B					
	Δ (m)				Δ_y=	0.103	Δ (m)				Δ_y=	0.083	Δ (m)				Δ_y=	0.111
	SDOF undamaged	Residual	Undamaged + Residual	SDOF Procedure1	Ductility	Ratio	SDOF undamaged	Residual	Undamaged + Residual	SDOF Procedure1	Ductility	Ratio	SDOF undamaged	Residual	Undamaged + Residual	SDOF Procedure1	Ductility	Ratio
I	0.076	-0.001	0.078	0.076	1.000	1.020	0.041	0.000	0.041	0.041	1.000	1.000	0.076	-0.007	0.083	0.076	1.000	1.094
II	0.107	0.002	0.109	0.104	1.058	1.050	0.071	0.000	0.071	0.074	1.000	0.956	0.109	-0.010	0.119	0.105	1.069	1.129
III	0.153	0.035	0.188	0.159	1.823	1.183	0.093	0.010	0.103	0.107	1.237	0.957	0.182	-0.063	0.245	0.284	2.205	0.862
IV	0.165	-0.003	0.168	0.193	1.633	0.873	0.109	0.026	0.135	0.140	1.628	0.963	0.197	-0.059	0.256	0.274	2.305	0.932
V	0.222	-0.014	0.237	0.255	2.298	0.926	0.148	0.063	0.212	0.200	2.549	1.058	0.289	0.003	0.292	0.492	2.633	0.594
VI	0.240	0.011	0.251	0.337	2.439	0.744	0.160	0.075	0.235	0.186	2.828	1.259	0.334	0.028	0.362	0.561	3.265	0.646

Deformation Level	Elcentro																	
	F5S4B						F5S7B						F8S3B					
	Δ_{max} (m)						Δ_{max} (m)						Δ_{max} (m)					
	SDOF undamaged	Residual	Undamaged + Residual	SDOF Procedure1	Ductility	Ratio	SDOF undamaged	Residual	Undamaged + Residual	SDOF Procedure1	Ductility	Ratio	SDOF undamaged	Residual	Undamaged + Residual	SDOF Procedure1	Ductility	Ratio
I	0.074	-0.002	0.076	0.074	1.000	1.026	0.041	0.003	0.044	0.041	1.000	1.078	0.076	0.004	0.080	0.076	1.000	1.056
II	0.103	-0.002	0.105	0.101	1.025	1.044	0.071	0.005	0.077	0.072	1.000	1.066	0.109	0.006	0.114	0.101	1.031	1.134
III	0.150	-0.017	0.167	0.177	1.628	0.946	0.091	0.010	0.102	0.111	1.223	0.914	0.182	0.043	0.224	0.202	2.022	1.112
IV	0.169	-0.027	0.196	0.210	1.901	0.933	0.109	-0.011	0.120	0.142	1.449	0.849	0.197	0.038	0.235	0.210	2.121	1.119
V	0.220	-0.056	0.275	0.213	2.676	1.290	0.147	-0.023	0.170	0.190	2.052	0.895	0.289	0.078	0.367	0.289	3.308	1.270
VI	0.241	-0.053	0.294	0.254	2.858	1.160	0.160	-0.026	0.186	0.224	2.240	0.829	0.334	0.078	0.412	0.305	3.708	1.351

A5 Continued

Deformation Level	Pacoima Dam																	
	F5S4B						F5S7B						F8S3B					
	Δ_{max} (m)						Δ_{max} (m)						Δ_{max} (m)					
	SDOF undamaged	Residual	Undamaged + Residual	SDOF Procedure1	Ductility	Ratio	SDOF undamaged	Residual	Undamaged + Residual	SDOF Procedure1	Ductility	Ratio	SDOF undamaged	Residual	Undamaged + Residual	SDOF Procedure1	Ductility	Ratio
I	0.072	0.000	0.072	0.075	1.000	0.965	0.041	0.000	0.041	0.041	1.000	1.006	0.078	-0.003	0.080	0.078	1.000	1.038
II	0.102	0.000	0.102	0.117	1.000	0.870	0.071	0.000	0.071	0.081	1.000	0.886	0.107	-0.004	0.111	0.112	1.000	0.990
III	0.155	0.050	0.205	0.202	1.994	1.015	0.093	0.012	0.104	0.150	1.257	0.697	0.180	0.033	0.214	0.206	1.925	1.037
IV	0.165	0.059	0.223	0.224	2.171	0.996	0.108	0.024	0.132	0.189	1.585	0.697	0.200	0.048	0.248	0.231	2.236	1.073
V	0.226	0.067	0.293	0.363	2.848	0.808	0.148	0.047	0.196	0.344	2.361	0.570	0.289	0.092	0.381	0.402	3.435	0.948
VI	0.240	0.064	0.304	0.377	2.956	0.808	0.159	0.051	0.209	0.375	2.521	0.557	0.334	0.076	0.410	0.452	3.690	0.907
Deformation Level	Parkfield																	
	F5S4B						F5S7B						F8S3B					
	Δ_{max} (m)						Δ_{max} (m)						Δ_{max} (m)					
	SDOF undamaged	Residual	Undamaged + Residual	SDOF Procedure1	Ductility	Ratio	SDOF undamaged	Residual	Undamaged + Residual	SDOF Procedure1	Ductility	Ratio	SDOF undamaged	Residual	Undamaged + Residual	SDOF Procedure1	Ductility	Ratio
I	0.072	0.001	0.073	0.072	1.000	1.012	0.042	0.000	0.042	0.042	1.000	1.000	0.076	-0.001	0.077	0.076	1.000	1.007
II	0.106	0.001	0.106	0.112	1.034	0.953	0.071	0.000	0.071	0.067	1.000	1.065	0.109	-0.001	0.109	0.109	1.000	0.999
III	0.151	0.021	0.172	0.159	1.671	1.084	0.093	0.007	0.099	0.072	1.199	1.375	0.183	0.058	0.241	0.242	2.171	0.995
IV	0.163	0.030	0.193	0.171	1.878	1.127	0.108	0.014	0.121	0.093	1.463	1.303	0.196	0.069	0.265	0.288	2.387	0.919
V	0.222	0.081	0.303	0.236	2.944	1.285	0.148	-0.003	0.152	0.112	1.830	1.354	0.287	0.104	0.391	0.471	3.523	0.831
VI	0.240	0.083	0.323	0.260	3.142	1.243	0.160	-0.008	0.168	0.127	2.024	1.326	0.335	0.080	0.415	0.582	3.739	0.714

A5 Continued

Deformation Level	El Centro 79a																	
	F5S4B						F5S7B						F8S3B					
	Δ_{max} (m)						Δ_{max} (m)						Δ_{max} (m)					
	SDOF undamaged	Residual	Undamaged + Residual	SDOF Procedure1	Ductility	Ratio	SDOF undamaged	Residual	Undamaged + Residual	SDOF Procedure1	Ductility	Ratio	SDOF undamaged	Residual	Undamaged + Residual	SDOF Procedure1	Ductility	Ratio
I	0.076	-0.001	0.077	0.075	1.000	1.029	0.041	-0.001	0.041	0.041	1.000	1.019	0.079	0.001	0.079	0.079	1.000	1.007
II	0.107	0.002	0.109	0.080	1.057	1.364	0.070	0.000	0.070	0.068	1.000	1.028	0.109	0.001	0.109	0.107	1.000	1.026
III	0.154	-0.005	0.159	0.135	1.547	1.181	0.093	0.003	0.095	0.102	1.147	0.930	0.182	0.036	0.218	0.125	1.965	1.741
IV	0.165	-0.013	0.177	0.148	1.724	1.201	0.108	0.009	0.117	0.140	1.410	0.833	0.196	-0.084	0.279	0.185	2.517	1.508
V	0.222	-0.049	0.271	0.166	2.638	1.632	0.147	0.019	0.166	0.140	2.001	1.184	0.289	-0.008	0.297	0.289	2.672	1.026
VI	0.241	-0.060	0.301	0.171	2.923	1.757	0.160	0.022	0.182	0.143	2.188	1.274	0.334	0.063	0.397	0.384	3.580	1.034

Deformation Level	El Centro 79b																	
	F5S4B						F5S7B						F8S3B					
	Δ_{max} (m)						Δ_{max} (m)						Δ_{max} (m)					
	SDOF undamaged	Residual	Undamaged + Residual	SDOF Procedure1	Ductility	Ratio	SDOF undamaged	Residual	Undamaged + Residual	SDOF Procedure1	Ductility	Ratio	SDOF undamaged	Residual	Undamaged + Residual	SDOF Procedure1	Ductility	Ratio
I	0.076	-0.002	0.078	0.076	1.000	1.022	0.041	0.000	0.041	0.041	1.000	1.009	0.078	-0.002	0.079	0.078	1.000	1.024
II	0.107	0.001	0.109	0.112	1.056	0.973	0.071	0.001	0.072	0.076	1.000	0.949	0.109	-0.003	0.111	0.121	1.002	0.922
III	0.154	0.012	0.167	0.170	1.619	0.977	0.093	0.011	0.103	0.110	1.245	0.941	0.180	-0.075	0.256	0.249	2.304	1.026
IV	0.165	0.005	0.170	0.202	1.652	0.843	0.109	0.027	0.136	0.133	1.642	1.025	0.196	-0.091	0.286	0.265	2.581	1.082
V	0.224	-0.120	0.343	0.375	3.338	0.917	0.148	-0.033	0.181	0.179	2.185	1.011	0.290	-0.176	0.466	0.313	4.201	1.490
VI	0.243	-0.140	0.383	0.390	3.722	0.983	0.160	-0.043	0.203	0.195	2.440	1.039	0.335	-0.193	0.529	0.344	4.763	1.537

A5 Continued

Deformation Level	Chi-Chi																	
	F5S4B						F5S7B						F8S3B					
	Δ_{max} (m)						Δ_{max} (m)						Δ_{max} (m)					
	SDOF undamaged	Residual	Undamaged + Residual	SDOF Procedure1	Ductility	Ratio	SDOF undamaged	Residual	Undamaged + Residual	SDOF Procedure1	Ductility	Ratio	SDOF undamaged	Residual	Undamaged + Residual	SDOF Procedure1	Ductility	Ratio
I	0.076	0.000	0.077	0.078	1.000	0.987	0.041	0.000	0.041	0.041	1.000	1.000	0.078	0.000	0.078	0.078	1.000	1.000
II	0.106	0.000	0.106	0.121	1.029	0.875	0.071	0.000	0.071	0.077	1.000	0.925	0.109	0.000	0.109	0.107	1.000	1.018
III	0.153	0.025	0.178	0.176	1.725	1.010	0.091	0.009	0.101	0.104	1.214	0.973	0.182	-0.008	0.189	0.219	1.706	0.866
IV	0.165	-0.009	0.173	0.197	1.685	0.882	0.109	0.026	0.136	0.124	1.633	1.091	0.197	-0.014	0.211	0.244	1.904	0.867
V	0.222	-0.065	0.287	0.244	2.793	1.180	0.148	0.025	0.173	0.240	2.088	0.721	0.289	0.177	0.466	0.405	4.197	1.150
VI	0.240	-0.087	0.327	0.302	3.176	1.082	0.160	0.026	0.186	0.269	2.235	0.689	0.334	0.209	0.543	0.632	4.895	0.860

Deformation Level	Northridge-Pacoima																	
	F5S4B						F5S7B						F8S3B					
	Δ_{max} (m)						Δ_{max} (m)						Δ_{max} (m)					
	SDOF undamaged	Residual	Undamaged + Residual	SDOF Procedure1	Ductility	Ratio	SDOF undamaged	Residual	Undamaged + Residual	SDOF Procedure1	Ductility	Ratio	SDOF undamaged	Residual	Undamaged + Residual	SDOF Procedure1	Ductility	Ratio
I	0.076	0.000	0.077	0.076	1.000	1.006	0.042	0.000	0.042	0.042	1.000	1.000	0.076	0.001	0.077	0.076	1.000	1.007
II	0.107	0.000	0.108	0.109	1.046	0.987	0.070	0.000	0.070	0.071	1.000	0.990	0.109	0.001	0.109	0.107	1.000	1.025
III	0.154	-0.046	0.201	0.145	1.949	1.380	0.093	0.009	0.101	0.090	1.222	1.129	0.180	-0.035	0.215	0.173	1.938	1.246
IV	0.165	-0.055	0.220	0.148	2.134	1.487	0.109	-0.007	0.116	0.113	1.394	1.024	0.196	-0.047	0.243	0.184	2.185	1.319
V	0.222	-0.052	0.275	0.181	2.670	1.520	0.148	-0.036	0.185	0.160	2.225	1.156	0.287	-0.141	0.429	0.258	3.864	1.660
VI	0.240	-0.049	0.289	0.208	2.808	1.390	0.160	-0.041	0.201	0.163	2.417	1.229	0.335	-0.192	0.527	0.330	4.752	1.599

A5 Continued

Deformation Level	Cape Mendocino																	
	F5S4B						F5S7B						F8S3B					
	Δ_{max} (m)						Δ_{max} (m)						Δ_{max} (m)					
	SDOF undamaged	Residual	Undamaged + Residual	SDOF Procedure1	Ductility	Ratio	SDOF undamaged	Residual	Undamaged + Residual	SDOF Procedure1	Ductility	Ratio	SDOF undamaged	Residual	Undamaged + Residual	SDOF Procedure1	Ductility	Ratio
I	0.076	-0.001	0.078	0.076	1.000	1.020	0.041	0.000	0.041	0.041	1.000	1.003	0.076	-0.001	0.077	0.076	1.000	1.007
II	0.107	-0.006	0.113	0.116	1.103	0.981	0.071	0.000	0.071	0.069	1.000	1.028	0.109	-0.001	0.109	0.112	1.000	0.975
III	0.153	-0.028	0.181	0.173	1.755	1.044	0.093	-0.008	0.101	0.089	1.214	1.137	0.180	-0.004	0.184	0.249	1.658	0.738
IV	0.165	-0.033	0.198	0.206	1.927	0.964	0.109	-0.008	0.118	0.122	1.416	0.965	0.196	0.010	0.206	0.272	1.852	0.757
V	0.222	-0.001	0.224	0.477	2.172	0.469	0.148	-0.024	0.173	0.189	2.084	0.915	0.290	0.097	0.387	0.335	3.485	1.154
VI	0.240	0.016	0.256	0.488	2.485	0.524	0.160	-0.029	0.189	0.200	2.275	0.945	0.335	0.125	0.460	0.337	4.149	1.367

Deformation Level	Northridge																	
	F5S4B						F5S7B						F8S3B					
	Δ_{max} (m)						Δ_{max} (m)						Δ_{max} (m)					
	SDOF undamaged	Residual	Undamaged + Residual	SDOF Procedure1	Ductility	Ratio	SDOF undamaged	Residual	Undamaged + Residual	SDOF Procedure1	Ductility	Ratio	SDOF undamaged	Residual	Undamaged + Residual	SDOF Procedure1	Ductility	Ratio
I	0.075	-0.001	0.076	0.078	1.000	0.975	0.041	0.000	0.041	0.041	1.000	1.000	0.078	-0.001	0.079	0.078	1.000	1.018
II	0.106	0.002	0.108	0.124	1.051	0.874	0.071	0.000	0.071	0.078	1.000	0.910	0.107	-0.002	0.109	0.112	1.000	0.971
III	0.154	0.049	0.203	0.151	1.973	1.348	0.093	-0.012	0.105	0.090	1.266	1.170	0.180	-0.072	0.252	0.228	2.272	1.105
IV	0.165	0.052	0.217	0.189	2.104	1.148	0.110	-0.009	0.119	0.107	1.439	1.118	0.197	-0.089	0.287	0.245	2.583	1.169
V	0.222	-0.044	0.266	0.323	2.585	0.822	0.148	0.015	0.164	0.162	1.974	1.010	0.287	-0.099	0.387	0.299	3.486	1.294
VI	0.240	-0.053	0.293	0.349	2.848	0.840	0.160	0.022	0.182	0.182	2.192	1.002	0.335	-0.056	0.391	0.333	3.524	1.176

A.6 SECTION PROPERTIES FOR CASE BUILDING

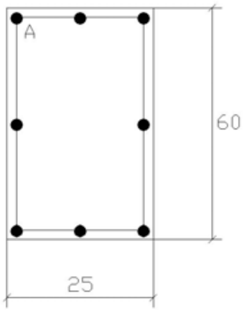

Column S1
(25/50)
A = 201 mm^2
cover = 35 mm

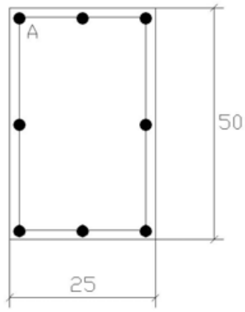

Column S2
(25/60)
A = 229 mm^2
cover = 35 mm

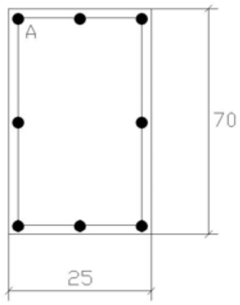

Column S3
(25/70)
A = 254 mm^2
cover = 35 mm

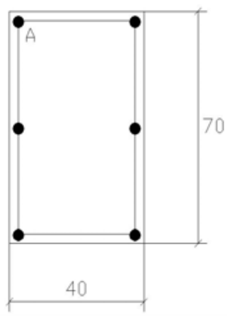

Column S4
(40/70)
A = 254 mm^2
cover = 35 mm

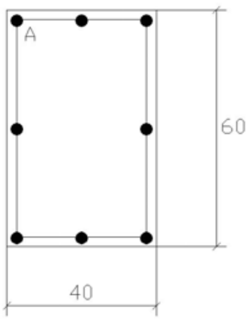

Column S5
(40/60)
A = 254 mm^2
cover = 35 mm

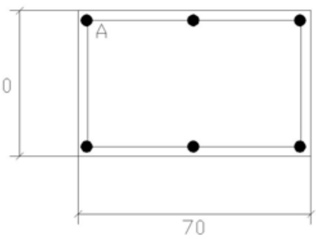

Column S6
(70/40)
A = 254 mm^2
cover = 35 mm

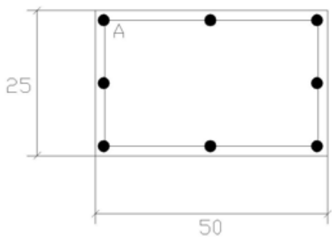

Column S7
(50/25)
A = 201 mm^2
cover = 35 mm

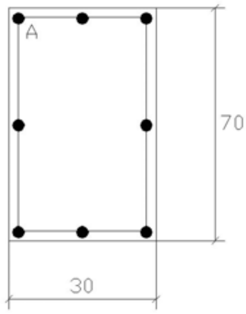

Column S8
(30/70)
A = 178 mm^2
cover = 35 mm

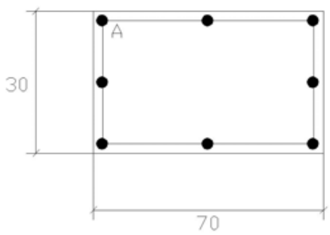

Column S9
(70/30)
A = 178 mm^2
cover = 35 mm

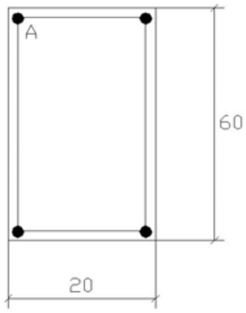

Beam
(20/60)
A = 201 mm^2
cover = 35 mm